RESEARCH ARTICLE

Comparative Analysis of Intensity Scintillation and Phase Structure Functions under Three Atmospheric Turbulence Spectral Models

Rui Wang[1,2,*] **and Xizheng Ke**[1,3]

[1] Faculty of Automation and Information Engineering, Xi'an University of Technology, Xi'an 710048, China
[2] Faculty of Information, Xi'an University of Finance and Economics, Xi'an 710100, China
[3] Shaanxi Civil-Military Integration Key Laboratory of Intelligence Collaborative Networks, Xi'an 710126, China

Abstract

To investigate the effects of different atmospheric turbulence power spectrum models on the statistical characteristics of optical field propagation, this study considers the non-Kolmogorov spectrum, the generalized von Kármán spectrum and the generalized modified atmospheric spectrum. The spectral distributions of the three models over different spatial-frequency ranges are compared, and the intensity scintillation indices and phase structure functions of plane and spherical waves under different turbulence conditions are analyzed. Based on the relevant theoretical models, the effects of propagation distance, power-law spectral exponent, and turbulence inner scale on intensity fluctuations, and of the power-law spectral exponent on wavefront phase distortions, are examined numerically, while the roles of the turbulence inner and outer scales are analyzed through the spectral models and spatial filtering functions. Analytical expressions for the phase structure functions under the three spectral models are derived and compared. The results indicate that the spectral models differ in their descriptions of low-frequency energy limitation, high-frequency dissipation and spectral corrections near the dissipation range, which changes the predicted intensity scintillation and phase fluctuations. Plane and spherical waves also respond differently because the propagation geometry changes how turbulence-induced disturbances accumulate along the path. The derived expressions relate the spectral parameters directly to the scintillation index and phase structure function and can be used to evaluate atmospheric optical links.

Keywords: atmospheric turbulence power spectrum, intensity scintillation index, phase structure function.

1 Introduction

The wireless optical communication system mainly uses the atmospheric channel to realize the long-distance transmission of optical signals.

Submitted: 28 September 2026
Revised: 05 November 2026
Accepted: 07 November 2026
Published: 21 November 2026

Vol. 2, **No.** 1, 2027.
10.62762/OWC.2026.211491

***Corresponding author:**
✉ Rui Wang
2005010006@xaufe.edu.cn

Citation
Wang, R., & Ke, X. (2026). Comparative Analysis of Intensity Scintillation and Phase Structure Functions under Three Atmospheric Turbulence Spectral Models. *Optical Wireless Communication*, 2(1), 1–47.

© 2026 by the Authors. Published by Institute of Central Computation and Knowledge. This is an open access article under the CC BY license (https://creativecommons.org/licenses/by/4.0/).

Atmospheric turbulence is composed of a superposition of eddies of different scales. Its energy is input by the outer scale, cascades through the inertial region to the small scale, and finally dissipates through the viscous effect at the inner scale, showing obvious statistical randomness and inhomogeneity [1, 2]. The random variation of temperature, pressure and wind speed in the atmosphere will cause the random fluctuation of refractive index in space and time, which makes the atmosphere appear as a random turbulent medium with multi-scale structure, thus forming atmospheric turbulence. When the laser beam is transmitted in the atmospheric link, the random fluctuation of the refractive index caused by atmospheric turbulence will lead to the intensity fluctuation and phase distortion of the transmitted light field. The intensity fluctuation leads to the fluctuation of the signal-to-noise ratio at the receiving end, and the phase distortion causes the wavefront distortion, which affects the coherent detection and wavefront correction effect, thereby reducing the performance of the communication link.

The light intensity scintillation index reflects the degree of random fluctuation of the received light intensity [3–9], which is a key index to evaluate the link fading characteristics and error performance. The phase structure function describes the variation of the phase with the spatial distance [10], which shows the degree of wavefront distortion of the beam. The influence of atmospheric turbulence on light field transmission is studied by using the intensity scintillation index and the phase structure function as the statistics to describe the intensity fluctuation and phase distortion, respectively.

2 Atmospheric turbulence

The power spectrum of atmospheric turbulence is a key model for the physical characteristics of atmospheric turbulence and the statistical characteristics of light field. The Kolmogorov spectrum model is often used in traditional atmospheric turbulence research. However, in the actual atmospheric environment, due to the inner and outer scale effect and the existence of a non-classical energy cascade process, the Kolmogorov spectrum cannot fully describe the characteristics of atmospheric turbulence. Therefore, the non-Kolmogorov spectrum, the generalized von Kármán spectrum and the generalized modified atmospheric spectrum have been proposed successively. These models can describe the characteristics of atmospheric turbulence under different physical conditions by introducing generalized power-law spectral index, finite inner and outer scale correction, and spectral correction parameters. These three power spectra are different in describing non-Kolmogorov turbulence, turbulent dissipation region and inner and outer scale effects. However, there is no systematic comparative study on the analytical relationship between the scintillation index and the phase structure function under different spectral models.

2.1 The physical mechanism of atmospheric turbulence formation

Atmospheric turbulence is a multi-scale random motion driven by hydrodynamic instability. The atmospheric motion is driven by wind shear, buoyancy and temperature gradient, which makes the coupling disturbance of velocity field and density field in the gas medium. When this disturbance is amplified under certain conditions and gradually evolves into a multi-scale random structure, the originally ordered laminar motion will be transformed into a turbulent state. The incompressible viscous fluid motion satisfies the Navier-Stokes equation [2], and its expression is

$$\frac{\partial \vec{V}}{\partial t} + (\vec{V} \cdot \nabla)\vec{V} = -\frac{1}{\rho_m}\nabla P + \frac{\mu}{\rho_m}\Delta \vec{V} \quad (\nabla \cdot \vec{V} = 0) \tag{1}$$

where $\vec{V}$ is the velocity field, P is the pressure, ρ_m is the fluid density, $(\vec{V} \cdot \nabla)\vec{V}$ is called the nonlinear convection term (turbulence term), and $\nu\Delta\vec{V}$ with $\nu = \mu/\rho_m$ is called the momentum diffusion term. The coefficient μ is the dynamic viscosity coefficient $(\mathrm{kg}/(\mathrm{m}\cdot\mathrm{s}))$, and ν is the kinematic viscosity coefficient $(\mathrm{m}^2/\mathrm{s})$.

The nonlinear convection term reflects the transport process of fluid momentum in space, and the momentum diffusion term is generated by the viscous effect. In the atmospheric environment, the generation of turbulence is derived from the competitive relationship between these two physical processes. When the nonlinear convection term is dominant, the small disturbance inside the fluid will be continuously amplified and form a complex vortex structure. When the viscous diffusion term is dominant, the disturbance will be dissipated quickly and the fluid will remain laminar. This competitive relationship is usually expressed by the Reynolds number, which was introduced by Reynolds as the criterion for the transition from laminar to

turbulent flow [11]. According to the similarity theory, the Reynolds number is the ratio of the nonlinear convection (inertial) term to the viscous term [2], and its expression is

$$R = \frac{|(\vec{V} \cdot \nabla)\vec{V}|}{|\nu \Delta \vec{V}|} \sim \frac{lV}{\nu} \quad (2)$$

where l is the characteristic scale of fluid motion. When R is less than the critical value R_c, viscous dissipation inhibits the growth of velocity disturbance and the fluid maintains a stable laminar structure. When $R > R_c$, the fluid system enters a dynamic unstable state, and the velocity disturbance is continuously amplified and gradually forms a random vortex structure, resulting in turbulence. In the atmospheric boundary layer, the Reynolds number can usually reach the order of $10^7 \sim 10^9$, and the atmospheric motion is generally in a highly developed turbulent state.

(1) Turbulent energy cascade and scale structure

The dynamic evolution process of atmospheric turbulence is a cascade transmission process of energy in scale space. In the atmosphere, energy is usually first injected into the fluid system by large-scale motions such as wind shear, convection, or surface heating, and then gradually transferred to smaller-scale vortices [2] through nonlinear interactions until it reaches the viscous dissipation scale and eventually converted into heat energy. This process makes the atmospheric turbulence show an obvious multi-scale hierarchical structure. Two basic scale parameters, turbulent outer scale L_0 and turbulent inner scale l_0, are usually introduced to describe this structural feature [2].

The outer scale L_0 of atmospheric turbulence represents the maximum characteristic scale of the turbulent energy injection end, which corresponds to the typical spatial scale of the average flow field injecting kinetic energy into turbulence. When the fluid characteristic scale $l > L_0$, the fluid motion is affected by boundary conditions or external driving mechanisms, and the turbulence in this region has obvious anisotropic characteristics. The turbulent inner scale l_0 represents the minimum characteristic scale of viscous dissipation of turbulent energy. The scale is determined by the energy dissipation rate per unit mass ε_1 and the fluid viscosity. Below this scale, the turbulent vortex structure decays rapidly and the kinetic energy is converted into heat energy. There is a wide scale interval between L_0 and l_0, which is called the inertial region. In the inertial region, turbulent energy is transmitted in cascade through nonlinear interaction, and viscous dissipation has not yet played a significant role. In Kolmogorov theory, the velocity scale of the inertial region of homogeneous isotropic turbulence satisfies $V(r) \sim (\varepsilon_1 r)^{1/3}$, and the turbulence energy spectrum shows a power-law distribution $\Phi(\kappa) \propto \kappa^{-11/3}$, where κ is the wavenumber. In the tropopause, stratosphere and near-surface regions of the actual atmosphere, the turbulence spectrum still maintains power-law characteristics, and the index often deviates from $-11/3$ [12]. Non-Kolmogorov turbulence models have therefore been adopted in the performance analysis of free-space optical links, including links with receive diversity in anisotropic turbulence [13].

Atmospheric turbulence can be divided into three regions in the scale space. The region where the size of the turbulent vortex is larger than the outer scale L_0 is the energy injection region. The energy is injected into the system by the large-scale dynamic process, and the turbulence has obvious anisotropy [14]. The region where the size of the turbulent vortex is smaller than the outer scale L_0 and larger than the inner scale l_0 is the inertial region. The energy is cascaded between the vortices of different scales, and the turbulence is approximately isotropic. The region where the size of the turbulent vortex is smaller than the inner scale l_0 is the dissipative region, the viscous effect is dominant, and the turbulent energy dissipates rapidly [2], as shown in Figure 1.

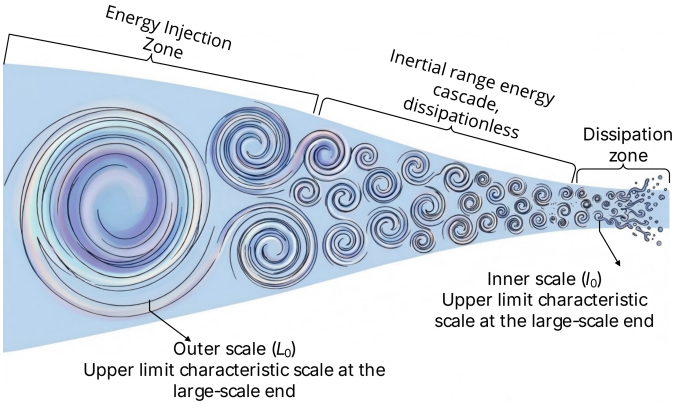


Figure 1. Inner scale and outer scale of atmospheric turbulence.

(2) Refractive index fluctuation

Atmospheric turbulence is characterized by the randomness of the velocity field, which will lead to the fluctuation of temperature and density, and cause the random fluctuation of refractive index field. For

the problem of light wave propagation, the refractive index fluctuation is a key physical quantity to describe the influence of atmospheric turbulence.

If the statistical properties of the refractive index perturbation $n_1(\vec{r},t)$ satisfy the translation invariance, the spatial correlation function $B_n(\vec{r}_1,\vec{r}_2)$ depends only on $\vec{r}_1-\vec{r}_2$, and the random medium can be regarded as a local homogeneous random medium [3], as shown in (3).

$$B_n\left(\vec{r}_1,\vec{r}_2\right)=B_n\left(\vec{r}_1-\vec{r}_2\right)=B_n\left(\vec{r}_d\right) \tag{3}$$

In the propagation of light waves in the atmosphere, since the correlation length in the vertical direction is much smaller than that in the horizontal direction, the refractive index fluctuation often exhibits obvious anisotropy. The expression of its spatial correlation function is

$$B_n(\vec{r}_d)=\langle n_1^2\rangle \exp\left[-\left(x/r_x\right)^2-\left(y/r_y\right)^2-\left(z/r_z\right)^2\right] \tag{4}$$

where r_x, r_y, r_z can be seen as the coherent length of the refractive index fluctuation in the x, y, z directions.

According to the Wiener-Khinchin theorem, the power spectral density of the refractive index fluctuation $\Phi_n(\vec{k}_s)$ is the Fourier transform of the correlation function $B_n(\vec{r}_d)$, namely

$$\Phi_n(\vec{k}_s)=\frac{1}{(2\pi)^3}\int_{\infty} B_n(\vec{r}_d)\exp(i\vec{k}_s\cdot\vec{r}_d)dV_d \tag{5}$$

(3) Characteristic scale related to light wave propagation

The refractive index inhomogeneous structure in atmospheric turbulence has a continuous spatial scale distribution, in which the inner scale l_0 and the outer scale L_0 are the characteristic scale parameters that characterize the characteristics of the two ends of the turbulent refractive index power spectrum at high and low spatial frequencies. The outer scale L_0 mainly reflects the scale characteristics of the low spatial frequency end, and the inner scale l_0 mainly reflects the scale characteristics of the transition from the inertial zone to the dissipation zone at the high spatial frequency end. The two describe the characteristic scales at both ends of the atmospheric turbulence power spectrum, which are not equal to the large-scale turbulence structure and the small-scale turbulence structure, respectively. Large-scale and small-scale turbulent structures [6–8] are relatively divided according to the spatial scale of the refractive index inhomogeneous structure. The structure with larger spatial scale [6–8] corresponds to a lower spatial frequency, and the structure with smaller spatial scale [6–8] corresponds to a higher spatial frequency. Since the spatial scale of the turbulence structure is continuously distributed, the large scale and the small scale are not strictly separated by a fixed spatial scale value, but are used to describe the relative size of the spatial scale of different atmospheric turbulence structures. Here, the large and small represent the relative size of the spatial scale of the turbulence structure, rather than the strength of its effect on light propagation [6–8]. In the study of the influence of atmospheric turbulence on light propagation, it is also necessary to introduce the characteristic scales related to light propagation, such as Fresnel scale, spatial coherence scale and scattering disk scale [3, 9], as shown in Table 1. These light propagation characteristic scales do not belong to the large-scale or small-scale turbulence structure itself, and are used as reference scales for analyzing the interaction between light waves and turbulence structures of different scales. By comparing the relative relationship between the scale of turbulence structure and these characteristic scales of light propagation, the effective range, mode of action and contribution of different scale turbulence structures to the fluctuation of light field under specific propagation conditions can be judged. The related strong turbulence theory [7] also shows that the effect of different scale turbulence structures on scintillation depends on the relationship between its scale and the propagation scale such as the coherent scale of the light field, and the strength of its effect cannot be judged only by the structure size itself. Therefore, the inner and outer scales are used to characterize the characteristic scales at both ends of the turbulence power spectrum [4], the large and small scales are used to describe the relative contributions of different spatial scales of the continuous turbulence structure to scintillation [6, 7], and the light propagation characteristic scale is used to analyze the specific effects of different scale turbulence structures on light wave propagation. The objects and physical meanings described by the three are different, but they are interrelated in the analysis of atmospheric turbulence light propagation.

The spatial coherence radius ρ_0 of the light wave refers

Table 1. Characteristic scales related to optical propagation.

Scale	Symbol	Physical meaning
Spatial coherence radius of the optical wave	ρ_0	Characteristic scale describing wavefront coherence
First Fresnel zone	$\sqrt{L/k}$	Most effective turbulent cell size for generating scintillation
Beam radius	W	Characterizes the transverse beam size
Scattering disk	$L/k\rho_0$	Effective region formed by strong turbulent scattering

to the distance corresponding to the 1 / e point of the coherence function. After the light wave has propagated over a sufficiently long distance L, only turbulent eddies of certain characteristic sizes, namely the Fresnel scale, the spatial coherence radius and the scattering disk discussed below, can effectively cause the diffusion and amplitude fluctuation of the light wave. The Fresnel zone defines the most effective turbulent cell size for generating scintillation at a distance L from the source. A spatial coherence region of size ρ_0 at the receiver corresponds to a region of size $L/k\rho_0$ near the emitter, which is called the scattering disk [15]. The Fresnel zone, spatial coherence radius and inner scale are the most important scale sizes when studying light intensity scintillation. Under weak turbulence, the first Fresnel zone scale determines the most effective turbulence cell size to generate scintillation at a distance of L. As the propagation distance increases or the turbulence intensity increases, the spatial coherence radius will gradually decrease, and the scattering disk scale will increase. The scale that controls the intensity scintillation therefore shifts from the Fresnel scale to the coherence radius and the scattering disk scale. Under the condition of strong turbulence, only the eddy whose scale is larger than the scattering disk or smaller than the spatial coherence radius will have an effect on the light intensity fluctuation, and the turbulence scale between the two has less effect on the scintillation. In the analysis of light intensity scintillation under medium to strong turbulence conditions, it is necessary to use a spatial filter to filter out turbulent vortices of the corresponding scale. This scale selection effect shows that the influence of atmospheric turbulence on light wave propagation is essentially a spatial filtering process. Under the condition of strong turbulence, the field in a spatial coherence region of size ρ_0 at the receiving end is determined by the field within the scattering disk $L/k\rho_0$ near the transmitting end. The turbulent vortex with a scale larger than the scattering disk can change the direction of the light entering the coherent unit and affect the field distribution in the region, as shown in Figure 2.

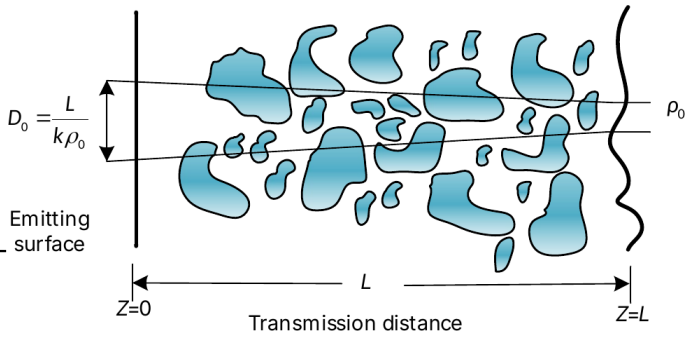


Figure 2. The relationship between the field of scattering disk size at $z = 0$ and the field of spatial coherence radius size at $z = L$.

2.2 Three kinds of atmospheric turbulence power spectrum models

2.2.1 Non-Kolmogorov Spectrum (NKS)

Atmospheric turbulence is a random process, and it is usually necessary to carry out complete statistical analysis with the help of corresponding statistics. The non-Kolmogorov spectrum is the basic power-law spectral model, and the generalized power-law spectral index α varies from 3 to 5. The spectrum does not consider the influence of inner scale and outer scale, and it is considered that turbulence follows a unified power-law distribution at all spatial frequencies. Since it does not contain truncation, it means that the phase difference is infinite when the distance is infinite, which is unphysical and is only applicable to the inertial region where the observation scale is much larger than the inner scale and much smaller than the outer scale. The expression of non-Kolmogorov spectrum [12] is

$$\Phi_n(\kappa, \alpha) = A(\alpha)\tilde{C}_n^2\kappa^{-\alpha} \quad 3 < \alpha < 5 \tag{6}$$

where α represents the generalized power-law spectral index. $A(\alpha)$ is called the consistency function, which is dimensionless, and its role is to establish the integral relationship between the turbulent refractive index structure function and the power spectrum within a given range of α. $\Gamma[\cdot]$ is the gamma function. The expression of $A(\alpha)$ [12, 16–18] has three forms, as shown in Table 2.

The three expressions of $A(\alpha)$ are equivalent, and Figure 3 shows the variation curve of $A(\alpha)$ with the

Table 2. Expressions of $A(\alpha)$.

Form	Expression
Stribling	$A(\alpha) = 2^{\alpha-6}(\alpha^2 - 5\alpha + 6)\pi^{-3/2}\frac{\Gamma[(\alpha-2)/2]}{\Gamma[(5-\alpha)/2]}$
Beland	$A(\alpha) = -2^{\alpha-4}\pi^{-3/2}\frac{\Gamma(\alpha/2)}{\Gamma[(3-\alpha)/2]}$
Toselli	$A(\alpha) = \frac{\Gamma(\alpha-1)}{4\pi^2}\cos\left(\frac{\alpha\pi}{2}\right)$

All three forms are valid for $3 < \alpha < 5$.

power law exponent α of the power spectrum. The abscissa represents the parameter α, ranging from 3 to 5, and the ordinate is $A(\alpha)$, ranging from 0.00 to 0.07. The curve in the plot shows a single peak shape of rising first and then falling, reaching a maximum value of about 0.06 at α of about 4.4, and the function values at the two endpoints of $\alpha = 3$ and $\alpha = 5$ are close to zero. For the non-Kolmogorov spectrum, the one-dimensional spectral exponent is no longer fixed at $-5/3$, and the three-dimensional spectral exponent α is no longer fixed at $11/3$, but changes within a certain range. In order to ensure the continuity of the parameters, the absolute value of the three-dimensional spectral power α is usually 3-5 when studying the light propagation characteristics in atmospheric turbulence.

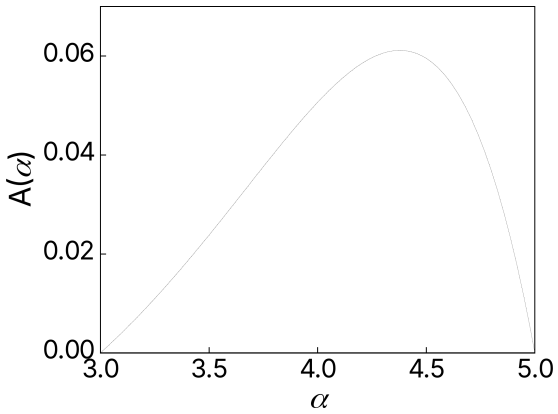


Figure 3. Variation of $A(\alpha)$ with α.

2.2.2 *Generalized von Kármán Spectrum (GVKS)*

The generalized von Kármán spectrum introduces the outer-scale-dependent low-frequency limitation κ_0 and the inner-scale-dependent high-frequency dissipation κ_m. The low spatial frequency end is modified by the outer scale parameters κ_0 to limit the low spectral energy corresponding to the larger spatial scale turbulence structure. The dissipation characteristics of the high spatial frequency end are described by the inner scale parameters κ_m, and the high spectral energy corresponding to the smaller spatial scale turbulence structure is suppressed. Thus, the variation characteristics of turbulent power spectrum in the inertial region and its two ends can be described more completely. It should be pointed out that the inner-scale and outer-scale parameters l_0 and L_0 represent the characteristic scales of the high-frequency dissipation end and the low-frequency cutoff end of the power spectrum, respectively. They are spectral domain boundary parameters, rather than representing a certain type of small-scale or large-scale turbulent structure, respectively. The large-scale and small-scale turbulent structures are relatively divided according to the spatial scale, which mainly correspond to lower and higher spatial frequencies, respectively. The inner scale is usually in the order of several millimeters, and the outer scale is usually in the order of several meters. The expression of the generalized von Kármán spectrum [19, 20] is

$$\Phi_n(\kappa,\alpha) = A(\alpha)\tilde{C}_n^2\frac{\exp(-\kappa^2/\kappa_m^2)}{(\kappa^2+\kappa_0^2)^{\alpha/2}} \tag{7}$$

where κ is the spatial frequency in rad / m, $A(\alpha) = \Gamma(\alpha-1)\cos(\alpha\pi/2)/4\pi^2$. $\tilde{C}_n^2(\alpha,z)$ is a non-Kolmogorov refractive index structure constant in the unit of $m^{3-\alpha}$. The parameter κ_m and κ_0 are the spatial cutoff frequencies related to the inner scale and the outer scale, respectively, $\kappa_m = c(\alpha)/l_0$,$c(\alpha) = \{\Gamma[(5-\alpha)/2]\cdot A(\alpha)\cdot 2\pi/3\}^{1/(\alpha-5)}$,$\kappa_0 = 2\pi/L_0$.

2.2.3 *Generalized Modified Atmospheric Spectrum (GMAS)*

The generalized modified atmospheric spectrum is the von Kármán spectrum with added Hill protrusions [21], which are expressed in terms of a_1 and b_1, to describe the small protrusions on the power spectral density curve at high frequencies. Compared with the former two, it is more consistent with the experimental observation results in describing the upper atmospheric turbulence. The expression of the generalized modified atmospheric spectrum [22] is

$$\begin{aligned}\Phi_n(\kappa,\alpha) &= A(\alpha)\tilde{C}_n^2\kappa^{-\alpha}f(\kappa,\alpha,l_0,L_0)\\ 0<\kappa<\infty &\quad 3<\alpha<5\\ f(\kappa,\alpha,l_0,L_0) &= [1+a_1(\frac{\kappa}{\kappa_l}) - b_1(\frac{\kappa}{\kappa_l})^\beta]\\ &\times\exp(-\frac{\kappa^2}{\kappa_l^2})[1-\exp(-\frac{\kappa^2}{\kappa_0^2})]\end{aligned} \tag{8}$$

Considering the protrusions at high frequencies, the spatial cut-off frequency κ_l [22] corresponding to the inner scale correlation is redefined as

$$\kappa_l = \frac{c_h(\alpha)}{l_0} \tag{9}$$

The expression of $c_h(\alpha)$ is

$$\begin{aligned} c_h(\alpha) =& \{\pi A(\alpha)\left[\Gamma(\frac{3-\alpha}{2})(\frac{3-\alpha}{3})\right. \\ &+a_1\Gamma(2-\frac{\alpha}{2})(\frac{4-\alpha}{3}) \\ &\left.-b_1\Gamma(\frac{3-\alpha+\beta}{2})(\frac{3-\alpha+\beta}{3})\right]\}^{\frac{1}{\alpha-5}} \end{aligned} \tag{10}$$

The values of parameters a_1, b_1 and β [23] in formulas (8) and (10) depend on the experimental results. The two coefficients a_1 and b_1 control the height and width of the protrusion. They reflect the phenomenon of kinetic energy accumulation at the edge of the dissipative layer during the cascade of energy from the larger spatial scale turbulent structure to the smaller spatial scale turbulent structure. β determines the rate of change of the correction term with spatial frequency.

Atmospheric turbulence with non-Kolmogorov properties appears in the upper troposphere or the upper atmosphere of the stratosphere, and the outer scale of the turbulent vortex is large. Some experimental results show that the inner scale of turbulence can change from a few millimeters near the ground to a few centimeters in the upper atmosphere. Let $L_0 = \infty$ in (8), the expression of generalized modified atmospheric spectrum is simplified [22] as

$$\begin{aligned} &\Phi_n(\kappa,\alpha) = A(\alpha)\tilde{C}_n^2\kappa^{-\alpha}f(\kappa,\alpha,l_0) \\ &\quad 0<\kappa<\infty \quad 3<\alpha<5 \\ &f(\kappa,\alpha,l_0) = [1+a_1(\frac{\kappa}{\kappa_l})-b_1(\frac{\kappa}{\kappa_l})^\beta]\exp(-\frac{\kappa^2}{\kappa_l^2}) \end{aligned} \tag{11}$$

2.2.4 Comparison of the characteristics of different atmospheric turbulence power spectrum models

(1) Characteristics of different atmospheric turbulence power spectrum models

Considering that the actual atmospheric measurements are mostly concentrated in the vicinity of the classical Kolmogorov value $\alpha = 11/3$, the analysis interval of α is defined in the range of (3,4). The non-Kolmogorov spectral formula, the generalized von Kármán spectral formula and the generalized modified atmospheric spectral formula are used respectively. The outer scale is L_0 = 10 m, the inner scale is l_0 = 1 mm and the three typical values of α are 3.3, 3.67 and 3.9, respectively. The parameters are a_1=1.802, b_1=0.254 and β= 7 / 6. The double logarithmic coordinates are used to describe the distribution characteristics of the three power spectra of the spatial frequency κ in the range of 10^{-2} to 10^4, as shown in Figure 4. Figure 4 (a) is the curve of three different atmospheric turbulence power spectra at $\alpha = 3.67$, Figure 4 (b) is the curve of non-Kolmogorov spectrum under different conditions α, Figure 4 (c) is the curve of generalized von Kármán spectrum under different conditions α, Figure 4 (d) is the curve of generalized modified atmospheric spectrum under different conditions α.

Figure 4 (a) shows the difference between the three atmospheric turbulence power spectrum models with the change of spatial frequency κ. The non-Kolmogorov model is represented by a curve with a circular symbol, strictly following the ideal power law, and is expressed as a straight line in the logarithmic coordinate, indicating the ideal state of turbulent energy transfer. The generalized von Kármán spectral model is represented by a curve with a square symbol. In the low frequency band, the divergence at low wavenumbers is suppressed by a smooth saturation trend, showing the real physical characteristics limited by the outer scale. The generalized modified atmospheric spectral model is represented by a curve with a triangular symbol. Before entering the dissipation layer, a significant Hill uplift is formed, which reflects the accumulation characteristics of energy near the edge of the dissipation zone at higher spatial frequencies. In the high frequency band, it drops rapidly with a very steep slope, reflecting the rapid dissipation of turbulent energy. Figure 4 (b) shows the influence of the change of the power exponent α on the change of the refractive index power spectrum $\Phi_n(\kappa)$ of atmospheric turbulence under the non-Kolmogorov turbulence model. The curve with square symbol represents α = 3.3, the curve with circular symbol represents $\alpha = 3.67$, and the curve with triangular symbol represents α = 3.9. When α increases from 3.3 to 3.9, the inclination of the atmospheric turbulence power spectrum curve in the double logarithmic coordinate system changes. In the low spatial frequency κ region, the larger α value corresponds to a higher energy distribution, and the triangle curve is at the top, indicating that the low spectral energy corresponding to the larger spatial scale turbulence structure increases relatively. With

the increase of spatial frequency κ, the larger the α is, the more intense the attenuation is. The atmospheric turbulence power spectrum curve intersects near $\kappa \approx 10^0$ and changes its position. In the high spatial frequency κ region, the curve with larger α decreases the fastest, and its ordinate value is the lowest.

Figure 4 (c) shows the variation of the generalized von Kármán spectrum with the spatial frequency κ under different α. In the low frequency region $\kappa < 1$, the power spectrum of atmospheric turbulence is saturated, and the magnitude of spectral energy increases significantly with the increase of α value, indicating that the low spectral energy corresponding to the larger spatial turbulence structure increases with the increase of α value. When entering the middle and high frequency region, the three curves all show a significant downward trend, and the larger the α, the steeper the slope of the curve decays with the increase of frequency. At the end of the high frequency $\kappa > 10^2$, there is an opposite characteristic to the low frequency band. The curve with smaller α retains higher residual energy at high frequencies instead. This phenomenon of spectral line overlap and conversion from low frequency to high frequency reflects the redistribution of turbulent energy space by α.

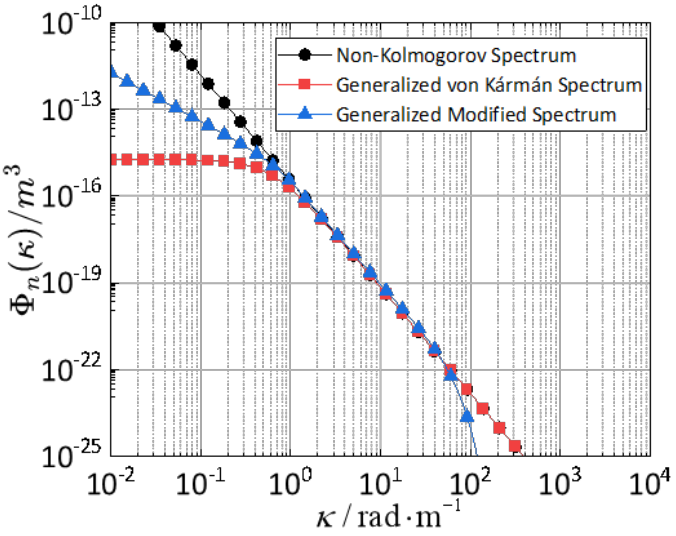
Figure 4 (d) shows the evolution of the generalized modified atmospheric spectral refractive index power spectrum $\Phi_n(\kappa)$ with the spatial frequency κ, which reflects the influence of α on the turbulent energy distribution. When $\alpha = 3.3$, the spectral curve drops sharply at a very low spatial frequency, indicating that the spectral energy is more concentrated in the low spatial frequency range under this parameter, and the energy of the high frequency component decays faster. When α increases to the classical Kolmogorov value $\alpha = 3.67$, the curve shows a wider decline interval, reflecting the process of energy transfer from a larger spatial scale to a smaller spatial scale in the inertial region. When α increases to 3.9, the curve rises as a whole, and the downward trend is gentler, which reflects that relatively more spectral energy is retained in the high spatial frequency range, and the relative influence of smaller spatial scale turbulence structure is enhanced. The characteristics of the three power spectrum models are shown in Table 3.

(2) The influence of atmospheric turbulence power spectrum on intensity scintillation.

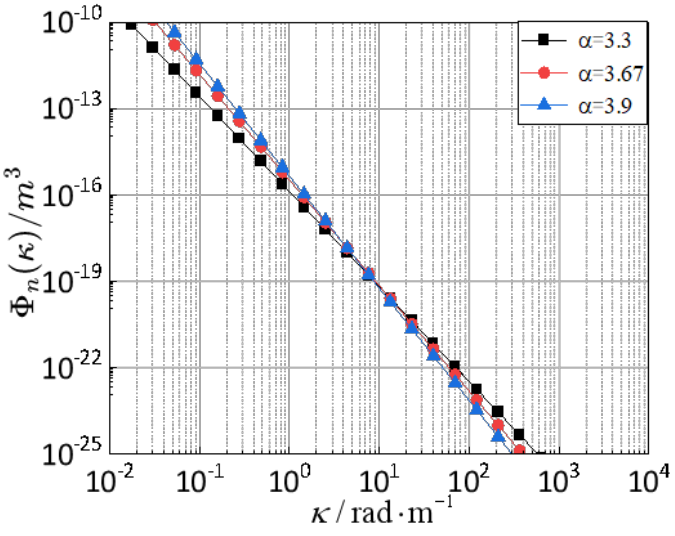
Light intensity scintillation is a random fluctuation of light intensity formed by the transformation of atmospheric refractive index fluctuation through light wave propagation and diffraction. It is sensitive to the refractive index fluctuation near the Fresnel scale and in the range of related high spatial frequency. The influence of non-Kolmogorov spectrum on intensity fluctuation depends on α. When α increases, due to the lack of inner scale truncation, there is a lack of spectral attenuation caused by viscous dissipation at the high spatial frequency end. The calculated scintillation index may deviate from the measured value at the high frequency end, and there are some limitations in the description of the high spatial frequency refractive index fluctuation and its scintillation contribution. Since the generalized von Kármán spectrum takes into account the inner scale l_0, it can describe the energy attenuation after the transition from the inertial region to the dissipative region at the high spatial frequency end, and it can effectively suppress the influence of the refractive index fluctuation of the minimum spatial scale on the light intensity scintillation. The intensity fluctuation will decrease with the increase of the inner scale, which is more in line with the actual laser atmospheric transmission law. The generalized modified atmospheric spectrum describes the high-frequency turbulence components in detail by introducing the spectral protrusions in the high spatial frequency region. The protrusion will change the energy distribution in the spatial frequency range related to the light intensity scintillation, thus affecting the light intensity fluctuation.

(3) The influence of atmospheric turbulence power spectrum on wavefront phase distortion

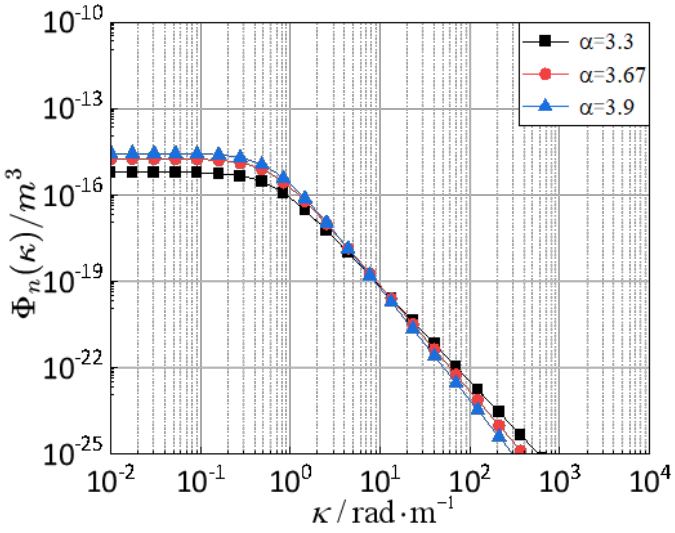
The wavefront phase perturbation caused by atmospheric turbulence includes the combined effects of refractive index fluctuations at different spatial scales. The large-scale refractive index fluctuations at low spatial frequencies have a significant effect on wavefront tilt and low-order phase distortion, while the smaller-scale refractive index fluctuations at higher spatial frequencies mainly affect local phase changes and higher-order wavefront distortion. Since the non-Kolmogorov spectrum ignores the outer scale L_0, it cannot describe the characteristics of the actual turbulence limited by the outer scale at the large-scale end, and will overestimate the energy of the low frequency part. The corresponding phase structure function continues to increase with the increase of the lateral spacing, which cannot reflect the large spacing saturation characteristics under the condition of limited outer scale. By introducing a low spatial frequency correction term corresponding to the



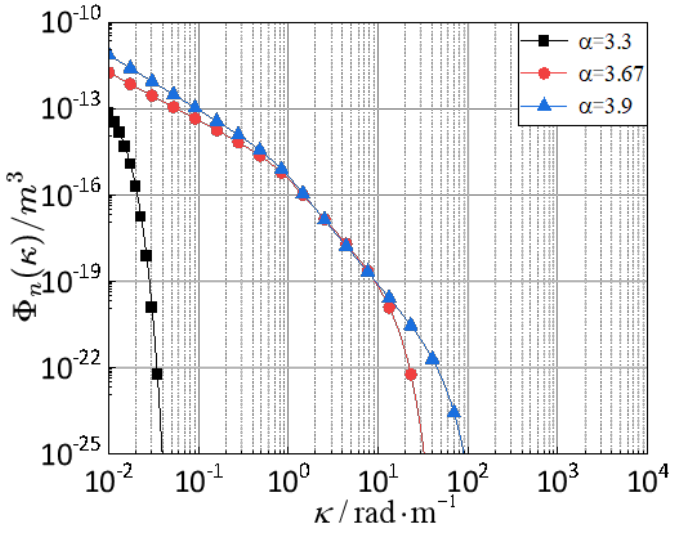
(a) Comparison of the three turbulence spectra



(b) Non-Kolmogorov spectrum



(c) Generalized von Kármán spectrum



(d) Generalized modified atmospheric spectrum

Figure 4. Characteristic curves of the three atmospheric turbulence power spectrum models.

Table 3. Characteristics of the three atmospheric turbulence power spectrum models.

Type	Power spectrum	Influence of inner scale	Influence of outer scale	Frequency response
Fundamental spectrum	Non-Kolmogorov spectrum	Not considered; no correction for the dissipation range	Not considered; no upper limit of energy	Full-band linear slope
Theoretical analysis spectrum	Generalized von Kármán spectrum	Considered; an exponential decay term characterizes dissipation	Considered; κ_0 limits the growth of low-frequency energy	Smooth truncation at both ends
Physical spectrum	Generalized modified atmospheric spectrum	Considered; describes the energy bump before the dissipation range	Considered; κ_0 ensures finite large-scale energy	High-frequency bump correction

outer scale L_0, the generalized von Kármán spectrum limits the spectral energy at the low spatial frequency and avoids the divergence of the ideal power-law spectrum at low wavenumbers. When the lateral spacing increases to be equivalent to or larger than the outer scale L_0, the phase structure function gradually

shows a saturation trend, which can describe the low spatial frequency phase disturbance more reasonably. Based on the generalized von Kármán spectrum, the generalized modified atmospheric power spectrum adds Hill protrusions near the dissipative region. In addition to maintaining the limitation of the finite outer scale on the low spatial frequency phase disturbance, it can also reflect the influence of the high spatial frequency energy change on the local phase fluctuation and the higher-order wavefront distortion. The Hill protrusion reflects the nonlinear accumulation of small-scale energy in front of the dissipative region, rather than the enhancement of large-scale phase distortion.

3 Analysis of light intensity scintillation characteristics of different atmospheric turbulence power spectrum models

3.1 Physical model of light intensity scintillation index

Light intensity scintillation is a turbulence effect caused by laser propagation in atmospheric turbulence. The random fluctuation of refractive index caused by atmospheric turbulence leads to wavefront phase distortion. As the propagation distance of the beam increases, the phase distortion gradually transforms into the fluctuation of the beam amplitude through the diffraction process. At the same time, atmospheric turbulence will directly attenuate the amplitude of the beam. The two effects on the amplitude jointly determine the instantaneous energy distribution at the receiving end and cause the fluctuation of the light intensity. From the perspective of physical mechanism, the fluctuation of light intensity is the result of the synergistic effect of various effects, and the visual expression of the fluctuation of light intensity is the scintillation of light intensity.

3.1.1 Method for solving light intensity scintillation index

In the study of atmospheric turbulence, the theory of Rytov approximation (Rytov theory) [4] establishes a theoretical model of light wave propagation in random turbulent media by first-order perturbation expansion of the logarithmic amplitude of electromagnetic waves, and can accurately describe the characteristics of light intensity scintillation under weak turbulence conditions. When the turbulence intensity increases, the first-order approximation of the Rytov theory will no longer be applicable. In order to overcome this limitation, the theory is usually extended to the medium-strong turbulence range by introducing a correction term of the logarithmic amplitude variance or reconstructing it in an exponential form. This method is called the extended Rytov theory [4]. The method of solving the intensity scintillation index is limited by the condition of atmospheric turbulence intensity, and the commonly used method is shown in Table 4.

3.1.2 Light intensity scintillation index model

Different approximations are used for different turbulence strengths. In the analysis of the intensity scintillation index, the weak-fluctuation approximation is applicable to weak-turbulence conditions, while the strong-fluctuation approximation is used to characterize intensity fluctuations under strong-turbulence conditions. The unified model is employed to analyze the variation of the intensity scintillation index across different turbulence strengths. The validity of each approximation depends on the turbulence strength, the power spectrum model and the propagation conditions. The extended Rytov theory with modulation process [4] is applied to analyze the nonlinear evolution process from medium turbulence to strong turbulence.

(1) Spatial filtering function

According to the extended Rytov theory, the spatial filtering function is used to screen the effective spatial frequency components involved in the formation of light intensity scintillation under medium to strong turbulence conditions, and the scale components with weak contribution to light intensity scintillation are suppressed. An effective generalized atmospheric turbulent refractive index power spectrum expression [4, 24] including large-scale and small-scale spatial filtering functions is

$$\begin{aligned}\Phi_{ne}(\kappa,\alpha) =&\Phi_n(\kappa,\alpha)G(\kappa,l_0,L_0,\alpha)\\ =&\Phi_n(\kappa,\alpha)[G_X(\kappa,l_0,L_0,\alpha)+G_Y(\kappa,\alpha)]\end{aligned} \tag{12}$$

where $G(\kappa,l_0,L_0,\alpha)$ is a spatial filter including a large-scale spatial filtering function $G_X(\kappa,l_0,L_0,\alpha)$ [4, 24] and a small-scale spatial filtering function $G_Y(\kappa,\alpha)$ [4, 24].

$G(\kappa,l_0,L_0,\alpha)$ is a linear spatial filter that allows only the spatial frequency of $\kappa < \kappa_X$ and $\kappa > \kappa_Y$ to pass through, filtering out the spatial frequency between κ_X and κ_Y that does not contribute to the intensity scintillation in the moderate to strong turbulence region. The correction factors related to the inner and outer scales are explicitly introduced

Table 4. Common methods for calculating the optical intensity scintillation index.

Turbulence condition	Method	Physical core and applicability
Weak turbulence (weak fluctuation)	Born approximation	The perturbation terms are assumed to be additive.
	Rytov approximation	The perturbation terms enter as a product, consistent with the lognormal amplitude distribution.
Moderate-to-strong turbulence (moderate-to-strong fluctuation)	Extended Huygens–Fresnel principle; extended Rytov theory	The extended Huygens–Fresnel principle yields the first- and second-order moments of the optical field from weak to strong turbulence; the extended Rytov theory extends weak-fluctuation results to moderate-to-strong fluctuations by accounting for multiple scattering and modulation by large-scale eddies.
Saturated strong turbulence (strong fluctuation)	Asymptotic theory	Assumes statistical independence of the optical field under very strong perturbations; used to derive the scintillation index in the saturation regime.

into the large-scale spatial filtering function [4, 24] to characterize the influence of the finite inner and outer scales on the large-scale intensity fluctuation components. The inner scale correction factor is no longer introduced into the small-scale spatial filtering function. The influence of the inner scale is reflected by the parameters such as the spatial coherence radius, the scattering disk and the corresponding cut-off spatial frequency. It is considered that κ_Y contains the inner scale effect. The expressions of large-scale and small-scale spatial filtering functions [4, 24] are

$$G_X(\kappa, l_0, L_0, \alpha) = f(\kappa, l_0, \alpha) g(\kappa L_0) \exp(-\frac{\kappa^2}{\kappa_X^2}) \quad \kappa < \kappa_X \tag{13}$$

$$G_Y(\kappa, \alpha) = \frac{\kappa^\alpha}{(\kappa^2 + \kappa_Y^2)^{\alpha/2}} \quad \kappa > \kappa_Y \tag{14}$$

Among them, $f(\kappa, l_0, \alpha)$ and $g(\kappa L_0)$ are the factors related to the inner scale and the outer scale, respectively [4, 24]. The inner scale can affect the filtering characteristics by affecting the spatial coherence radius ρ_0 and the scattering disk $L/k\rho_0$. κ_X is the cutoff spatial frequency of the large-scale light intensity fluctuation component, which is dominated by refraction [4], and κ_Y is the cutoff spatial frequency of the small-scale light intensity fluctuation component, which is dominated by diffraction [4]. The outer scale L_0 and the inner scale l_0 represent the physical scale boundary of the low and high spatial frequency ends of the turbulent power spectrum, respectively, while κ_X and κ_Y are the effective spatial frequency cutoff parameters determined by the propagation scale and the turbulence intensity in the extended Rytov model, which are used to limit the frequency range of large-scale refractive and small-scale diffractive intensity fluctuations, respectively. The physical meanings of the two are different and do not correspond to L_0 and l_0 one by one [4]. In the case of zero inner scale and ignoring the influence of outer scale, we choose $f(\kappa, l_0, \alpha) = g(\kappa L_0) = 1$, and the large-scale and small-scale spatial filtering functions in Eqs. (13) and (14) [4, 24] become

$$G_X(\kappa, \alpha) = \exp(-\frac{\kappa^2}{\kappa_X^2}) \quad \kappa < \kappa_X \tag{15}$$

$$G_Y(\kappa, \alpha) = \frac{\kappa^\alpha}{(\kappa^2 + \kappa_Y^2)^{\alpha/2}} \quad \kappa > \kappa_Y \tag{16}$$

Under different scale models, the factors of inner scale and outer scale are shown in Table 5.

Table 5. Inner-scale and outer-scale factors.

Model	Condition	Inner-scale factor $f(\kappa, l_0, \alpha)$	Outer-scale factor $g(\kappa L_0)$
Zero inner scale	Inner and outer scales ignored	1	1
Non-zero inner scale	Inner scale considered	$\exp(-\kappa^2/\kappa_m^2)$	1
Inner and outer scales	Inner and outer scales considered	$\exp(-\kappa^2/\kappa_m^2)$	$1 - \exp(-\kappa^2/\kappa_0^2)$

Under weak-fluctuation conditions, the turbulence components of different spatial scales are involved in the effect of light wave propagation, so that

$G_X(\kappa,\alpha) + G_Y(\kappa,\alpha) \approx 1$, the effective spectrum $\Phi_{ne}(\kappa,\alpha)$ is the same as the generalized power spectrum $\Phi_n(\kappa,\alpha)$. Under the condition of medium to strong light intensity fluctuation, the contribution of turbulence components corresponding to some spatial scales to scintillation is suppressed by propagation coherence and multiple scattering, $\Phi_{ne}(\kappa,\alpha) \neq \Phi_n(\kappa,\alpha)$. Under strong intensity fluctuations, the cutoff spatial frequencies corresponding to the large scale κ_X and small scale κ_Y is used to define the spatial frequency range that has an effective influence on the intensity scintillation [3–6]. When the light wave enters the atmospheric turbulence and transmits at any distance L, it corresponds to the effective scattering disk scale L/kl_X of the large-scale component and the effective scale upper limit l_Y of the small-scale component, respectively. The relationship between these propagation scales and the corresponding cut-off frequencies [4, 24] is

$$\frac{L}{kl_X} = \frac{1}{\kappa_X} \cong \begin{cases} \sqrt{\frac{L}{k}} & \tilde{\sigma}_R^2 \ll 1 \\ \frac{L}{k\rho_0} & \tilde{\sigma}_R^2 \gg 1 \end{cases} \tag{17}$$

$$l_Y = \frac{1}{\kappa_Y} \cong \begin{cases} \sqrt{\frac{L}{k}} & \tilde{\sigma}_R^2 \ll 1 \\ \rho_0 & \tilde{\sigma}_R^2 \gg 1 \end{cases} \tag{18}$$

The general expressions of the cut-off spatial frequencies κ_X and κ_Y are

$$\frac{1}{\kappa_X^2} = c_1(\alpha)\frac{L}{k} + c_2(\alpha)(\frac{L}{k\rho_0})^2 \tag{19}$$

$$\kappa_Y^2 = c_3(\alpha)\frac{k}{L} + c_4(\alpha)\frac{1}{\rho_0^2} \tag{20}$$

where $c_1(\alpha), c_2(\alpha), c_3(\alpha), c_4(\alpha)$ are the scaling constants of medium to strong generalized power spectrum turbulence.

The large-scale spatial filtering function $G_X(\kappa,\alpha)$ retains the spatial scale larger than the lower limit of its effective scale to characterize the large-scale light intensity fluctuation component dominated by refraction [4]. The small-scale spatial filtering function of $G_Y(\kappa,\alpha)$ retains the spatial scale less than the upper limit of its effective scale l_Y, to characterize the small-scale light intensity fluctuation component dominated by diffraction [4]. The large-scale and small-scale boundaries here are determined by the propagation conditions and the corresponding cut-off spatial frequencies [3–6]. The selection of large-scale and small-scale spatial filtering functions for different light waves under different scale models is shown in Table 6.

where $\kappa_{X_0}^2 = \kappa_X^2\kappa_0^2/(\kappa_X^2 + \kappa_0^2)$ and $\kappa_m = c(\alpha)/l_0$.

(2) The model of light intensity scintillation index

When studying the intensity fluctuation caused by atmospheric turbulence, the received light intensity is a modulation process. The scintillation index model decomposes the normalized light intensity into a statistically independent product of the large-scale light intensity fluctuation component and the small-scale light intensity fluctuation component, which is used to characterize the light intensity modulation formed by turbulence at different effective spatial scales. The large scale and small scale here belong to the statistical stratification of light intensity fluctuation, which is not equivalent to the outer scale and inner scale of turbulence power spectrum. According to the modulation process, under the assumption that X and Y are statistically independent, the normalized intensity expression [4] is

$$\hat{I} = \frac{I}{\langle I \rangle} = XY \tag{21}$$

Among them, X is the modulation component of large-scale light intensity [4], which mainly reflects the refraction effect of large spatial scale turbulence structure. Y characterizes the small-scale light intensity modulation component [4], which mainly reflects the diffraction effect of the smaller spatial scale turbulence structure. $\langle I \rangle$ is the average light intensity, $\langle I \rangle = 1$, the expression of the second moment of normalized light intensity [4] is

$$\left\langle \hat{I}^2 \right\rangle = \frac{\langle I^2 \rangle}{\langle I \rangle^2} = \left\langle (XY)^2 \right\rangle = \left\langle X^2 \right\rangle \left\langle Y^2 \right\rangle \tag{22}$$

In order to characterize the intensity fluctuation of light intensity, the normalized intensity fluctuation variance is also known as the intensity scintillation index. The intensity scintillation index is a dimensionless physical quantity, and its expression [4] is

$$\begin{aligned} \sigma_I^2 &= \frac{\langle I^2 \rangle}{\langle I \rangle^2} - 1 \\ &= \left\langle X^2 \right\rangle \left\langle Y^2 \right\rangle - 1 \\ &= (1+\sigma_X^2)(1+\sigma_Y^2) - 1 \\ &= \sigma_X^2 + \sigma_Y^2 + \sigma_X^2\sigma_Y^2 \end{aligned} \tag{23}$$

Table 6. Large-scale and small-scale spatial filtering functions.

Wave	Scale	Zero inner scale	Non-zero inner scale	Inner and outer scales
Plane	Large	$\exp\left(-\frac{\kappa^2}{\kappa_X^2}\right)$	$\exp\left[-\left(\frac{\kappa^2}{\kappa_m^2}+\frac{\kappa^2}{\kappa_X^2}\right)\right]$	$\exp\left(-\frac{\kappa^2}{\kappa_m^2}\right)\left[\exp\left(-\frac{\kappa^2}{\kappa_X^2}\right)-\exp\left(-\frac{\kappa^2}{\kappa_{X_0}^2}\right)\right]$
	Small	$\frac{\kappa^\alpha}{(\kappa^2+\kappa_Y^2)^{\alpha/2}}$	$\frac{\kappa^\alpha}{(\kappa^2+\kappa_Y^2)^{\alpha/2}}$	$\frac{\kappa^\alpha}{(\kappa^2+\kappa_Y^2)^{\alpha/2}}$
Spherical	Large	$\exp\left(-\frac{\kappa^2}{\kappa_X^2}\right)$	$\exp\left[-\left(\frac{\kappa^2}{\kappa_m^2}+\frac{\kappa^2}{\kappa_X^2}\right)\right]$	$\exp\left(-\frac{\kappa^2}{\kappa_m^2}\right)\left[\exp\left(-\frac{\kappa^2}{\kappa_X^2}\right)-\exp\left(-\frac{\kappa^2}{\kappa_{X_0}^2}\right)\right]$
	Small	$\frac{\kappa^\alpha}{(\kappa^2+\kappa_Y^2)^{\alpha/2}}$	$\frac{\kappa^\alpha}{(\kappa^2+\kappa_Y^2)^{\alpha/2}}$	$\frac{\kappa^\alpha}{(\kappa^2+\kappa_Y^2)^{\alpha/2}}$

Large-scale filters are denoted G_X and small-scale filters G_Y.

where σ_X^2 and σ_Y^2 are the normalized variances of X and Y, respectively, $\langle X\rangle = \langle Y\rangle = 1$.

There is a mapping relationship between the logarithmic amplitude of the light wave and the light intensity $\chi = (1/2)\ln(I/A_0^2), A_0 = |U_0(r,L)|$. According to the Rytov theory [4], when $\sigma_\chi^2 \ll 1$, $\sigma_I^2 = \exp(4\sigma_\chi^2) - 1$, the relation between logarithmic scintillation index and logarithmic amplitude is $\sigma_{\ln I}^2 = 4\sigma_\chi^2$. The relation between the scintillation index and the log-intensity variance [4] is

$$\sigma_I^2 = \exp(\sigma_{\ln I}^2) - 1 \quad \sigma_\chi^2 \ll 1 \tag{24}$$

The expression of the scintillation index corresponding to the large-scale and small-scale light intensity fluctuation components [4] is

$$\sigma_X^2 = \exp(\sigma_{\ln X}^2) - 1 \quad \sigma_Y^2 = \exp(\sigma_{\ln Y}^2) - 1 \tag{25}$$

where $\sigma_{\ln X}^2$ and $\sigma_{\ln Y}^2$ are called the variances of large-scale and small-scale logarithmic light intensity fluctuations [4], respectively, and they are independent of each other.

Substituting Eq. (25) into Eq. (23), the expression of the relationship between the scintillation index of light intensity and the variance of large-scale and small-scale logarithmic light intensity fluctuation [4] is

$$\sigma_I^2 = \exp(\sigma_{\ln X}^2 + \sigma_{\ln Y}^2) - 1 \tag{26}$$

Combining Eq.(24) and Eq. (26), the expression of light intensity scintillation index [4] is

$$\sigma_I^2 = \exp(\sigma_{\ln I}^2) - 1 = \exp(\sigma_{\ln X}^2 + \sigma_{\ln Y}^2) - 1 \tag{27}$$

(3) Light intensity scintillation index model under weak turbulence condition

In the weak turbulence region, the scintillation index model of light intensity directly reflects the spatial integral characteristics of the light wave front and the refractive index power spectrum of atmospheric turbulence.

(a) Light intensity scintillation index model of plane wave

The intensity scintillation index model of plane wave reflects the average fluctuation of long-distance transmission of laser in the atmosphere, and its expression [24, 25] is

$$\sigma_{L,PL}^2(\alpha) = 8\pi^2 k^2 L \int_0^1 \int_0^\infty \kappa\Phi_n(\alpha,\kappa)[1-\cos(\frac{L\kappa^2}{k}\xi)]d\kappa d\xi \quad \tilde{\sigma}_R^2 < 1 \tag{28}$$

(b) Scintillation index model of spherical wave intensity

The light intensity scintillation index model of spherical wave introduces the path weighting factor $\xi(1-\xi)$, which reflects the unique geometric expansion effect of point source divergence. Its expression [24] is

$$\sigma_{L,SP}^2(\alpha) = 8\pi^2 k^2 L \int_0^1 \int_0^\infty \kappa\Phi_n(\alpha,\kappa)\left\{1-\cos\left[\frac{L\kappa^2}{k}\xi(1-\xi)\right]\right\} d\kappa d\xi \quad \tilde{\sigma}_R^2 < 1 \tag{29}$$

(4) Scintillation index model of light intensity under saturated strong turbulence condition

When the propagation distance of light increases or the turbulence intensity increases, the intensity fluctuation no longer continues to increase, and the phenomenon of light intensity saturation occurs. This is because the loss of spatial coherence caused by strong turbulence

inhibits the growth of fluctuations. The general model expression of scintillation index of intensity fluctuation and scintillation index of plane wave and spherical wave [8, 26, 27] is

$$\sigma_{IS}^2(\alpha) = 1 + 32\pi^2 k^2 L \int_0^1 \int_0^\infty \kappa \Phi_n(\kappa,\alpha) \sin^2\left[\frac{L\kappa^2\xi}{2k}\right] \times \exp\left\{-\int_0^1 D_S\left[\frac{L\kappa}{k} w(\tau,\xi),\alpha\right] d\tau\right\} d\kappa d\xi \quad \tilde{\sigma}_R^2 \gg 1 \tag{30}$$

Approximate $\sin^2\left(\frac{L\kappa^2\xi}{2k}\right) \cong \frac{L^2\kappa^4\xi^2}{4k^2}$ by sine function, (30) becomes

$$\sigma_{IS}^2(\alpha) = 1 + 8\pi^2 L^3 \int_0^1 \int_0^\infty \xi^2 \kappa^5 \Phi_n(\kappa,\alpha) \times \exp\{-\int_0^1 D_S[\frac{L\kappa}{k} w(\tau,\xi),\alpha] d\tau\} d\kappa d\xi \quad \tilde{\sigma}_R^2 \gg 1 \tag{31}$$

where τ is the normalized distance variable. The exponential function acts as a low-pass spatial filter formed by the phase structure function $D_S(\rho,\alpha)$ of the plane wave. The expression [8] is

$$D_{S,PL}(\rho,\alpha) = \pi^2 k^2 L \rho^2 \int_0^1 \int_0^\infty \kappa^3 \Phi_n(\kappa,\alpha)[1+\cos(\frac{L\kappa^2\xi}{k})] d\kappa d\xi \tag{32}$$

The expression of function $w(\tau,\varepsilon)$ is

$$w(\tau,\varepsilon) = \begin{cases} \tau(1-\bar{\Theta}\varepsilon) & \tau < \varepsilon \\ \varepsilon(1-\bar{\Theta}\tau) & \tau > \varepsilon \end{cases} \tag{33}$$

where $\bar{\Theta} = 1 - \Theta$, the refraction parameter Θ is the receiving plane beam parameter, the plane wave $\Theta = 1$, the spherical wave $\Theta = 0$.

(5) The intensity scintillation index model under arbitrary turbulence intensity from weak to strong

A set of universal models of intensity scintillation index with spatial filtering function adapted to arbitrary turbulence intensity from weak to strong is established.

(a) Light intensity scintillation index model of plane wave

The universal model of the intensity scintillation index of plane waves is to integrate the spatial frequency components corresponding to large-scale and small-scale intensity fluctuations by introducing a filter function. According to Eq.(27), the expression of the intensity scintillation index model of plane waves [28] is

$$\sigma_{I,PL}^2 = \exp[\sigma_{\ln X,PL}^2(\alpha) + \sigma_{\ln Y,PL}^2(\alpha)] - 1 \tag{34}$$

where $\sigma_{\ln X,PL}^2$ and $\sigma_{\ln Y,PL}^2$ are the large-scale and small-scale logarithmic intensity fluctuation variances of plane waves, respectively, and their expressions are

$$\sigma_{\ln X,PL}^2(\alpha) = 8\pi^2 k^2 \int_0^L \int_0^\infty \kappa \Phi_n(\kappa,\alpha) G_X(\kappa,\alpha) \times \left[1 - \cos\left(\kappa^2 z/k\right)\right] d\kappa\, dz \tag{35}$$

$$\sigma_{\ln Y,PL}^2(\alpha) = 8\pi^2 k^2 \int_0^L \int_0^\infty \kappa \Phi_n(\kappa,\alpha) G_Y(\kappa,\alpha) \times \left[1 - \cos\left(\kappa^2 z/k\right)\right] d\kappa\, dz \tag{36}$$

(b) Spherical wave intensity scintillation index

The universal model of intensity scintillation index of spherical wave adopts filtering mechanism and considers the influence of wavefront curvature of spherical wave. According to formula (27), the expression of intensity scintillation index model of spherical wave is

$$\sigma_{I,SP}^2 = \exp[\sigma_{\ln X,SP}^2(\alpha) + \sigma_{\ln Y,SP}^2(\alpha)] - 1 \tag{37}$$

where $\sigma_{\ln X,SP}^2$ and $\sigma_{\ln Y,SP}^2$ are the large-scale and small-scale logarithmic intensity fluctuation variances of spherical waves, respectively, and their expressions are

$$\sigma_{\ln X,SP}^2(\alpha) = 8\pi^2 k^2 \int_0^L \int_0^\infty \kappa \Phi_n(\alpha,\kappa) G_X(\kappa,\alpha) \times \left\{1 - \cos\left[\frac{\kappa^2}{k} z\left(1 - \frac{z}{L}\right)\right]\right\} d\kappa\, dz \tag{38}$$

$$\sigma_{\ln Y,SP}^2(\alpha) = 8\pi^2 k^2 \int_0^L \int_0^\infty \kappa \Phi_n(\alpha,\kappa) G_Y(\kappa,\alpha) \times \left\{1 - \cos\left[\frac{\kappa^2}{k} z\left(1 - \frac{z}{L}\right)\right]\right\} d\kappa\, dz \tag{39}$$

When the inner and outer scale effects are ignored, $f(\kappa, l_0, \alpha) = g(\kappa L_0) = 1$, the plane wave / spherical wave model can be reduced to the classical Rytov form.

(6) The Rytov variance of non-Kolmogorov spectrum

Under the condition of Kolmogorov spectrum weak turbulence, the scintillation index σ_R^2 of plane wave

light intensity is called Rytov variance, and its expression [9] is

$$\sigma_{I,PL}^2(L) = 1.23C_n^2k^{7/6}L^{11/6} = \sigma_R^2 \tag{40}$$

Under the condition of non-Kolmogorov spectral weak turbulence, the intensity scintillation index $\tilde{\sigma}_R^2$ of the plane wave is called the generalized Rytov variance, and its expression is

$$\tilde{\sigma}_R^2 = -8\pi^2A(\alpha)\Gamma(1-\alpha/2)\alpha^{-1}\sin(\alpha\pi/4)\tilde{C}_n^2k^{3-\alpha/2}L^{\alpha/2} \tag{41}$$

Under the condition of power spectrum without inner and outer scales, the generalized Rytov variance is used to distinguish the strong and weak turbulence. Under the condition of the power spectrum containing inner and outer scales, strong and weak turbulence are distinguished by the ratio $L/(k\rho_{PL}^2)$, i.e., the size of the effective scattering disk relative to the spatial coherence radius. Different strength fluctuation conditions are shown in Table 7.

Table 7. Optical intensity fluctuation conditions.

Type of power spectrum	Weak fluctuation	Strong fluctuation
Without inner and outer scales	$\tilde{\sigma}_R^2 < 1$	$\tilde{\sigma}_R^2 \gg 1$
With inner and outer scales	$L/[k\rho_{PL}^2(\alpha)] \ll 1$	$L/[k\rho_{PL}^2(\alpha)] \gg 1$

where $\rho_{PL}(\alpha)$ represents the spatial coherence radius of the plane wave of the non-Kolmogorov spectrum.

3.2 The intensity scintillation index of plane wave

The light intensity scintillation effect caused by atmospheric turbulence is the spatial effect of random fluctuation accumulation of refractive index. The intensity scintillation index of plane wave under different generalized spectral models and different atmospheric turbulence intensities is analyzed.

3.2.1 Plane wave intensity scintillation index under weak turbulence condition

Under the condition of weak turbulence, the scintillation is caused by the Fresnel-scale turbulent vortex.

(1) The intensity scintillation index of plane wave in non-Kolmogorov spectrum

The non-Kolmogorov spectrum is the benchmark model, which reflects the ideal state of energy cascade under power-law distribution. Substituting the non-Kolmogorov spectrum (6) into (28), using the gamma function formula $\Gamma(1-\alpha/2) = -(\alpha/2)\Gamma(-\alpha/2)$, the plane wave intensity scintillation index [29] becomes

$$\sigma_{I,PL}^2(\alpha) = \beta_1(\alpha)\cdot A(\alpha)\tilde{C}_n^2\pi^2k^{3-\alpha/2}L^{\alpha/2} \tag{42}$$

where $\sigma_{I,PL}^2(\alpha) = \tilde{\sigma}_R^2 = \sigma_{R,PL}^2(\alpha)$, $\beta_1(\alpha) = 4\Gamma(-\alpha/2)\cdot\sin(\pi\alpha/4)$.

(2) Intensity scintillation index of plane wave in generalized von Kármán spectrum

The generalized von Kármán spectrum introduces the correction of the outer scale L_0 and the inner scale l_0, which physically reflects the energy dissipation and generation characteristics of atmospheric turbulence at both ends of the inertial region. Substituting the generalized von Kármán spectrum Eq. (7) into Eq.(28), the expression of the intensity scintillation index of the plane wave [29] is

$$\sigma_{I,PLvk}^2(\alpha) = \frac{\tilde{\sigma}_R^2}{\sin(\alpha\pi/4)}\left[\left(1+\frac{1}{Q_m^2(\alpha)}\right)^{\alpha/4}\sin\left(\frac{\alpha}{2}\tan^{-1}Q_m(\alpha)\right) - \frac{\alpha}{2}Q_m^{1-\frac{\alpha}{2}}(\alpha)\right] \tag{43}$$

where $Q_m(\alpha) = [c(\alpha)]^2L/\left(kl_0^2\right)$ is the normalized scale parameter.

(3) Intensity scintillation index of plane wave in generalized modified atmospheric spectrum

The refractive index fluctuation bulge phenomenon caused by the inner scale is reflected in the generalized modified atmospheric spectrum, which can describe the light intensity fluctuation in the high frequency region. Substituting the generalized modified atmospheric spectrum (8) into Equation (28), the expression of the intensity scintillation index of the plane wave [29] is

$$\sigma_{I,PLhill}^2 = \frac{\tilde{\sigma}_R^2}{\sin(\alpha\pi/4)}\left\{\left\{1+\frac{1}{[Q_l(\alpha)]^2}\right\}^{\alpha/4}\left\{\sin\left[\frac{\alpha}{2}\tan^{-1}Q_l(\alpha)\right]\right.\right.$$
$$+\frac{a_1\alpha\Gamma(3/2-\alpha/2)}{(\alpha-1)\Gamma(1-\alpha/2)}\left\{1+[Q_l(\alpha)]^2\right\}^{-1/4}\sin\left[\frac{\alpha-1}{2}\tan^{-1}Q_l(\alpha)\right]$$
$$\left.-\frac{b_1\alpha\Gamma(1-\alpha/2+\beta/2)}{(\alpha-\beta)\Gamma(1-\alpha/2)}\left\{1+[Q_l(\alpha)]^2\right\}^{-\beta/4}\sin\left[\frac{\alpha-\beta}{2}\tan^{-1}Q_l(\alpha)\right]\right\}$$
$$\left.-\left[\frac{\alpha}{2}+\frac{a_1\alpha\Gamma(3/2-\alpha/2)}{2\Gamma(1-\alpha/2)}-\frac{b_1\alpha\Gamma(1-\alpha/2+\beta/2)}{2\Gamma(1-\alpha/2)}\right][Q_l(\alpha)]^{1-\alpha/2}\right\} \tag{44}$$

where $Q_l(\alpha) = [c_h(\alpha)]^2 L/\left(kl_0^2\right)$, $\kappa_l = c_h(\alpha)/l_0$ and $\kappa_0 = 2\pi/L_0$. The expression of $c_h(\alpha)$ is

$$c_h(\alpha) = \left\{\pi A(\alpha)\left[\Gamma\left(\frac{3-\alpha}{2}\right)\left(\frac{3-\alpha}{3}\right)+a_1\Gamma\left(2-\frac{\alpha}{2}\right)\left(\frac{4-\alpha}{3}\right)\right.\right.$$
$$\left.\left.-b_1\Gamma\left(\frac{3-\alpha+\beta}{2}\right)\left(\frac{3-\alpha+\beta}{3}\right)\right]\right\}^{\frac{1}{\alpha-5}} \tag{45}$$

3.2.2 *Plane wave intensity scintillation index under saturated strong turbulence condition*

With the increase of beam propagation distance or atmospheric turbulence intensity, the spatial coherence scale of the light field gradually decreases, and the effective contribution of the refractive index fluctuation of different spatial scales to the light intensity scintillation is redistributed, so that the growth of the light intensity scintillation is suppressed and gradually enters the saturation region.

(1) The intensity scintillation index of plane wave in non-Kolmogorov spectrum

In the saturation region, the phase structure function D_s is the key to the evolution of the intensity scintillation index, which reflects the inhibitory effect of the spatial coherence radius ρ_0 on the intensity scintillation. Assuming that the inner scale of atmospheric turbulence is less than the spatial coherence radius ρ_0 of plane wave, the expression of phase structure function under non-Kolmogorov spectrum [8] is

$$D_{S,PL}(\rho,\alpha) = 4\pi^2 A(\alpha)\tilde{C}_n^2 k^2 L\cdot\left[-\frac{\Gamma(1-\alpha/2)}{\alpha/2}\cdot\left(\frac{\rho^2}{4}\right)^{\frac{\alpha}{2}-1}\right] \tag{46}$$

Substituting Eq. (46) into the integral part of the exponential term in Eq. (31), the expression is obtained as follows:

$$\int_0^1 D_{S,PL}\left[\frac{L\kappa}{k}w(\tau,\varepsilon),\alpha\right]d\tau = -\frac{\pi^2}{1.23}\cdot 4^{2-\frac{\alpha}{2}}\cdot\frac{\Gamma(1-\alpha/2)}{\Gamma(\alpha/2)}\cdot\frac{A(\alpha)}{R(\alpha)}$$
$$\times\tilde{\sigma}_R^2\left(\frac{L}{k}\right)^{\frac{\alpha}{2}-1}\kappa^{\alpha-2}\xi^{\alpha-2}\left(1+\frac{2-\alpha}{\alpha-1}\xi\right) \tag{47}$$

Substituting Eq. (6) and Eq. (47) into Eq.(31), the expression of the scintillation index of plane wave intensity is obtained as follows:

$$\sigma_{IS,PL}^2(\alpha) = 1 + r_1(\alpha)\cdot I_1(\alpha)\cdot\sigma_{R(PL)}^{\frac{4(\alpha-4)}{\alpha-2}}(\alpha) \tag{48}$$

The expressions of $r_1(\alpha)$ and $I_1(\alpha)$ are

$$r_1(\alpha) = \frac{1}{\alpha-2}\cdot[2]^{\frac{(3-\alpha)(\alpha-10)}{\alpha-2}}\cdot\left[-\frac{\Gamma(1-\alpha/2)}{\Gamma(\alpha/2)}\right]^{\frac{\alpha-6}{\alpha-2}}\cdot\Gamma\left(\frac{6-\alpha}{\alpha-2}\right)\cdot[\beta_1(\alpha)]^{\frac{8-2\alpha}{\alpha-2}}$$
$$I_1(\alpha) = \frac{1}{\alpha-3}{}_2F_1\left(\frac{6-\alpha}{\alpha-2},\alpha-3;\alpha-2;\frac{\alpha-2}{\alpha-1}\right)$$
$${}_2F_1(A,B;C;Z) = \frac{\Gamma(C)}{\Gamma(B)\cdot\Gamma(C-B)}\int_0^1 t^{B-1}\cdot(1-t)^{C-B-1}\cdot(1-tZ)^{-A}dt \tag{49}$$

(2) Intensity scintillation index of plane wave in generalized von Kármán spectrum

Under strong turbulence, the inner scale l_0 shows a high-frequency truncation effect on small-scale fluctuations. Under the geometric optics approximation, the intensity scintillation index under strong fluctuation conditions is therefore limited by the small-scale components of the light field. Assuming that the inner scale of atmospheric turbulence is smaller than the spatial coherence radius of plane wave, the expression of phase structure function under the generalized von Kármán spectrum [8] is

$$D_{S,PL}(\rho,\alpha) = 0.5\Xi A(\alpha)\pi^2\Gamma(2-\alpha/2)\tilde{C}_n^2 k^2 L\kappa_m^{4-\alpha}\rho^2 \quad \rho \ll l_0 \tag{50}$$

where $Q_m(\alpha) = [c(\alpha)]^2 L/\left(kl_0^2\right)$, the Ξ expression is

$$\Xi = 1+\frac{2\sin\left[\frac{\alpha-2}{2}\tan^{-1}Q_m(\alpha)\right]}{(\alpha-2)\left[Q_m(\alpha)\right]^{2-\alpha/2}}\left\{1+\frac{1}{[Q_m(\alpha)]^2}\right\}^{\frac{\alpha-2}{4}} \tag{51}$$

Substituting Eq.(50) into the integral part of the exponential term in Eq. (31), the expression is obtained as follows:

$$\int_0^1 D_{S,PL}\left[\frac{L\kappa}{k}w(\tau,\xi),\alpha\right]d\tau = -\frac{\alpha\Gamma(2-\alpha/2)\,\Xi}{16\Gamma\left(1-\frac{\alpha}{2}\right)\sin\left(\frac{\pi\alpha}{4}\right)} \times \tilde{\sigma}_R^2\left[Q_m(\alpha)\right]^{2-\frac{\alpha}{2}}\left(\frac{L\kappa^2}{k}\right)\xi^2\left(1-\frac{2}{3}\xi\right) \tag{52}$$

By using the geometric optics approximation $L\kappa^2/k \ll 1$, the trigonometric function term in (31) is expressed as

$$\sin^2\left(\frac{L\kappa^2\xi}{2k}\right) \cong \frac{L^2\kappa^4\xi^2}{4k^2} \tag{53}$$

Substituting Eq.(7) and Eq.(53) into Eq.(31), the expression of the scintillation index of plane wave intensity [8] is

$$\sigma_{IS,PL}^2 \approx 1 + \frac{C_{PL}(\alpha)}{\left\{\tilde{\sigma}_R^2\left[Q_m(\alpha)\right]^{3-\alpha/2}\right\}^{2-\alpha/2}} - \frac{\alpha\Gamma(2-\alpha/2)\tilde{\sigma}_R^2\left[Q_m(\alpha)\right]^{2-\alpha/2}}{16\Gamma\left(1-\alpha/2\right)\sin(\alpha\pi/4)} \gg 1 \tag{54}$$

The expression of $C_{PL}\left(\alpha\right)$ is

$$C_{PL}(\alpha) = \frac{-\alpha\Gamma(3-\alpha/2)}{2\Gamma(1-\alpha/2)\sin(\alpha\pi/4)} \times \int_0^1 \frac{\xi^2}{\left\{\tilde{\sigma}_R^2\left[Q_m(\alpha)\right]^{\alpha/2-3} - \frac{\alpha\Gamma(2-\alpha/2)\Xi}{16\Gamma(1-\alpha/2)\sin(\alpha\pi/4)}\xi^2\left(1-\frac{2}{3}\xi\right)\right\}^{3-\alpha/2}}d\xi \tag{55}$$

(3) Plane wave intensity scintillation index under generalized modified atmospheric spectrum

Assuming that the inner scale of atmospheric turbulence is smaller than the spatial coherence radius of plane wave, the expression of phase structure function under the condition of generalized modified atmospheric spectrum [8] is

$$D_{S,PL}(\rho,\alpha) = 0.5\pi^2 A(\alpha)\Xi(\alpha)\tilde{C}_n^2 k^2 L\kappa_l^{4-\alpha}\rho^2 \tag{56}$$

The expressions of $\Xi(\alpha)$ and $\Delta(\alpha,u)$ are

$$\Xi(\alpha) = \left[\Gamma\left(\frac{4-\alpha}{2}\right)\Delta(\alpha,0) + a_1\Gamma\left(\frac{5-\alpha}{2}\right)\Delta(\alpha,1) - b_1\Gamma\left(\frac{4-\alpha+\beta}{2}\right)\Delta(\alpha,\beta)\right]$$
$$\Delta(\alpha,u) = 1 + \frac{2\sin\left[\frac{\alpha-u-2}{2}\tan^{-1}Q_l(\alpha)\right]}{(\alpha-u-2)[Q_l(\alpha)]^{2-(\alpha-u)/2}\left[1+\frac{1}{Q_l(\alpha)^2}\right]^{\frac{\alpha-u}{4}}} \tag{57}$$

Substituting Eq.(56) into the integral part of the exponential term in Eq. (31), the expression is obtained as follows:

$$\int_0^1 D_{S,PL}\left[\frac{L\kappa}{k}w(\tau,\xi)\right]d\tau = -\frac{\alpha\,\Xi(\alpha)}{16\Gamma(1-\alpha/2)\sin(\alpha\pi/4)} \times \tilde{\sigma}_R^2\left[Q_l(\alpha)\right]^{2-\frac{\alpha}{2}}\left(\frac{L\kappa^2}{k}\right)\xi^2\left(1-\frac{2\xi}{3}\right) \tag{58}$$

Substituting Eq. (8), Eq.(53) and Eq. (58) into Eq. (31), the expression of the scintillation index of plane wave intensity is

$$\sigma_{IS,PL}^2(\alpha) = 1 + \frac{C_{PL}(\alpha)}{\{\tilde{\sigma}_R^2[Q_l(\alpha)]^{3-\alpha/2}\}^{2-\alpha/2}} \tag{59}$$

The expressions of $C_{PL}\left(\alpha\right)$, A_{PL1}, A_{PL2} and A_{PL3} are

$$C_{PL}(\alpha) = -\frac{\alpha\Gamma(3-\alpha/2)}{2\Gamma(1-\alpha/2)\sin(\alpha\pi/4)}\left\{\tilde{\sigma}_R^2\left[Q_l(\alpha)\right]^{3-\frac{\alpha}{2}}\right\}^{3-\frac{\alpha}{2}} \times \left[A_{PL1} + \frac{a_1\Gamma(7/2-\alpha/2)}{\Gamma(3-\alpha/2)} \times A_{PL2} - \frac{b_1\Gamma(3-\alpha/2+\beta/2)}{\Gamma(3-\alpha/2)} \times A_{PL3}\right]$$
$$A_{PL1} = \int_0^1 \frac{\xi^2}{\left\{1-\xi^2(1-2\xi/3)\left[\alpha\Xi(\alpha)\tilde{\sigma}_R^2\left[Q_l(\alpha)\right]^{3-\frac{\alpha}{2}}\right]/\left[16\Gamma(1-\alpha/2)\sin(\alpha\pi/4)\right]\right\}^{\frac{6-\alpha}{2}}}$$
$$A_{PL2} = \int_0^1 \frac{\xi^2}{\left\{1-\xi^2(1-2\xi/3)\left[\alpha\Xi(\alpha)\tilde{\sigma}_R^2\left[Q_l(\alpha)\right]^{3-\frac{\alpha}{2}}\right]/\left[16\Gamma(1-\alpha/2)\sin(\alpha\pi/4)\right]\right\}^{\frac{7-\alpha}{2}}}d\xi$$
$$A_{PL3} = \int_0^1 \frac{\xi^2}{\left\{1-\xi^2(1-2\xi/3)\left[\alpha\Xi(\alpha)\tilde{\sigma}_R^2\left[Q_l(\alpha)\right]^{3-\frac{\alpha}{2}}\right]/\left[16\Gamma(1-\alpha/2)\sin(\alpha\pi/4)\right]\right\}^{3+\frac{\beta-\alpha}{2}}}d\xi \tag{60}$$

3.2.3 *Plane wave intensity scintillation index under arbitrary turbulence intensity from weak to strong*

According to the extended Rytov theory, the light intensity fluctuation is divided into large-scale and small-scale light intensity fluctuation components, which shows the change process of the light intensity scintillation index of the plane wave when the turbulence intensity is arbitrary from weak to strong.

(1) The intensity scintillation index of plane wave in non-Kolmogorov spectrum with zero inner scale

Under the zero-inner-scale non-Kolmogorov spectrum, the scintillation index of light intensity from weak to strong turbulence is constructed by the asymptotic form of cut-off frequencies η_X and η_Y, which reflects that the scintillation index of light intensity increases first and then tends to saturation constant with the generalized Rytov index. Substituting the non-Kolmogorov spectrum Eq. (6), Eq.(15) and Eq.(16) into Eq.(35) and Eq.(36), and using the geometric optics approximation $1-\cos x \approx x^2/2$, the large-scale and small-scale logarithmic intensity fluctuation variances of plane waves are obtained. The expressions [24] are

$$\sigma^2_{\ln X,PL}(\alpha) = [2\Gamma(3-\alpha/2)/3\beta_1(\alpha)] \cdot \eta^{3-\frac{\alpha}{2}}_{X,PL}(\alpha) \cdot \sigma^2_{R,PL}(\alpha) \tag{61}$$

$$\sigma^2_{\ln Y,PL}(\alpha) = [8/(\alpha-2)\beta_1(\alpha)] \cdot \eta^{1-\frac{\alpha}{2}}_{Y,PL}(\alpha) \cdot \sigma^2_{R,PL}(\alpha) \tag{62}$$

where $\eta_{X,PL}(\alpha) = L\kappa^2_{X,PL}(\alpha)/k$, $\eta_{Y,PL}(\alpha) = L\kappa^2_{Y,PL}(\alpha)/k$.

Under the condition of arbitrary turbulence intensity from weak to strong, the expression of light intensity scintillation index of plane wave [26] is

$$\sigma^2_{I,PL} = \begin{cases} \sigma^2_{\ln X,PL}(\alpha) + \sigma^2_{\ln Y,PL}(\alpha) \approx \sigma^2_{R,PL}(\alpha) & \sigma^2_{R,PL}(\alpha) \ll 1 \\ \exp\left[\sigma^2_{\ln X,PL}(\alpha) + \sigma^2_{\ln Y,PL}(\alpha)\right] - 1 \approx \sigma^2_{IS,PL}(\alpha) & \sigma^2_{R,PL}(\alpha) \gg 1 \end{cases} \tag{63}$$

The expressions of $\eta_{X,PL}(\alpha)$ and $\eta_{Y,PL}(\alpha)$ are

$$\begin{cases} \eta_{X,PL}(\alpha) \approx 1/c_{1,PL}(\alpha),\ \eta_{Y,PL}(\alpha) \approx c_{3,PL}(\alpha) & \sigma^2_{R,PL} \ll 1 \\ \eta_{X,PL}(\alpha) \approx k\rho^2_{0,PL}(\alpha)/\left[L\, c_{2,PL}(\alpha)\right], & \sigma^2_{R,PL} \gg 1 \\ \eta_{Y,PL}(\alpha) \approx L\, c_{4,PL}(\alpha)/\left[k\rho^2_{0,PL}(\alpha)\right] \end{cases} \tag{64}$$

where $\rho_{0,PL}(\alpha)$ is the coherent radius of the plane wave, so that the phase structure function $D_{S,PL}(\rho_{0,PL}(\alpha),\alpha) = 2$. The expression of $\rho_{0,PL}(\alpha)$ is

$$\rho_{0,PL}(\alpha) = \left\{-\frac{\Gamma(\alpha/2)}{\Gamma(1-\alpha/2)\cdot 2^{3-\alpha}}\right\}^{1/(\alpha-2)} \times \left[\pi^2 A(\alpha)\tilde{C}^2_n k^2 L\right]^{-1/(\alpha-2)} \tag{65}$$

According to different conditions, the expressions of $c_{1,PL}$, $c_{2,PL}$, $c_{3,PL}$ and $c_{4,PL}$ are obtained by substituting equations (42) and (48) into equations (63)and substituting equations (64) into equations (61) and (62) respectively.

$$\begin{aligned} c_{1,PL}(\alpha) &= \left[\frac{2\Gamma(3-\alpha/2)}{3\beta_1(\alpha)\times 0.49}\right]^{\frac{2}{6-\alpha}} \\ c_{2,PL}(\alpha) &= \left[\frac{3\beta_1(\alpha)\cdot r_1(\alpha)\cdot I_1(\alpha)}{4\Gamma(3-\alpha/2)}\right]^{\frac{2}{\alpha-6}} \cdot [\rho_1(\alpha)\cdot\beta_1(\alpha)]^{\frac{2}{\alpha-2}} \\ c_{3,PL}(\alpha) &= \left[\frac{0.51\times(\alpha-2)\cdot\beta_1(\alpha)}{8}\right]^{\frac{2}{2-\alpha}} \\ c_{4,PL}(\alpha) &= \left[\frac{(\alpha-2)\cdot\ln 2}{8\cdot\rho_1(\alpha)}\right]^{\frac{2}{2-\alpha}} \end{aligned} \tag{66}$$

In Eq. (66), $\rho_1(\alpha) = -\Gamma(\alpha/2)/[2^{3-\alpha}\Gamma(1-\alpha/2)]$ is the coefficient in the coherence radius of Eq. (65), i.e., $\rho_{0,PL}(\alpha) = \rho_1^{1/(\alpha-2)}[\pi^2 A(\alpha)\tilde{C}^2_n k^2 L]^{-1/(\alpha-2)}$. Substituting Eq.(66) into Eq.(19) and Eq.(20), $\kappa^2_{X,PL}(\alpha)$ and $\kappa^2_{Y,PL}(\alpha)$ are obtained, and the analytical expressions of $\eta_{X,PL}(\alpha)$ and $\eta_{Y,PL}(\alpha)$ under moderate to strong non-Kolmogorov turbulence are as follows:

$$\begin{aligned} \eta_{X,PL}(\alpha) &= \frac{\left[\frac{3\beta_1(\alpha)\times 0.49}{2\Gamma(3-\alpha/2)}\right]^{\frac{2}{6-\alpha}}}{1 + f_{X,PL}(\alpha)\,\sigma^{\frac{4}{\alpha-2}}_{R,PL}(\alpha)} \\ \eta_{Y,PL}(\alpha) &= \left[\frac{0.51\times(\alpha-2)\,\beta_1(\alpha)}{8}\right]^{\frac{2}{2-\alpha}} \\ &\quad \times \left[1 + f_{Y,PL}(\alpha)\,\sigma^{\frac{4}{\alpha-2}}_{R,PL}(\alpha)\right] \end{aligned} \tag{67}$$

where $f_{X,PL}(\alpha) = \left[\frac{r_1(\alpha)\cdot I_1(\alpha)}{2\times 0.49}\right]^{\frac{2}{\alpha-6}}$ $f_{Y,PL}(\alpha) = \left(\frac{\ln 2}{0.51}\right)^{\frac{2}{2-\alpha}}$

The formula (67) is substituted into formula (61) and formula (62) respectively. According to formula (34), the expression of the scintillation index of plane wave intensity at zero inner scale is

$$\sigma^2_{I,PL}(\alpha) = \exp\left\{\frac{0.49\,\sigma^2_{R,PL}(\alpha)}{\left[1 + f_{X,PL}(\alpha)\,\sigma^{\frac{4}{\alpha-2}}_{R,PL}(\alpha)\right]^{3-\frac{\alpha}{2}}} + \frac{0.51\,\sigma^2_{R,PL}(\alpha)}{\left[1 + f_{Y,PL}(\alpha)\,\sigma^{\frac{4}{\alpha-2}}_{R,PL}(\alpha)\right]^{\frac{\alpha}{2}-1}}\right\} - 1 \tag{68}$$

where $\sigma^2_{R,PL}$ is the intensity scintillation index of plane wave under non-Kolmogorov spectrum in weak turbulence.

(2) The intensity scintillation index of plane wave in the generalized von Kármán spectrum with inner scale and outer scale

Under the generalized von Kármán spectrum with inner scale and outer scale, the intensity scintillation index model reflects the limitation of the outer scale on the low spatial frequency refractive index fluctuation and the inner scale on the high spatial frequency refractive index fluctuation. Through the low-pass and high-pass spatial filtering characteristics, the influence of different spatial frequency turbulence components on the large-scale and small-scale intensity fluctuation

components is distinguished [24]. According to (12), choose $f(\kappa, l_0, \alpha) = \exp(-\kappa^2/\kappa_m^2)$ and $g(\kappa L_0) = 1 - \exp\left(-\kappa^2/\kappa_0^2\right)$. The expressions of large-scale and small-scale spatial filters are

$$G_X(\kappa, l_0, L_0, \alpha) = \exp\left(-\frac{\kappa^2}{\kappa_m^2}\right)\left[\exp\left(-\frac{\kappa^2}{\kappa_X^2}\right) - \exp\left(-\frac{\kappa^2}{\kappa_{X_0}^2}\right)\right] \tag{69}$$

$$G_Y(\kappa, \alpha) = \frac{\kappa^\alpha}{(\kappa^2 + \kappa_Y^2)^{\alpha/2}} \quad \kappa > \kappa_Y \tag{70}$$

where $\kappa_{X_0}^2 = \kappa_X^2\kappa_0^2/(\kappa_X^2 + \kappa_0^2)$.

The large-scale logarithmic intensity fluctuation variance expression of plane wave [24] is

$$\sigma_{\ln X,PL}^2(l_0, L_0, \alpha) = \sigma_{\ln X,PL}^2(l_0, \alpha) - \sigma_{\ln X,PL}^2(L_0, \alpha) \tag{71}$$

According to the extended Rytov theory, substituting Eq. (71) into Eq. (27), the intensity scintillation index of plane wave [24] can be expressed as

$$\sigma_{I,PL}^2(l_0, L_0, \alpha) = \exp\left[\sigma_{\ln X,PL}^2(l_0, \alpha) - \sigma_{\ln X,PL}^2(L_0, \alpha) + \sigma_{\ln Y,PL}^2(l_0, \alpha)\right] - 1 \tag{72}$$

where $\sigma_{\ln Y,PL}^2(l_0, \alpha)$ is a small-scale logarithmic intensity scintillation including the inner-scale effect.

The variance expression of large-scale logarithmic intensity fluctuation of plane wave including inner scale effect is

$$\begin{aligned}\sigma_{\ln X,PL}^2(l_0, \alpha) &= 8\pi^2k^2L\int_0^1\int_0^\infty \kappa\Phi_n(\kappa, \alpha)\exp\left(-\frac{\kappa^2}{\kappa_m^2}\right)\exp\left(-\frac{\kappa^2}{\kappa_X^2}\right) \\ &\quad\times\left[1 - \cos\left(\frac{L\kappa^2}{k}\xi\right)\right]d\kappa\, d\xi \\ &\approx -\frac{\alpha}{4\Gamma(1-\alpha/2)\sin(\alpha\pi/4)}\tilde{\sigma}_R^2\int_0^1\xi^2 d\xi\int_0^\infty \eta^{2-\alpha/2} \\ &\quad\times\exp\left(-\frac{\eta}{Q_m(\alpha)} - \frac{\eta}{\eta_{X,PL}(\alpha)}\right)d\eta\end{aligned} \tag{73}$$

Using $1 - \cos\left(L\kappa^2\xi/k\right) \cong \left(L\kappa^2\xi/k\right)^2/2, \kappa \ll \kappa_X$ and $\eta = L\kappa^2/k, \eta_{X,PL}(\alpha) = L\kappa_{X,PL}^2/k$, (73) becomes

$$\begin{aligned}\sigma_{\ln X,PL}^2(l_0, \alpha) = &-\frac{\alpha\Gamma(3-\alpha/2)}{12\Gamma(1-\alpha/2)\sin(\alpha\pi/4)}\tilde{\sigma}_R^2 \\ &\times\left[\frac{\eta_{X,PL}(\alpha)Q_m(\alpha)}{\eta_{X,PL}(\alpha) + Q_m(\alpha)}\right]^{3-\alpha/2}\end{aligned} \tag{74}$$

When the inner scale is zero, $Q_m \to \infty$, (74)is reduced to

$$\sigma_{\ln X,PL}^2(l_0, \alpha) = -\frac{\alpha\Gamma(3-\alpha/2)}{12\Gamma(1-\alpha/2)\sin(\alpha\pi/4)}\tilde{\sigma}_R^2\eta_{X,PL}^{3-\alpha/2}(\alpha) \tag{75}$$

Under arbitrary turbulence intensity from weak to strong, the variance expression of large-scale logarithmic intensity fluctuation of plane wave [24] is

$$\sigma_{\ln X,PL}^2(l_0, \alpha) = \begin{cases} 0.49\tilde{\sigma}_R^2 & L/\left[k\rho_{PL}^2(\alpha)\right] \ll 1 \\ \frac{C_{PL}(\alpha)}{2\left\{\tilde{\sigma}_R^2[Q_m(\alpha)]^{3-\alpha/2}\right\}^{2-\alpha/2}} & L/\left[k\rho_{PL}^2(\alpha)\right] \gg 1 \end{cases} \tag{76}$$

Under arbitrary turbulence intensity from weak to strong, the dimensionless low-pass cut-off spatial frequency $\eta_{X,PL}$ asymptotic form expression [24] is

$$\begin{aligned}\eta_{X,PL}(\alpha) &= \frac{1}{c_{1,PL}(\alpha) + c_{2,PL}(\alpha)L/\left[k\rho_{PL}^2(\alpha)\right]} \\ &\approx \begin{cases} 1/c_{1,PL}(\alpha) & L/\left[k\rho_{PL}^2(\alpha)\right] \ll 1 \\ k\rho_{PL}^2(\alpha)/\left[L\, c_{2,PL}(\alpha)\right] & L/\left[k\rho_{PL}^2(\alpha)\right] \gg 1 \end{cases}\end{aligned} \tag{77}$$

where $c_{1,PL}(\alpha)$ and $c_{2,PL}(\alpha)$ are undetermined parameters.

According to different conditions, (77) is substituted into(75) respectively, and (76) is solved simultaneously. The expressions of $c_{1,PL}(\alpha)$ and $c_{2,PL}(\alpha)$ are obtained as follows

$$c_{1,PL}(\alpha) = \left[-\frac{5.88\Gamma(1-\alpha/2)\sin(\alpha\pi/4)}{\alpha\Gamma(3-\alpha/2)}\right]^{2/(\alpha-6)} \tag{78}$$

$$\begin{aligned}c_{2,PL}(\alpha) = \Bigg\{ &-\frac{C_{PL}(\alpha)}{2\left\{\tilde{\sigma}_R^2\left[Q_m(\alpha)\right]^{3-\alpha/2}\right\}^{2-\alpha/2}} \\ &\cdot\frac{12\Gamma(1-\alpha/2)\sin(\alpha\pi/4)}{\alpha\Gamma(3-\alpha/2)\tilde{\sigma}_R^2}\Bigg\}^{2/(\alpha-6)} \times\frac{k\rho_{PL}^2(\alpha)}{L}\end{aligned} \tag{79}$$

Substituting Eq. (78) and Eq. (79) into Eq. (77), the expression of $\eta_{X,PL}$ is obtained as

$$\eta_{X,PL}(\alpha) = \frac{1/c_{1,PL}(\alpha)}{1 + \left[1.02C_{PL}(\alpha)\right]^{\frac{2}{\alpha-6}}\tilde{\sigma}_R^2\left[Q_m(\alpha)\right]^{2-\alpha/2}} \tag{80}$$

Substituting Eq. (80) into Eq. (74), the large-scale logarithmic intensity fluctuation variance expression of plane wave including inner scale effect is obtained [24] :

$$\sigma^2_{\ln X,PL}(l_0,\alpha) = -\frac{\alpha\Gamma(3-\alpha/2)}{12\Gamma(1-\alpha/2)\sin(\alpha\pi/4)}\tilde{\sigma}_R^2 \times\left\{\frac{Q_m(\alpha)}{1+c_{1,PL}(\alpha)Q_m(\alpha)+c_{1,PL}(\alpha)\left[1.02C_{PL}(\alpha)\right]^{\frac{2}{\alpha-6}}\tilde{\sigma}_R^2\left[Q_m(\alpha)\right]^{3-\frac{\alpha}{2}}}\right\}^{3-\alpha/2} \tag{81}$$

The large-scale logarithmic intensity fluctuation variance expression [24] of the plane wave including the outer-scale effect is

$$\sigma^2_{\ln X,PL}(L_0,\alpha) = -\frac{\alpha\Gamma(3-\alpha/2)}{12\Gamma(1-\alpha/2)\sin(\alpha\pi/4)}\tilde{\sigma}_R^2 \times\left[\frac{\eta_{X0,PL}(\alpha)Q_m(\alpha)}{\eta_{X0,PL}(\alpha)+Q_m(\alpha)}\right]^{3-\alpha/2} \tag{82}$$

The expression of $\eta_{X0,PL}(\alpha)$ is

$$\begin{aligned}\eta_{X0,PL}(\alpha) &= \frac{\eta_{X,PL}(\alpha)Q_0}{\eta_{X,PL}(\alpha)+Q_0} \\ &= \frac{Q_0}{1+c_{1,PL}(\alpha)Q_0+c_{1,PL}(\alpha)\left[1.02C_{PL}(\alpha)\right]^{\frac{2}{\alpha-6}}\tilde{\sigma}_R^2Q_0\left[Q_m(\alpha)\right]^{2-\frac{\alpha}{2}}} \\ Q_0 &= L\kappa_0^2/k = 4\pi^2L/(kL_0^2)\end{aligned} \tag{83}$$

The small-scale logarithmic intensity fluctuation variance expression of plane wave [24] is

$$\sigma^2_{\ln Y,PL}(l_0,\alpha) = -\frac{\alpha}{(\alpha-2)\Gamma(1-\alpha/2)\sin(\alpha\pi/4)}\tilde{\sigma}_R^2\eta_{Y,PL}^{1-\alpha/2}(\alpha) \tag{84}$$

where $\eta_{Y,PL}(\alpha) = L\kappa_Y^2(\alpha)/k$ is the dimensionless high-pass cut-off spatial frequency.

Under the condition of arbitrary turbulence intensity, the expression of small-scale logarithmic intensity scintillation of plane wave is

$$\sigma^2_{\ln Y,PL}(l_0,\alpha) = \begin{cases}0.51\sigma^2_{I,PLvk}(\alpha) & L/\left[k\rho^2_{PL}(\alpha)\right] \ll 1 \\ \ln 2 & L/\left[k\rho^2_{PL}(\alpha)\right] \gg 1\end{cases} \tag{85}$$

Under the condition of arbitrary turbulence intensity, $\eta_{Y,PL}(\alpha)$ represents the effective truncation position of the high spatial frequency component in the turbulence spectrum, and its variation with α reflects the distribution characteristics of small-scale disturbance energy under different spectral indices. The asymptotic expression of the dimensionless high-pass cutoff spatial frequency $\eta_{Y,PL}(\alpha)$ [24] is

$$\begin{aligned}\eta_{Y,PL}(\alpha) &= c_{3,PL}(\alpha)+\frac{c_{4,PL}(\alpha)L}{k\rho^2_{PL}(\alpha)} \\ &\approx \begin{cases}c_{3,PL}(\alpha) & L/\left[k\rho^2_{PL}(\alpha)\right] \ll 1 \\ c_{4,PL}(\alpha)L/\left[k\rho^2_{PL}(\alpha)\right] & L/\left[k\rho^2_{PL}(\alpha)\right] \gg 1\end{cases}\end{aligned} \tag{86}$$

According to different conditions, (86) is substituted into (84) respectively, and (85) is solved simultaneously. The expressions of $c_{3,PL}(\alpha)$ and $c_{4,PL}(\alpha)$ are obtained as follows

$$c_{3,PL}(\alpha) = \left[-\frac{0.51\sigma^2_{I,PLvk}(\alpha)(\alpha-2)\Gamma(1-\alpha/2)\sin(\alpha\pi/4)}{\tilde{\sigma}_R^2\cdot\alpha}\right]^{\frac{2}{2-\alpha}} \tag{87}$$

$$c_{4,PL}(\alpha) = \left[-\frac{\ln 2\cdot(\alpha-2)\Gamma(1-\alpha/2)\sin(\alpha\pi/4)}{\tilde{\sigma}_R^2\cdot\alpha}\right]^{\frac{2}{2-\alpha}} \times\frac{k\rho^2_{PL}(\alpha)}{L} \tag{88}$$

Substituting Eq. (87) and Eq. (88) into Eq. (86), we obtain the expression of $\eta_{Y,PL}$ [24] :

$$\eta_{Y,PL}(\alpha) = \left[-\frac{\alpha}{0.51(\alpha-2)\Gamma(1-\alpha/2)\sin(\alpha\pi/4)}\frac{\tilde{\sigma}_R^2}{\sigma^2_{I,PLvk}(\alpha)}\right]^{\frac{2}{\alpha-2}} \times\left(1+0.73^{\frac{2}{\alpha-2}}\sigma_{I,PL}^{\frac{4}{\alpha-2}}(\alpha)\right) \tag{89}$$

Substituting Eq. (89) into Eq. (84), the small-scale logarithmic intensity fluctuation variance expression of plane wave can be obtained [24] :

$$\sigma^2_{\ln Y,PL}(l_0,\alpha) = 0.51\sigma^2_{I,PLvk}(\alpha)\left(1+0.73^{\frac{2}{\alpha-2}}\sigma_{I,PLvk}^{\frac{4}{\alpha-2}}\right)^{1-\frac{\alpha}{2}} \tag{90}$$

where $\sigma^2_{I,PLvk}(\alpha)$ is the intensity scintillation index of the plane wave under the generalized von Kármán spectrum in the case of weak turbulence.

The cut-off frequency κ_Y of the small-scale spatial filter depends on the inner scale, and the variance of the small-scale logarithmic light intensity fluctuation given by formula (90) also includes the inner scale effect. Because the influence of the outer scale

on the variance of the small-scale logarithmic light intensity fluctuation is very small, it is neglected here. Substituting Eq. (81), Eq. (82) and Eq. (90) into Eq. (72), the intensity scintillation index of plane wave in the generalized von Kármán spectrum under arbitrary atmospheric turbulence intensity including inner-scale and outer-scale effects is obtained. The expression [24] is

$$\begin{aligned}\sigma_{I,PL}^2(l_0,L_0,\alpha)=\exp\Bigg\{&\beta_3(\alpha)\tilde{\sigma}_R^2\left[\frac{\eta_{X,PL}(\alpha)Q_m(\alpha)}{\eta_{X,PL}(\alpha)+Q_m(\alpha)}\right]^{3-\frac{\alpha}{2}}\\&-\beta_3(\alpha)\tilde{\sigma}_R^2\left[\frac{\eta_{X0,PL}(\alpha)Q_m(\alpha)}{\eta_{X0,PL}(\alpha)+Q_m(\alpha)}\right]^{3-\frac{\alpha}{2}}\\&+0.51\,\sigma_{I,PLvk}^2(\alpha)\left(1+0.73^{\frac{2}{\alpha-2}}\sigma_{I,PLvk}^{\frac{4}{\alpha-2}}(\alpha)\right)^{1-\frac{\alpha}{2}}\Bigg\}-1\end{aligned} \tag{91}$$

The expressions of $\beta_3(\alpha)$ and $\frac{\eta_{X,PL}(\alpha)Q_m(\alpha)}{\eta_{X,PL}(\alpha)+Q_m(\alpha)}$ are

$$\begin{aligned}\beta_3(\alpha)=&-\frac{\alpha\Gamma(3-\alpha/2)}{12\Gamma(1-\alpha/2)\sin(\alpha\pi/4)}\\\frac{\eta_{X,PL}(\alpha)Q_m(\alpha)}{\eta_{X,PL}(\alpha)+Q_m(\alpha)}=&Q_m(\alpha)\Big/\Big\{1+c_{1,PL}(\alpha)Q_m(\alpha)\\&+c_{1,PL}(\alpha)\left[1.02C_{PL}(\alpha)\right]^{\frac{2}{\alpha-6}}\tilde{\sigma}_R^2\left[Q_m(\alpha)\right]^{3-\frac{\alpha}{2}}\Big\}\end{aligned} \tag{92}$$

(3) The intensity scintillation index of plane wave in the generalized modified atmospheric spectrum with inner scale

Under the condition of generalized modified atmospheric spectrum including inner scale, considering that the finite aperture of the actual photodetector will produce aperture averaging effect, the intensity scintillation index model couples the inner scale of atmospheric turbulence and the geometric parameters of the receiver, which reflects the filtering effect of system parameters on intensity scintillation in engineering applications. Here, the outer scale effect is ignored, and the corresponding large-scale spatial filter only contains the inner scale parameters. The expression of scintillation index of plane wave intensity [24] is

$$\begin{aligned}\sigma_{I,PL}^2(\alpha,D,l_0)=\exp\Big[&\sigma_{\ln X,PL}^2(\alpha,D,l_0)\\&+\sigma_{\ln Y,PL}^2(\alpha,D,l_0)\Big]-1\end{aligned} \tag{93}$$

The optical communication system is approximated as an ABCD optical system [4, 30], and the receiving antenna with a diameter of D is equivalent to a Gaussian lens. The large-scale logarithmic intensity fluctuation variance of the plane wave is obtained, and its expression [24] is

$$\begin{aligned}\sigma_{\ln X,PL}^2(\alpha,D,l_0)=&\frac{-\alpha\Gamma(3-\alpha/2)}{12\Gamma(1-\alpha/2)\sin(\alpha\pi/4)}\tilde{\sigma}_R^2\left[\frac{\eta_{xd}Q_l(\alpha)}{\eta_{xd}+Q_l(\alpha)}\right]^{3-\alpha/2}\\&\times\Bigg\{1+\frac{a_1\Gamma(7/2-\alpha/2)}{\Gamma(3-\alpha/2)}\left[\frac{\eta_{xd}}{\eta_{xd}+Q_l(\alpha)}\right]^{1/2}\\&-\frac{b_1\Gamma(3+\beta/2-\alpha/2)}{\Gamma(3-\alpha/2)}\left[\frac{\eta_{xd}}{\eta_{xd}+Q_l(\alpha)}\right]^{\beta/2}\Bigg\}\end{aligned} \tag{94}$$

where η_X is the dimensionless low-pass spatial cutoff frequency, $d=\sqrt{kD^2/(4L)}$ is the normalized receiving-aperture parameter, η_{xd} is the modified cut-off frequency, and $c_1(\alpha)$ is a constant. The expressions of η_X, η_{xd} and $c_1(\alpha)$ are

$$\begin{aligned}\eta_{xd}=&\frac{\eta_X}{1+d^2\eta_X/4}\\\eta_X=&\frac{1/c_1(\alpha)}{1+\left[1.02C_{PL}(\alpha)\right]^{\frac{2}{\alpha-6}}\tilde{\sigma}_R^2[Q_l(\alpha)]^{2-\alpha/2}}\\c_1(\alpha)=&\left[-\frac{5.88\Gamma(1-\alpha/2)\sin(\alpha\pi/4)}{\alpha\Gamma(3-\alpha/2)}\right]^{\frac{2}{\alpha-6}}\end{aligned} \tag{95}$$

The variance expression of small-scale logarithmic intensity fluctuation of plane wave with finite receiving aperture [24] is

$$\begin{aligned}\sigma_{\ln Y,PL}^2(\alpha,D,l_0)\approx&-\frac{\alpha}{2\Gamma(1-\alpha/2)\sin(\alpha\pi/4)}\tilde{\sigma}_R^2\left(\frac{d^2}{4}\right)^{\alpha/2-1}\\&\times\exp\left(\frac{d^2\eta_Y}{4}\right)\Gamma\left(1-\frac{\alpha}{2},\frac{d^2\eta_Y}{4}\right)\end{aligned} \tag{96}$$

where $\Gamma(a,z)$ is an incomplete Gamma function. η_Y is a dimensionless high-pass spatial cut-off frequency, and the expression of η_Y is

$$\begin{aligned}\eta_Y=&\left[-\frac{\alpha}{0.51(\alpha-2)\Gamma(1-\alpha/2)\sin(\alpha\pi/4)}\frac{\tilde{\sigma}_R^2}{\sigma_{I,PLhill}^2(\alpha)}\right]^{\frac{2}{\alpha-2}}\\&\times\left(1+0.73^{\frac{2}{\alpha-2}}\sigma_{I,PLhill}^{\frac{4}{\alpha-2}}(\alpha)\right)\end{aligned} \tag{97}$$

where $\sigma_{I,PLhill}^2(\alpha)$ denotes the intensity scintillation index of the plane wave under the generalized modified atmospheric spectrum in weak turbulence.

3.3 Intensity scintillation index of spherical wave

The study of the intensity scintillation index of spherical waves is to analyze the propagation

characteristics of spherical waves in the atmosphere. Spherical wave and plane wave show different path weighting characteristics and scale sensitivity due to the difference of wavefront geometry. The plane wave is more evenly affected by the atmospheric turbulence in the transmission. The wavefront fluctuation of the spherical wave causes the initial phase disturbance to gradually weaken with the geometric diffusion of the wavefront. This difference causes the spherical wave to be less affected by the large-scale vortex, and shows a smaller intensity scintillation index than the plane wave in the weak turbulence region. By studying the light intensity scintillation characteristics of two different waveforms, it can provide a theoretical basis for the study of atmospheric turbulence effects in wireless optical communication systems.

3.3.1 *Spherical wave intensity scintillation index under weak turbulence condition*

The spherical wave intensity scintillation index model contains a complex weighting factor, which reflects the influence of atmospheric turbulence fluctuation at different positions along the propagation path on the receiving end, and the influence of atmospheric turbulence at the front end of the beam propagation path is small.

(1) The intensity scintillation index of spherical wave in non-Kolmogorov spectrum

Substituting the non-Kolmogorov spectrum (6) into (29), the expression of the scintillation index of spherical wave intensity [24] is

$$\begin{aligned}\sigma_{I,SP}^2(\alpha) = & -4\pi^2\tilde{C}_n^2 k^{(6-\alpha)/2} L^{\alpha/2} A(\alpha) \\ & \times \sin(\pi\alpha/4)\,\Gamma(1-\alpha/2)\left[\Gamma(\alpha/2)\right]^2/\Gamma(\alpha) \\ = & \,\Gamma(\alpha/2)\Gamma(1+\alpha/2)\tilde{\sigma}_R^2/\Gamma(\alpha)\end{aligned} \tag{98}$$

By using variable substitution, (98) becomes

$$\begin{aligned}&\sigma_{I,SP}^2(\alpha) = \beta_2(\alpha)\cdot A(\alpha)\tilde{C}_n^2\pi^2 k^{3-\alpha/2} L^{\alpha/2} \\ &\beta_2(\alpha) = -4\Gamma(1-\alpha/2)\cdot\sin(\pi\alpha/4)\cdot\Gamma^2(\alpha/2)/\Gamma(\alpha)\end{aligned} \tag{99}$$

where $\sigma_{I,SP}^2(\alpha) = \sigma_{R,SP}^2(\alpha)$

(2) Intensity scintillation index of spherical wave in generalized von Kármán spectrum

Substituting the generalized von Kármán spectrum (7) into Eq. (29), the expression of the scintillation index of spherical wave intensity [24] is

$$\begin{aligned}\sigma_{I,SPvk}^2(\alpha) = \frac{\tilde{\sigma}_R^2}{\sin(\alpha\pi/4)}\Bigg\{&\frac{\left[1+(3/Q_m(\alpha))^2\right]^{\alpha/4}}{3^{\alpha/2-1}}\sin\left[\frac{\alpha}{2}\tan^{-1}\left(\frac{Q_m(\alpha)}{3}\right)\right] \\ &-\frac{\alpha}{2}Q_m^{1-\frac{\alpha}{2}}(\alpha)\Bigg\}\end{aligned} \tag{100}$$

(3) Intensity scintillation index of spherical wave in generalized modified atmospheric spectrum

Substituting the generalized modified atmospheric spectrum (8) into Eq. (29), the expression of the scintillation index of spherical wave intensity [29] is

$$\begin{aligned}\sigma_{I,SPhill}^2 = \frac{\tilde{\sigma}_R^2}{\sin(\alpha\pi/4)}\Bigg\{&3^{1-\alpha/2}\left\{1+\frac{9}{[Q_l(\alpha)]^2}\right\}^{\alpha/4}\sin\left[\frac{\alpha}{2}\tan^{-1}\left(\frac{Q_l(\alpha)}{3}\right)\right] \\ &+\frac{3^{1/2}a_1\alpha\Gamma(1.5-\alpha/2)}{(\alpha-1)\Gamma(1-\alpha/2)}\left\{9+[Q_l(\alpha)]^2\right\}^{-1/4}\sin\left[\frac{\alpha-1}{2}\tan^{-1}\left(\frac{Q_l(\alpha)}{3}\right)\right] \\ &-\frac{3^{\beta/2}b_1\alpha\Gamma\left(1-\frac{\alpha}{2}+\frac{\beta}{2}\right)}{(\alpha-\beta)\Gamma(1-\alpha/2)}\left\{9+[Q_l(\alpha)]^2\right\}^{-\beta/4}\sin\left[\frac{\alpha-\beta}{2}\tan^{-1}\left(\frac{Q_l(\alpha)}{3}\right)\right]\Bigg\} \\ &-\left[\frac{\alpha}{2}+\frac{a_1\alpha\Gamma(1.5-\alpha/2)}{2\Gamma(1-\alpha/2)}-\frac{b_1\alpha\Gamma\left(1-\frac{\alpha}{2}+\frac{\beta}{2}\right)}{2\Gamma(1-\alpha/2)}\right][Q_l(\alpha)]^{1-(\alpha/2)}\Bigg\}\end{aligned} \tag{101}$$

where $Q_l(\alpha) = [c_h(\alpha)]^2 L/\left(kl_0^2\right)$.

3.3.2 *The intensity scintillation index of spherical wave under saturated strong turbulence condition*

In the saturated strong turbulence region, the phase structure functions of plane wave and spherical wave differ through the path-weighting factor determined by the wavefront geometry (compare Eqs. (52) and (104)). Due to the wavefront diffusion effect, the small-scale logarithmic intensity fluctuation variance of spherical waves has different integral weights.

(1) The intensity scintillation index of spherical wave in non-Kolmogorov spectrum

Under the non-Kolmogorov spectrum of saturated strong turbulence, the expression of the intensity scintillation index of the spherical wave [8] is

$$\sigma_{IS,SP}^2(\alpha) = 1 + r_2(\alpha)\cdot I_2(\alpha)\cdot\sigma_{R(SP)}^{\frac{4(\alpha-4)}{\alpha-2}}(\alpha) \tag{102}$$

The expressions of $r_2(\alpha)$ and $I_2(\alpha)$ are

$$r_2(\alpha)=\frac{1}{\alpha-2}\cdot 2^{\frac{(3-\alpha)(\alpha-10)}{\alpha-2}}\cdot\left[-\frac{\Gamma(1-\alpha/2)}{\Gamma(\alpha/2)}\right]^{\frac{\alpha-6}{\alpha-2}}\times\Gamma\left(\frac{6-\alpha}{\alpha-2}\right)\cdot[\beta_2(\alpha)]^{\frac{8-2\alpha}{\alpha-2}}$$
$$I_2(\alpha)=(\alpha-1)^{\frac{6-\alpha}{\alpha-2}}\cdot\frac{\Gamma^2(\alpha-3)}{\Gamma(2\alpha-6)} \tag{103}$$

(2) Intensity scintillation index of spherical wave in generalized von Kármán spectrum

Under the generalized von Kármán spectrum of saturated strong turbulence, the integral expression of the phase structure function of spherical waves [8] is

$$\int_0^1 D_{S,SP}\left[\frac{L\kappa}{k}w(\tau,\xi),\alpha\right]d\tau=\frac{-\alpha\Gamma(2-\alpha/2)\,\Xi}{48\Gamma(1-\alpha/2)\sin(\pi\alpha/4)}\times\tilde{\sigma}_R^2\left[Q_m(\alpha)\right]^{2-\frac{\alpha}{2}}\left(\frac{L\kappa^2}{k}\right)\xi^2(1-\xi)^2 \tag{104}$$

Substituting Eq. (7) and Eq. (104) into Eq. (30), the expression of intensity scintillation index of spherical wave is obtained [8] :

$$\sigma_{IS,SP}^2\approx 1+\frac{C_{SP}(\alpha)}{\left\{\tilde{\sigma}_R^2\left[Q_m(\alpha)\right]^{3-\alpha/2}\right\}^{2-\alpha/2}},\quad -\frac{\alpha\Gamma(2-\alpha/2)\,\tilde{\sigma}_R^2\left[Q_m(\alpha)\right]^{2-\alpha/2}}{16\Gamma(1-\alpha/2)\sin(\alpha\pi/4)}\gg 1 \tag{105}$$

The expression of $C_{SP}(\alpha)$ is

$$C_{SP}(\alpha)=\frac{-\alpha\Gamma(3-\alpha/2)}{2\Gamma(1-\alpha/2)\sin(\alpha\pi/4)}\times\int_0^1\frac{\xi^2(1-\xi)^2}{\left\{\tilde{\sigma}_R^2\left[Q_m(\alpha)\right]^{\frac{\alpha}{2}-3}-\frac{\alpha\Gamma(2-\alpha/2)\Xi}{48\Gamma(1-\alpha/2)\sin(\alpha\pi/4)}\xi^2(1-\xi)^2\right\}^{3-\frac{\alpha}{2}}}d\xi \tag{106}$$

(3) Intensity scintillation index of spherical wave in generalized modified atmospheric spectrum

Under the generalized modified atmospheric spectrum in saturated strong turbulence, the integral expression of the phase structure function of spherical waves [25] is

$$\int_0^1 D_{S,SP}\left[\frac{L\kappa}{k}w(\tau,\xi)\right]d\tau=-\frac{\alpha\,\Xi(\alpha)}{48\Gamma(1-\alpha/2)\sin(\alpha\pi/4)}\times\tilde{\sigma}_R^2\left[Q_l(\alpha)\right]^{2-\alpha/2}\left(\frac{L\kappa^2}{k}\right)\xi^2(1-\xi)^2 \tag{107}$$

Substituting Eq. (8) and Eq. (107) into Eq. (30), the expression of the intensity scintillation index of the spherical wave [25] is

$$\sigma_{IS,SP}^2(\alpha)=1+\frac{C_{sp}(\alpha)}{\left\{\tilde{\sigma}_R^2\left[Q_l(\alpha)\right]^{3-\alpha/2}\right\}^{2-\alpha/2}} \tag{108}$$

The expression of $C_{SP}(\alpha)$ is

$$\begin{aligned}C_{SP}(\alpha)&=-\frac{\alpha\Gamma(3-\alpha/2)}{2\Gamma(1-\alpha/2)\sin(\alpha\pi/4)}\left\{\tilde{\sigma}_R^2[Q_l(\alpha)]^{3-\frac{\alpha}{2}}\right\}^{3-\frac{\alpha}{2}}\\&\times\left[A_{SP1}+\frac{a_1\Gamma(7/2-\alpha/2)}{\Gamma(3-\alpha/2)}\times A_{SP2}-\frac{b_1\Gamma(3-\alpha/2+\beta/2)}{\Gamma(3-\alpha/2)}\times A_{SP3}\right]\\A_{SP1}&=\int_0^1\frac{\xi^2(1-\xi)^2}{\left[1-\frac{\alpha\Xi(\alpha)\tilde{\sigma}_R^2[Q_l(\alpha)]^{3-\alpha/2}}{48\Gamma(1-\alpha/2)\sin(\alpha\pi/4)}\xi^2(1-\xi)^2\right]^{\frac{6-\alpha}{2}}}d\xi\\A_{SP2}&=\int_0^1\frac{\xi^2(1-\xi)^2}{\left[1-\frac{\alpha\Xi(\alpha)\tilde{\sigma}_R^2[Q_l(\alpha)]^{3-\alpha/2}}{48\Gamma(1-\alpha/2)\sin(\alpha\pi/4)}\xi^2(1-\xi)^2\right]^{\frac{7-\alpha}{2}}}d\xi\\A_{SP3}&=\int_0^1\frac{\xi^2(1-\xi)^2}{\left[1-\frac{\alpha\Xi(\alpha)\tilde{\sigma}_R^2[Q_l(\alpha)]^{3-\alpha/2}}{48\Gamma(1-\alpha/2)\sin(\alpha\pi/4)}\xi^2(1-\xi)^2\right]^{3+\frac{\beta-\alpha}{2}}}d\xi\end{aligned} \tag{109}$$

3.3.3 *The intensity scintillation index of spherical wave under arbitrary turbulence intensity from weak to strong*

(1) The intensity scintillation index of spherical wave under non-Kolmogorov spectrum with zero inner scale

Substituting the non-Kolmogorov spectrum Eq. (6), Eq. (15) and Eq. (16) into Eq. (38) and Eq. (39) respectively, and using the geometric optics approximation $1-\cos x\approx x^2/2$, the expressions of large-scale and small-scale logarithmic intensity fluctuation variance of spherical waves [24] are obtained as follows:

$$\sigma_{\ln X,SP}^2(\alpha)=\frac{2\Gamma(3-\alpha/2)}{30\beta_2(\alpha)}\cdot\eta_{X,SP}^{3-\frac{\alpha}{2}}(\alpha)\cdot\sigma_{R,SP}^2(\alpha) \tag{110}$$

$$\sigma_{\ln Y,SP}^2(\alpha)=\frac{8}{(\alpha-2)\beta_2(\alpha)}\cdot\eta_{Y,SP}^{1-\frac{\alpha}{2}}(\alpha)\cdot\sigma_{R,SP}^2(\alpha) \tag{111}$$

where $\eta_{X,SP}(\alpha)=L\kappa_{X,SP}^2(\alpha)/k$, $\eta_{Y,SP}(\alpha)=L\kappa_{Y,SP}^2(\alpha)/k$.

Under the condition of arbitrary turbulence intensity, the expression of the scintillation index of spherical wave intensity is

$$\sigma_{I,SP}^2 = \begin{cases} \sigma_{\ln X,SP}^2(\alpha) + \sigma_{\ln Y,SP}^2(\alpha) \approx \sigma_{R,SP}^2(\alpha), \\ \qquad \sigma_{R,SP}^2(\alpha) \ll 1 \\ \exp\left[\sigma_{\ln X,SP}^2(\alpha) + \sigma_{\ln Y,SP}^2(\alpha)\right] - 1 \approx \sigma_{IS,SP}^2(\alpha), \\ \qquad \sigma_{R,SP}^2(\alpha) \gg 1 \end{cases} \tag{112}$$

The general expressions for $\eta_{X,SP}(\alpha)$ and $\eta_{Y,SP}(\alpha)$ are

$$\begin{cases} \eta_{X,SP}(\alpha) \approx \frac{1}{c_{1,SP}(\alpha)}, \eta_{Y,SP}(\alpha) \approx c_{3,SP}(\alpha) & \sigma_{R,PL}^2 \ll 1 \\ \eta_{X,SP}(\alpha) \approx \frac{k \cdot \rho_{0,SP}^2(\alpha)}{L \cdot c_{2,SP}(\alpha)}, \eta_{Y,SP}(\alpha) \approx \frac{L \cdot c_{4,SP}(\alpha)}{k \cdot \rho_{0,SP}^2(\alpha)} & \sigma_{R,PL}^2 \gg 1 \end{cases} \tag{113}$$

where $\rho_{0,SP}(\alpha)$ is the coherence radius of the spherical wave, the expression is

$$\rho_{0,SP}(\alpha) = \left[-\frac{\Gamma(\alpha/2)(\alpha-1)}{\Gamma(1-\alpha/2)\cdot 2^{3-\alpha}}\right]^{\frac{1}{\alpha-2}} \cdot \left[\pi^2 A(\alpha) \tilde{C}_n^2 k^2 L\right]^{-\frac{1}{\alpha-2}} \tag{114}$$

According to different conditions, the expressions of $c_{1,SP}(\alpha)$, $c_{2,SP}(\alpha)$, $c_{3,SP}(\alpha)$ and $c_{4,SP}(\alpha)$ are obtained by substituting Eq. (99) and Eq. (102) into Eq. (112) and substituting Eq. (113) into Eq. (110) and Eq. (111) respectively.

$$\begin{aligned} c_{1,SP}(\alpha) &= \left[\frac{2\Gamma(3-\alpha/2)}{30\beta_2(\alpha)\times 0.49}\right]^{\frac{2}{6-\alpha}} \\ c_{2,SP}(\alpha) &= \left[\frac{3\beta_2(\alpha)\cdot r_2(\alpha)\cdot I_2(\alpha)}{4\Gamma(3-\alpha/2)}\right]^{\frac{2}{\alpha-6}} \cdot [\rho_2(\alpha)\cdot\beta_2(\alpha)]^{\frac{2}{\alpha-2}} \\ c_{3,SP}(\alpha) &= \left[\frac{0.51\times(\alpha-2)\cdot\beta_2(\alpha)}{8}\right]^{\frac{2}{2-\alpha}} \\ c_{4,SP}(\alpha) &= \left[\frac{(\alpha-2)\cdot\ln 2}{8\cdot\rho_2(\alpha)}\right]^{\frac{2}{2-\alpha}} \end{aligned} \tag{115}$$

In Eq. (115), $\rho_2(\alpha) = -(\alpha-1)\Gamma(\alpha/2)/[2^{3-\alpha}\Gamma(1-\alpha/2)]$ is the coefficient in the coherence radius of Eq. (114), i.e., $\rho_{0,SP}(\alpha) = \rho_2^{1/(\alpha-2)}[\pi^2 A(\alpha)\tilde{C}_n^2 k^2 L]^{-1/(\alpha-2)}$. Substituting Eq. (115) into Eq. (19) and Eq. (20), $\kappa_{X,SP}^2(\alpha)$ and $\kappa_{Y,SP}^2(\alpha)$ are obtained. The analytical expressions of $\eta_{X,SP}(\alpha)$ and $\eta_{Y,SP}(\alpha)$ under the condition of medium to strong non-Kolmogorov spectrum are obtained as follows:

$$\begin{aligned} \eta_{X,SP}(\alpha) &= \frac{L\kappa_{X,SP}^2}{k} = \frac{\left[\frac{30\beta_2(\alpha)\times 0.49}{2\Gamma(3-\alpha/2)}\right]^{\frac{2}{6-\alpha}}}{1 + f_{X,SP}(\alpha)\cdot\sigma_{R,SP}^{\frac{4}{\alpha-2}}(\alpha)} \\ \eta_{Y,SP}(\alpha) &= \frac{L\kappa_{Y,SP}^2}{k} = \left[\frac{0.51\times(\alpha-2)\cdot\beta_2(\alpha)}{8}\right]^{\frac{2}{2-\alpha}} \cdot \left[1 + f_{Y,SP}(\alpha)\cdot\sigma_{R,SP}^{\frac{4}{\alpha-2}}(\alpha)\right] \\ f_{X,SP}(\alpha) &= \left[\frac{r_2(\alpha)\cdot I_2(\alpha)}{2\times 0.49}\right]^{\frac{2}{\alpha-6}} \qquad f_{Y,SP}(\alpha) = \left(\frac{\ln 2}{0.51}\right)^{\frac{2}{2-\alpha}} \end{aligned} \tag{116}$$

At zero inner scale, the intensity scintillation index of spherical wave under non-Kolmogorov condition is expressed as

$$\sigma_{I,SP}^2(\alpha) = \exp\left\{\frac{0.49\,\sigma_{R,SP}^2(\alpha)}{\left[1 + f_{X,SP}(\alpha)\,\sigma_{R,SP}^{\frac{4}{\alpha-2}}(\alpha)\right]^{3-\frac{\alpha}{2}}} + \frac{0.51\,\sigma_{R,SP}^2(\alpha)}{\left[1 + f_{Y,SP}(\alpha)\,\sigma_{R,SP}^{\frac{4}{\alpha-2}}(\alpha)\right]^{\frac{\alpha}{2}-1}}\right\} - 1 \tag{117}$$

where $\sigma_{R,SP}^2$ is the intensity scintillation index of spherical wave under non-Kolmogorov spectrum in weak turbulence.

(2) The intensity scintillation index of spherical wave in the generalized von Kármán spectrum with inner scale and outer scale

The large-scale spatial filter expression (69) and the small-scale spatial filter expression (70) are selected. The large-scale logarithmic intensity fluctuation variance expression of spherical wave [24] is

$$\sigma_{\ln X,SP}^2(l_0, L_0, \alpha) = \sigma_{\ln X,SP}^2(l_0, \alpha) - \sigma_{\ln X,SP}^2(L_0, \alpha) \tag{118}$$

According to the extended Rytov theory, the expression of the total intensity scintillation index of spherical waves [24] is

$$\sigma_{I,SP}^2(l_0, L_0, \alpha) = \exp\left[\sigma_{\ln X,SP}^2(l_0, \alpha) - \sigma_{\ln X,SP}^2(L_0, \alpha) + \sigma_{\ln Y,SP}^2(l_0, \alpha)\right] - 1 \tag{119}$$

where $\sigma_{\ln Y,SP}^2(l_0, \alpha)$ denotes the small-scale logarithmic intensity scintillation of spherical wave with inner scale effect.

The large-scale logarithmic intensity fluctuation variance expression of spherical wave including inner scale [24] is

$$\sigma^2_{\ln X,SP}(l_0,\alpha) \approx \frac{-\alpha}{4\Gamma(1-\alpha/2)\sin(\alpha\pi/4)}\tilde{\sigma}_R^2 \int_0^1 \xi^2(1-\xi)^2 d\xi \int_0^\infty \eta^{2-\frac{\alpha}{2}} \times \exp\left(-\frac{\eta}{Q_m(\alpha)} - \frac{\eta}{\eta_{X,SP}(\alpha)}\right) d\eta \tag{120}$$

Using $1-\cos\left(L\kappa^2\xi/k\right) \cong \left(L\kappa^2\xi/k\right)^2/2, \kappa \ll \kappa_X$ and $\eta = L\kappa^2/k, \eta_{X,SP}(\alpha) = L\kappa^2_{X,SP}/k$, Eq. (120) becomes

$$\sigma^2_{\ln X,SP}(l_0,\alpha) = -\frac{\alpha\Gamma(3-\alpha/2)}{120\Gamma(1-\alpha/2)\sin(\alpha\pi/4)}\tilde{\sigma}_R^2 \times \left[\frac{\eta_{X,SP}(\alpha)Q_m(\alpha)}{\eta_{X,SP}(\alpha)+Q_m(\alpha)}\right]^{3-\frac{\alpha}{2}} \tag{121}$$

When the inner scale tends to zero ($l_0 \to 0$), $Q_m \to \infty$, Eq. (121) is simplified as

$$\sigma^2_{\ln X,SP}(l_0,\alpha) = -\frac{\alpha\Gamma(3-\frac{\alpha}{2})}{120\Gamma(1-\frac{\alpha}{2})\sin(\frac{\alpha\pi}{4})}\tilde{\sigma}_R^2\eta^{3-\frac{\alpha}{2}}_{X,SP}(\alpha) \tag{122}$$

Under the condition of arbitrary turbulence intensity, the variance expression of large-scale logarithmic intensity fluctuation of spherical wave is

$$\sigma^2_{\ln X,SP}(\alpha) = \begin{cases} 0.49\,\sigma^2_{R,SP}, & \tilde{\sigma}_R^2 < 1 \\ \dfrac{C_{SP}(\alpha)}{2\left\{\tilde{\sigma}_R^2\left[Q_m(\alpha)\right]^{3-\frac{\alpha}{2}}\right\}^{2-\alpha/2}}, & \\ -\dfrac{\alpha\Gamma(2-\alpha/2)\,\tilde{\sigma}_R^2\left[Q_m(\alpha)\right]^{2-\alpha/2}}{16\Gamma(1-\alpha/2)\sin(\alpha\pi/4)} \gg 1 & \end{cases} \tag{123}$$

where $\sigma^2_{R,SP}(\alpha)$ represents the intensity scintillation index of spherical wave under non-Kolmogorov spectrum in weak turbulence.

Under the condition of arbitrary turbulence intensity, the asymptotic expression of the dimensionless low-pass cutoff spatial frequency $\eta_{X,SP}$ is

$$\eta_{X,SP}(\alpha) = \frac{1}{c_{1,SP}(\alpha) + c_{2,SP}(\alpha)L/\left[k\rho^2_{SP}(\alpha)\right]} \approx \begin{cases} 1/c_{1,SP}(\alpha) & L/\left[k\rho^2_{SP}(\alpha)\right] \ll 1 \\ k\rho^2_{SP}(\alpha)/\left[L\,c_{2,SP}(\alpha)\right] & L/\left[k\rho^2_{SP}(\alpha)\right] \gg 1 \end{cases} \tag{124}$$

According to different conditions, the equation (124) is substituted into the equation (122), and the equation (123) is solved simultaneously. The expressions of parameters $c_{1,SP}(\alpha)$ and $c_{2,SP}(\alpha)$ can be obtained as follows:

$$c_{1,SP}(\alpha) = \left[-\frac{58.8\Gamma(1-\alpha/2)\sin(\alpha\pi/4)\Gamma(\alpha/2)\Gamma(1+\alpha/2)}{\alpha\Gamma(3-\alpha/2)\Gamma(\alpha)}\right]^{\frac{2}{\alpha-6}} \tag{125}$$

$$c_{2,SP}(\alpha) = \left\{-\frac{C_{SP}(\alpha)}{2\left\{\tilde{\sigma}_R^2\left[Q_m(\alpha)\right]^{3-\alpha/2}\right\}^{2-\frac{\alpha}{2}}} \cdot \frac{120\Gamma(1-\alpha/2)\sin(\alpha\pi/4)}{\alpha\Gamma(3-\alpha/2)\tilde{\sigma}_R^2}\right\}^{2/(\alpha-6)} \times \frac{k\rho^2_{SP}(\alpha)}{L} \tag{126}$$

Substituting Eq. (125) and Eq. (126) into Eq. (124), the expression of $\eta_{X,SP}(\alpha)$ is obtained as

$$\eta_{X,SP}(\alpha) = \frac{1/d_1(\alpha)}{1+\Delta(\alpha)} \tag{127}$$

The expressions of $d_1(\alpha)$ and $\Delta(\alpha)$ [24] are

$$d_1(\alpha) = \left[-\frac{58.8\Gamma(1-\alpha/2)\sin(\alpha\pi/4)\Gamma(\alpha/2)\Gamma(1+\alpha/2)}{\alpha\Gamma(3-\alpha/2)\Gamma(\alpha)}\right]^{\frac{2}{\alpha-6}}$$
$$\Delta(\alpha) = \left[\frac{1.02\Gamma(\alpha)C_{SP}(\alpha)}{\Gamma(\alpha/2)\Gamma(1+\alpha/2)}\right]^{\frac{2}{\alpha-6}} \tilde{\sigma}_R^2\left[Q_m(\alpha)\right]^{2-\frac{\alpha}{2}} \tag{128}$$

Substituting Eq. (127) into Eq. (122), the large-scale logarithmic intensity fluctuation variance of spherical wave including inner scale effect is obtained, and its expression is

$$\sigma^2_{\ln X,SP}(l_0,\alpha) = -\frac{\alpha\Gamma(3-\alpha/2)}{120\Gamma(1-\alpha/2)\sin(\alpha\pi/4)}\tilde{\sigma}_R^2 \times \left[\frac{Q_m(\alpha)}{1+d_1(\alpha)Q_m(\alpha)+d_1(\alpha)Q_m(\alpha)\Delta(\alpha)}\right]^{3-\alpha/2} \tag{129}$$

The variance expression of large-scale intensity fluctuation of spherical wave including outer scale effect [24] is

$$\sigma^2_{\ln X,SP}(L_0,\alpha) = -\frac{\alpha\Gamma(3-\alpha/2)}{120\Gamma(1-\alpha/2)\sin(\alpha\pi/4)}\tilde{\sigma}_R^2 \times \left[\frac{Q_0(\alpha)Q_m(\alpha)}{Q_0(\alpha)+d_1(\alpha)Q_m(\alpha)Q_0(\alpha)+d_1(\alpha)Q_0(\alpha)Q_m(\alpha)\Delta(\alpha)+Q_m(\alpha)}\right]^{3-\alpha/2} \tag{130}$$

The variance expression of small-scale logarithmic intensity fluctuation of spherical wave is

$$\sigma^2_{\ln Y,SP}(l_0,\alpha) = -\frac{\alpha}{(\alpha-2)\Gamma(1-\alpha/2)\sin(\alpha\pi/4)}\tilde{\sigma}_R^2\eta^{1-\frac{\alpha}{2}}_{Y,SP}(\alpha) \tag{131}$$

Under the condition of arbitrary turbulence intensity from weak to strong, the variance expression of small-scale logarithmic intensity fluctuation of spherical wave is

$$\sigma^2_{\ln Y,SP}(l_0,\alpha)=\begin{cases}0.51\sigma^2_{I,SPvk}(\alpha) & L/[k\rho^2_{SP}(\alpha)]\ll 1\\ \ln 2 & L/[k\rho^2_{SP}(\alpha)]\gg 1\end{cases} \tag{132}$$

Under arbitrary turbulence intensity from weak to strong, the asymptotic expression of the dimensionless high-pass cutoff spatial frequency $\eta_{Y,SP}(\alpha)$ is

$$\begin{aligned}\eta_{Y,SP}(\alpha)&=c_{3,SP}(\alpha)+\frac{c_{4,SP}(\alpha)L}{k\rho^2_{SP}(\alpha)}\\ &\approx\begin{cases}c_{3,SP}(\alpha) & L/\left[k\rho^2_{SP}(\alpha)\right]\ll 1\\ c_{4,SP}(\alpha)L/\left[k\rho^2_{SP}(\alpha)\right] & L/\left[k\rho^2_{SP}(\alpha)\right]\gg 1\end{cases}\end{aligned} \tag{133}$$

According to different conditions,(133) is substituted into (131) respectively, and (132) is solved simultaneously. The expressions of $c_{3,SP}(\alpha)$ and $c_{4,SP}(\alpha)$ are obtained as follows

$$c_{3,SP}(\alpha)=\left[-\frac{0.51\sigma^2_{I,SPvk}(\alpha)(\alpha-2)\Gamma(1-\alpha/2)\sin(\alpha\pi/4)}{\tilde{\sigma}^2_R\cdot\alpha}\right]^{\frac{2}{2-\alpha}} \tag{134}$$

$$c_{4,SP}(\alpha)=\left[-\frac{\ln 2\cdot(\alpha-2)\Gamma(1-\alpha/2)\sin(\alpha\pi/4)}{\tilde{\sigma}^2_R\cdot\alpha}\right]^{\frac{2}{2-\alpha}}\times\frac{k\rho^2_{SP}(\alpha)}{L} \tag{135}$$

Substituting Eq. (134) and Eq. (135) into Eq. (133), the expression of $\eta_{Y,SP}$ is obtained as

$$\begin{aligned}\eta_{Y,SP}(\alpha)=&\left[-\frac{\alpha}{0.51(\alpha-2)\Gamma(1-\alpha/2)\sin(\alpha\pi/4)}\frac{\tilde{\sigma}^2_R}{\sigma^2_{I,SPvk}(\alpha)}\right]^{\frac{2}{\alpha-2}}\\ &\times\left(1+0.73^{\frac{2}{\alpha-2}}\sigma^{\frac{4}{\alpha-2}}_{I,SPvk}(\alpha)\right)\end{aligned} \tag{136}$$

Substituting Eq. (136) into Eq. (131), the variance expression of small-scale logarithmic intensity fluctuation of spherical wave is obtained as follows:

$$\sigma^2_{\ln Y,SP}(l_0,\alpha)\cong 0.51\sigma^2_{I,SPvk}(\alpha)\left(1+0.73^{\frac{2}{\alpha-2}}\sigma^{\frac{4}{\alpha-2}}_{I,SPvk}\right)^{1-\frac{\alpha}{2}} \tag{137}$$

where $\sigma^2_{I,SPvk}(\alpha)$ denotes the intensity scintillation index of the spherical wave under the generalized von Kármán spectrum in weak turbulence.

The cutoff frequency of the small-scale spatial filter depends on the inner scale, and the small-scale logarithmic intensity fluctuation variance of the spherical wave given by Eq. (137) also includes the inner scale effect. Because the influence of the outer scale on the variance of the small-scale logarithmic light intensity fluctuation is very small, it is neglected here. Substituting Eq. (129), Eq. (130) and Eq. (137) into Eq. (119), the intensity scintillation index of spherical wave under generalized von Kármán spectrum with arbitrary turbulence intensity including inner scale and outer scale effects is obtained. The expression [24] is

$$\begin{aligned}\sigma^2_{I,SP}(l_0,L_0,\alpha)=\exp\Bigg\{&\beta_4(\alpha)\tilde{\sigma}^2_R\left[\frac{Q_m(\alpha)}{\beta_5(\alpha)}\right]^{3-\frac{\alpha}{2}}\\ &-\beta_4(\alpha)\tilde{\sigma}^2_R\left[\frac{Q_0(\alpha)Q_m(\alpha)}{\beta_5(\alpha)Q_0(\alpha)+Q_m(\alpha)}\right]^{3-\frac{\alpha}{2}}\\ &+0.51\,\sigma^2_{I,SPvk}(\alpha)\left(1+0.73^{\frac{2}{\alpha-2}}\sigma^{\frac{4}{\alpha-2}}_{I,SPvk}(\alpha)\right)^{1-\frac{\alpha}{2}}\Bigg\}-1,\\ &0\le\tilde{\sigma}^2_R<\infty\end{aligned} \tag{138}$$

The expressions of $\beta_4(\alpha)$ and $\beta_5(\alpha)$ are

$$\begin{aligned}\beta_4(\alpha)&=-\frac{\alpha\Gamma(3-\alpha/2)}{120\Gamma(1-\alpha/2)\sin(\alpha\pi/4)}\\ \beta_5(\alpha)&=1+d_1(\alpha)Q_m(\alpha)+d_1(\alpha)Q_m(\alpha)\Delta(\alpha)\end{aligned} \tag{139}$$

(3) The intensity scintillation index of spherical wave under the condition of generalized modified atmospheric spectrum with inner scale

The expression of the intensity scintillation index of spherical wave under the condition of generalized modified atmospheric spectrum with inner scale [20, 25] is

$$\sigma^2_{I,SP}(\alpha,D,l_0)=\exp\left[\sigma^2_{\ln X,SP}(\alpha,D,l_0)+\sigma^2_{\ln Y,SP}(\alpha,D,l_0)\right]-1 \tag{140}$$

The large-scale logarithmic intensity fluctuation variance expression of spherical wave [20, 25] is

$$\sigma^2_{\ln X,SP}(\alpha,D,l_0)=\frac{-\alpha\Gamma(3-\alpha/2)\,\tilde{\sigma}_R^2}{4\Gamma(1-\alpha/2)\sin(\alpha\pi/4)}\int_0^1\xi^2(1-\xi)^2\times\left[\frac{\eta_{xd\xi}Q_l(\alpha)}{\eta_{xd\xi}+Q_l(\alpha)}\right]^{3-\alpha/2}\times\left\{1+\frac{a_1\Gamma(7/2-\alpha/2)}{\Gamma(3-\alpha/2)}\left[\frac{\eta_{xd\xi}}{\eta_{xd\xi}+Q_l(\alpha)}\right]^{\frac{1}{2}}-\frac{b_1\Gamma(3+\beta/2-\alpha/2)}{\Gamma(3-\alpha/2)}\left[\frac{\eta_{xd\xi}}{\eta_{xd\xi}+Q_l(\alpha)}\right]^{\frac{\beta}{2}}\right\}d\xi \tag{141}$$

where η_X is the dimensionless low-pass spatial cutoff frequency. $d=\sqrt{kD^2/(4L)}$ is the normalized receiving-aperture parameter, $\eta_{xd\xi}$ is the modified cut-off frequency, and $c_2(\alpha)$ is a constant. The expressions of η_X, $\eta_{xd\xi}$ and $c_2(\alpha)$ are

$$\begin{aligned}\eta_{xd\xi}&=\frac{\eta_X}{1+d^2\xi^2\eta_X/4}\\ \eta_X&=\frac{1/c_2(\alpha)}{1+\left\{\left[\frac{1.02\Gamma(\alpha)}{\Gamma(\alpha/2)\Gamma(1+\alpha/2)}C_{sp}(\alpha)\right]^{\frac{2}{\alpha-6}}\tilde{\sigma}_R^2\left[Q_l(\alpha)\right]^{2-(\alpha/2)}\right\}}\\ c_2(\alpha)&=\left[-\frac{58.8\Gamma(1-\alpha/2)\sin(\alpha\pi/4)\Gamma(\alpha/2)\Gamma(1+\alpha/2)}{\alpha\Gamma(3-\alpha/2)\Gamma(\alpha)}\right]^{\frac{2}{\alpha-6}}\end{aligned} \tag{142}$$

The variance expression of small-scale logarithmic intensity fluctuation of spherical wave with finite receiving aperture is

$$\sigma^2_{\ln Y,SP}(\alpha,D,l_0)=\frac{-\alpha\,\tilde{\sigma}_R^2}{2\Gamma\left(1-\frac{\alpha}{2}\right)\sin\left(\frac{\alpha\pi}{4}\right)}\int_0^1\left(\frac{d^2\xi^2}{4}\right)^{\frac{\alpha}{2}-1}\times\exp\left(\frac{d^2\xi^2\eta_Y}{4}\right)\Gamma\left(1-\frac{\alpha}{2},\frac{d^2\xi^2\eta_Y}{4}\right)d\xi \tag{143}$$

The expression of η_Y is

$$\eta_Y=\left[-\frac{\alpha}{0.51(\alpha-2)\Gamma(1-\alpha/2)\sin(\alpha\pi/4)}\frac{\tilde{\sigma}_R^2}{\sigma^2_{I,SPhill}(\alpha)}\right]^{\frac{2}{\alpha-2}}\times\left(1+0.73^{\frac{2}{\alpha-2}}\sigma^{\frac{4}{\alpha-2}}_{I,SPhill}(\alpha)\right) \tag{144}$$

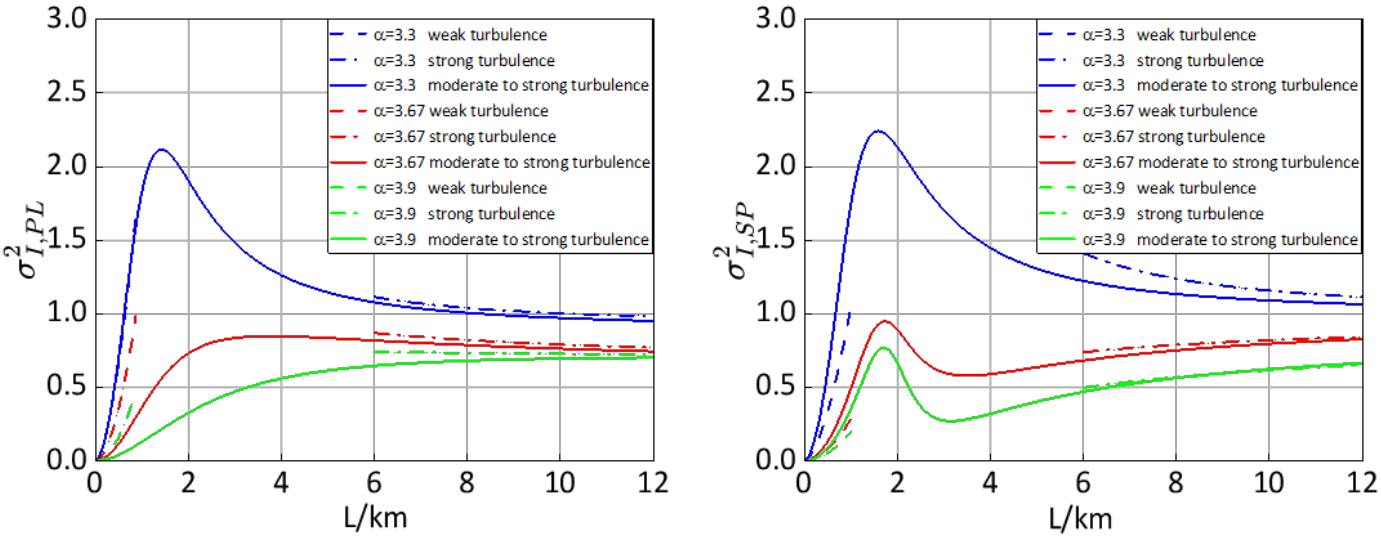
where $\sigma^2_{I,SPhill}(\alpha)$ represents the intensity scintillation index of the spherical wave under the generalized modified atmospheric spectrum in weak turbulence.

3.4 Analysis of the variation characteristics of the intensity scintillation index of plane wave and spherical wave

3.4.1 Analysis of the variation characteristics of the intensity scintillation index of plane wave and spherical wave of non-Kolmogorov spectrum

(1) Analysis of the variation characteristics of light intensity scintillation index with transmission distance

According to the expression (68) of the intensity scintillation index of plane wave with arbitrary turbulence intensity under non-Kolmogorov spectrum, the expression (42) of the intensity scintillation index of plane wave with weak turbulence intensity and the expression (48) of the intensity scintillation index of plane wave with saturated strong turbulence intensity under non-Kolmogorov spectrum, taking λ = 525 nm, non-Kolmogorov refractive index structure constant $\tilde{C}_n^2=10^{-14}m^{3-\alpha}$, selecting the generalized power-law spectral index $\alpha=3.3,\ 3.67,\ 3.9$, and the transmission distance is L ~ 0-12 km, the curve of the intensity scintillation index of plane wave with the change of transmission distance is obtained, as shown in Figure 5 (a). According to the expression of the scintillation index of spherical wave intensity with arbitrary turbulence intensity (117), the expression of the scintillation index of spherical wave intensity with weak turbulence intensity (99) and the expression of the scintillation index of spherical wave intensity with saturated strong turbulence intensity (102) under the condition of non-Kolmogorov spectrum, the curve of the scintillation index of spherical wave intensity with the transmission distance is obtained, as shown in Figure 5 (b). The solid line represents the intensity scintillation index of any turbulence intensity, the dashed line represents the intensity scintillation index of weak turbulence, and the dash-dotted line represents the intensity scintillation index of strong turbulence. Different symbols correspond to three different α. In the numerical analysis, the generalized power-law spectral index α is restricted to the range $3<\alpha<4$, because the closed-form expressions used here (e.g., Eq. (156)) are derived for this interval and measured values cluster near the Kolmogorov value, whereas the spectral model itself is defined for $3<\alpha<5$. The value $\alpha=11/3$ corresponds to the classical Kolmogorov turbulence spectrum. To investigate the influence of the spectral index on optical wave propagation, three representative values, $\alpha=3.3$, 11/3, and 3.9, are selected to characterize cases below, equal to, and above the classical Kolmogorov value, respectively.



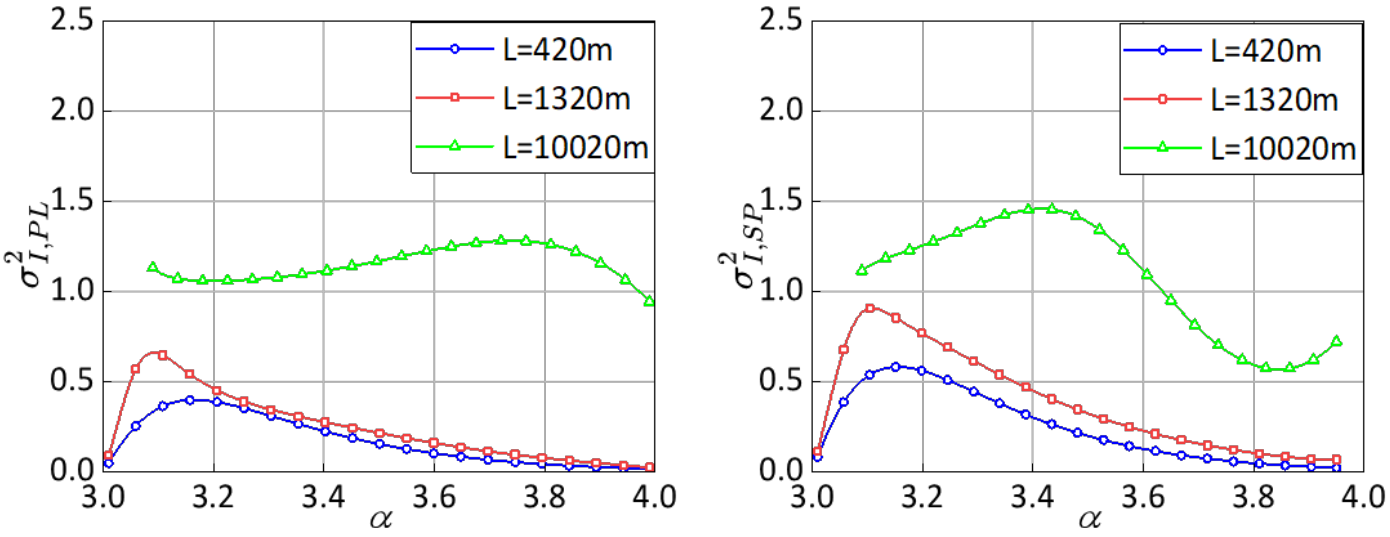
(a) Plane wave (b) Spherical wave

Figure 5. Optical intensity scintillation index versus propagation distance under the non-Kolmogorov spectrum.

According to Figure 5 (a), it can be seen that the intensity scintillation index of plane waves under non-Kolmogorov spectral conditions increases rapidly with the propagation distance in a short distance, and the smaller the α is, the higher the peak intensity scintillation index is, indicating that the refractive index fluctuation of higher spatial frequency has a stronger influence. With the increase of distance, the intensity scintillation index gradually decreases and tends to be saturated after reaching the peak, which is the result of the combined effect of multiple scattering and the loss of spatial coherence, so that the intensity fluctuation is smoothed. The light intensity scintillation index of weak turbulence is basically consistent with the light intensity scintillation index of arbitrary turbulence intensity in a short distance, while the light intensity scintillation index of saturated strong turbulence is close to the saturation value of the light intensity scintillation index of arbitrary turbulence intensity in a long distance. It shows that the three light intensity scintillation index expressions of weak turbulence, arbitrary turbulence intensity and saturated strong turbulence are asymptotically consistent in their respective applicable ranges. According to Figure 5 (b), it can be seen that the increase of the transmission distance of the intensity scintillation index of the spherical wave under the non-Kolmogorov spectrum increases first and then saturates. The smaller the α is, the more intense the fluctuation of the intensity scintillation index, indicating that the intensity scintillation index of the spherical wave is similar to that of the plane wave. With the increase of propagation distance, the influence of wavefront curvature and geometric diffusion of spherical wave, the scintillation index of light intensity decreases obviously at medium distance, forms depression at large distance, and then rises slowly and tends to be stable. By comparing Figure 5 (a) and Figure 5 (b), it can be seen that the intensity scintillation index of the plane wave shows a more regular single peak followed by saturation, whereas that of the spherical wave is shaped by the point source divergence characteristics. The response to refractive index fluctuations near the Fresnel scale and at higher spatial frequencies is relatively more obvious, resulting in a higher intensity scintillation peak than that of the plane wave in the moderate-turbulence region around the peak, although in the weak-turbulence region the spherical-wave scintillation index remains lower than that of the plane wave. The difference of the intensity scintillation index between the plane wave and the spherical wave shows that the light wave propagation mode changes the change process of the intensity scintillation index. With the increase of transmission distance, the intensity scintillation index of plane wave and spherical wave tends to be saturated in the long-distance region.

(2) Analysis of the variation characteristics of light intensity scintillation index with α

According to the expression (68) of the plane wave intensity scintillation index of arbitrary turbulence intensity under non-Kolmogorov spectral conditions, the wavelength $\lambda = 525$ nm, $\tilde{C}_n^2 = 10^{-14}m^{3-\alpha}$, $3 < \alpha < 4$, and the transmission distances $L = 420$ m, 1320 m and 10020 m, respectively. The curve of



(a) Plane wave (b) Spherical wave

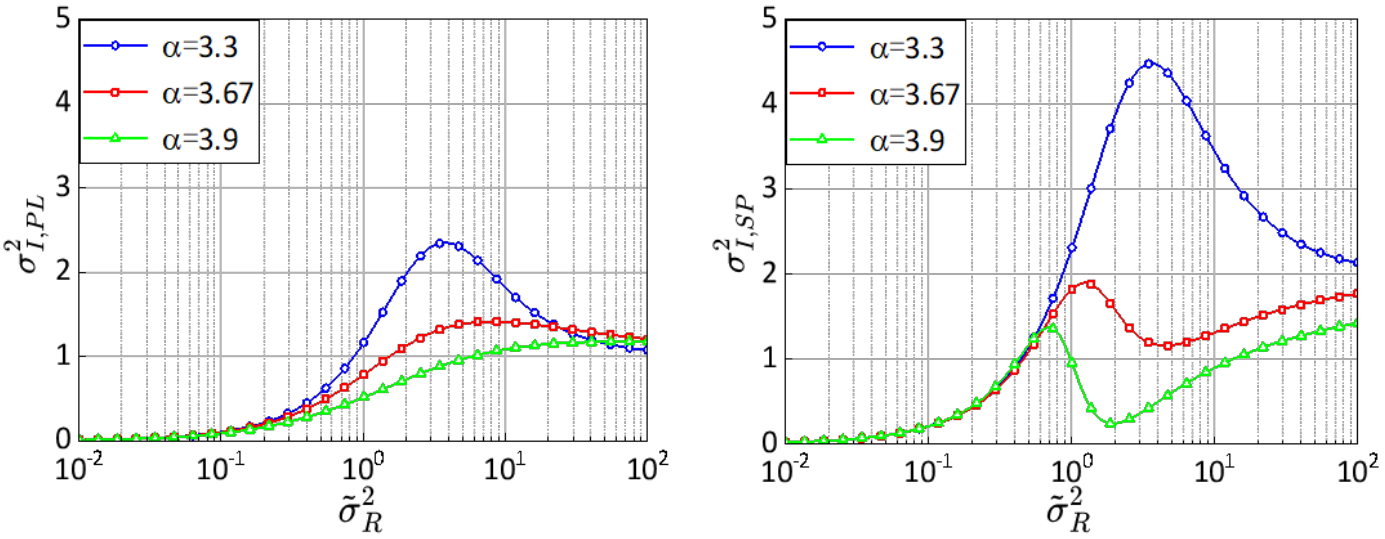
Figure 6. Optical intensity scintillation index versus α under the non-Kolmogorov spectrum.

the plane wave intensity scintillation index with α is obtained, as shown in Figure 6 (a). According to the expression (117) of the intensity scintillation index of spherical wave with arbitrary turbulence intensity under non-Kolmogorov spectral conditions, the curve of the intensity scintillation index of spherical wave with α is obtained, as shown in Figure 6 (b). Three curves of different symbols correspond to three different propagation distances.

According to Figure 6 (a), it is shown that under a given transmission distance, the plane wave intensity scintillation index reaches a larger value at a smaller power-law spectral index region $\alpha \approx 3.1$, and then decreases gradually with the increase of α. This shows that when α is small, the influence of the refractive index fluctuation in the higher spatial frequency range increases, which aggravates the light intensity scintillation effect. With the increase of propagation distance, the scintillation index of light intensity increases as a whole, and still maintains a high value in the larger α region, which is due to the enhancement of turbulence accumulation effect during long-distance propagation. Figure 6 (b) shows that the variation of the intensity scintillation index of the spherical wave with α is more complex than that of the plane wave. The peak value also appears at a smaller α at short and medium distances, and the peak value is slightly higher than that of the plane wave. Under the condition of long distance, the intensity scintillation index reaches a higher peak near α about 3.4-3.5, then decreases obviously, and increases again with the increase of α. This is because the intensity scintillation index of spherical wave is more affected by wavefront curvature and geometric diffusion. By comparing Figure 6 (a) and Figure 6 (b), it can be seen that the intensity scintillation index of plane wave changes smoothly with α, and the intensity scintillation index of spherical wave changes strongly with α under the same conditions. With the distance of 10020 m, the variation characteristics of the intensity scintillation index of the two wavefronts show a transition to the medium-strong turbulent saturation region. Due to the spatial filtering characteristics of the wavefront curvature, the intensity scintillation index of the spherical wave fluctuates with α and the intensity scintillation index of the plane wave is obviously different, which reflects the more complex random field redistribution mechanism of the spherical wave under different α conditions.

(3) Analysis of the variation characteristics of light intensity scintillation index with generalized Rytov variance $\tilde{\sigma}_R^2$

According to the expression (68) of the plane wave intensity scintillation index of arbitrary turbulence intensity under non-Kolmogorov spectral conditions, the wavelength $\lambda = 525$ nm, $\tilde{C}_n^2 = 10^{-14} m^{3-\alpha}$, and $3 < \alpha < 4$ are selected to obtain the curve of the plane wave intensity scintillation index with the generalized Rytov variance $\tilde{\sigma}_R^2$, as shown in Figure 7 (a). According to the expression (117) of the intensity scintillation index of spherical waves with arbitrary turbulence intensity under non-Kolmogorov spectral conditions, the curve of the intensity scintillation index of spherical waves with the generalized Rytov variance $\tilde{\sigma}_R^2$ is obtained, as shown in Figure 7 (b).



(a) Plane wave (b) Spherical wave

Figure 7. Optical intensity scintillation index versus $\tilde{\sigma}_R^2$ under the non-Kolmogorov spectrum.

According to Figure 7 (a), the intensity scintillation index of plane wave increases first and then tends to saturation with the increase of $\tilde{\sigma}_R^2$. The intensity scintillation index of plane wave in weak turbulence area is close to zero and rises slowly. After entering the medium turbulence area, it increases rapidly and peaks. The peak value is the highest when $\alpha = 3.3$ and the peak value is the lowest when $\alpha = 3.9$. This is because the smaller the α, the greater the influence of the refractive index fluctuation of the higher spatial frequency on the plane wave scintillation. The intensity scintillation index gradually decreases and tends to be saturated after reaching the peak value. This is because multiple scattering and the loss of spatial coherence under strong turbulence limit the increase of intensity fluctuation. According to Figure 7 (b), the variation characteristics of the scintillation index of the spherical wave are similar to those of the plane wave. When $\alpha = 3.3$, the peak value is higher than that of the plane wave, and when $\alpha = 3.9$, it falls back and recovers after the peak value. This is because the point source divergence characteristics of the spherical wave are more affected by the fluctuation of the refractive index of the higher spatial frequency. The spatial filtering effect leads to a higher scintillation peak in the medium-intensity turbulent region, and a fall and structured fluctuation after the peak. By comparing Figure 7 (a) and (b), it can be seen that the variation characteristics of the intensity scintillation index of the plane wave are close to the single peak and then slowly saturated. The variation characteristics of the intensity scintillation index of the spherical wave show stronger peaks and more obvious transition characteristics. Under the same $\tilde{\sigma}_R^2$ condition, the peak value of the spherical wave is generally slightly higher than that of the plane wave. This is because the light wave propagation mode changes the variation characteristics of the intensity scintillation index under different atmospheric turbulence intensities.

3.4.2 *Analysis of the variation characteristics of the intensity scintillation index of the plane wave and spherical wave of the generalized von Kármán spectrum*

(1) Analysis of the variation characteristics of light intensity scintillation index with transmission distance

According to the generalized von Kármán spectrum under the condition of arbitrary turbulence intensity plane wave intensity scintillation index expression (91), weak turbulence plane wave intensity scintillation index expression (43) and saturated strong turbulence plane wave intensity scintillation index expression (54), taking the wavelength $\lambda = 525$ nm, $\tilde{C}_n^2 = 10^{-14} m^{3-\alpha}$, selecting $\alpha = 3.3,\ 3.67,\ 3.9$, the transmission distance is $L \sim$ 0-12 km, the inner scale $l_0 = 1$ mm, the outer scale $L_0 = 1$ m, the curve of the plane wave intensity scintillation index with the transmission distance is obtained, as shown in Figure 8 (a). According to the generalized von Kármán spectrum under the condition of arbitrary turbulence intensity spherical wave light intensity scintillation index expression (138), weak turbulence spherical wave light intensity scintillation index expression (100) and saturated strong turbulence spherical wave light intensity scintillation index expression (105), the curve of spherical wave light intensity scintillation index

with transmission distance is obtained, as shown in Figure 8 (b). The solid line represents the intensity scintillation index of any turbulence intensity, the dashed line represents the intensity scintillation index of weak turbulence, and the dash-dotted line represents the intensity scintillation index of strong turbulence. Different symbols correspond to three different α.

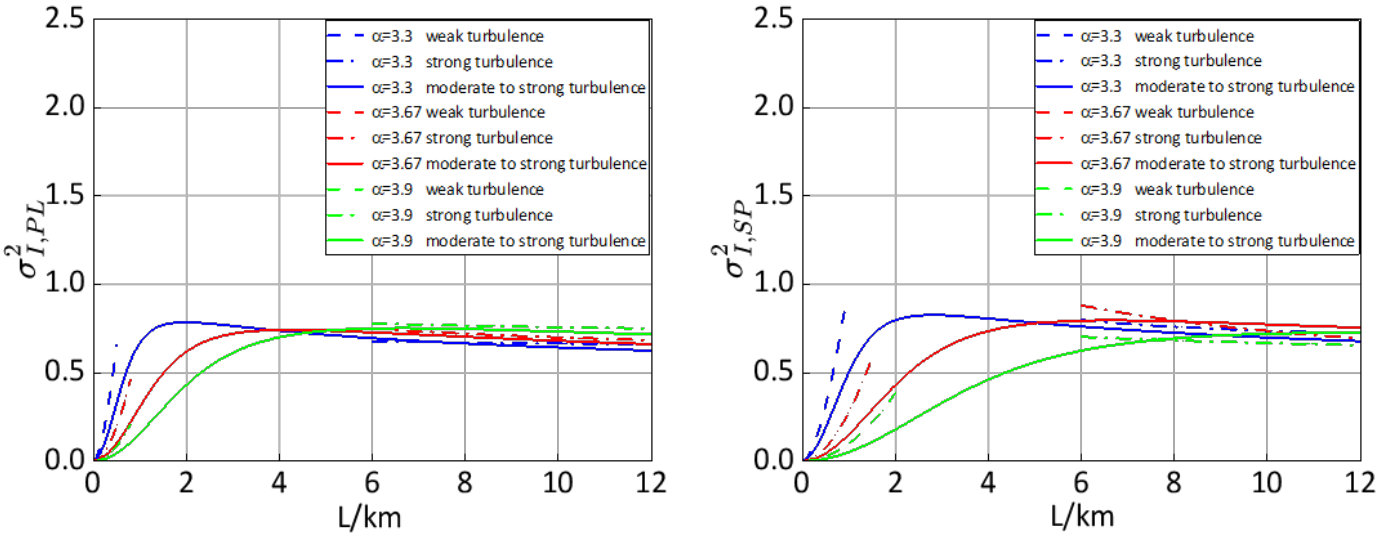
According to Figure 8 (a), the plane wave intensity scintillation index of the generalized von Kármán spectrum increases rapidly with the propagation distance, and then gradually decreases and saturates after reaching the peak value. The smaller the α is, the higher the peak value is and appears earlier, indicating that the lower α corresponds to the stronger small-scale disturbance. With the increase of transmission distance, multiple scattering and the loss of spatial coherence weaken the light intensity fluctuation. The scintillation index of plane wave light intensity decreases slowly and tends to be approximately saturated at medium and long distances. The expressions of weak turbulence and strong turbulence are approximate to the expressions of arbitrary turbulence intensity in their respective ranges. In Figure 8 (b), the intensity scintillation index of spherical wave increases rapidly to the peak value and then decreases slowly and tends to saturation with the increase of transmission distance. Subsequently, with the increase of transmission distance, the intensity scintillation index of spherical wave decreases slightly and then tends to be saturated. By comparing Figure 8 (a) and (b), it can be seen that the intensity scintillation index of the plane wave changes smoothly, and the peak value of the intensity scintillation index of the spherical wave is slightly higher than that of the plane wave. The peak value of the intensity scintillation index is because the wavefront curvature of the spherical surface is superimposed with the turbulence modulation in the moderate-turbulence region around the peak, which makes the light intensity fluctuate more. At medium and long distances, the intensity scintillation index of plane wave and spherical wave tends to be saturated.

(2) Analysis of the variation characteristics of light intensity scintillation index with α

According to the expression(91) of the intensity scintillation index of the plane wave with arbitrary turbulence intensity under the generalized von Kármán spectrum, the wavelength $\lambda = 525$ nm, $\tilde{C}_n^2 = 10^{-14} m^{3-\alpha}$, selecting $3 < \alpha < 4$, the transmission distance is $L = 420$ m, 1320 m and 10020 m, the inner scale is $l_0 = 1$ mm and 10 mm, and the outer scale is $L_0 = 1$ m. The curve of the intensity scintillation index of the plane wave with α is obtained, as shown in Figure 9 (a). According to the expression (138) of the scintillation index of spherical wave with arbitrary turbulence intensity under the condition of generalized von Kármán spectrum, the curve of the scintillation index of spherical wave with α is obtained, as shown in Figure 9 (b). The solid lines with markers represent the results for $l_0 = 1$ mm, and the solid lines without markers represent the results for $l_0 = 10$ mm.

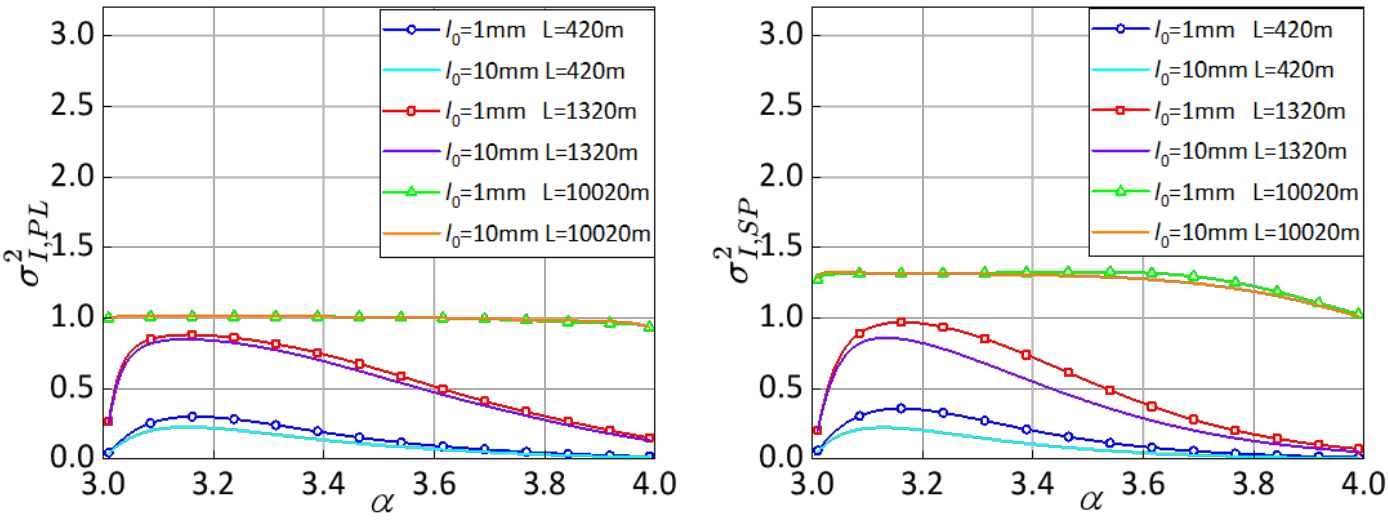
According to Figure 9 (a), under the condition of generalized von Kármán spectrum, when the transmission distance is 420 m and 1320 m respectively, the intensity scintillation index of plane wave has a peak at $\alpha \approx 3.1$, and decreases gradually with the increase of α. This is because a small α enhances the refractive index fluctuation at high spatial frequencies and thus increases the intensity scintillation. When the transmission distance increases to 10020 m, the light intensity scintillation index remains at a large value as a whole, which is due to the cumulative atmospheric turbulence effect in long-distance transmission. When the inner scale increases from 1 mm to 10 mm, the scintillation index of the light intensity in the short and medium transmission distance range decreases as a whole, and the peak value also decreases. This is due to the increase of the inner scale, which makes the turbulent energy attenuation at the high spatial frequency more obvious, thus weakening the influence of the refractive index fluctuation of the higher spatial frequency on the plane wave intensity scintillation. According to Figure 9 (b), the intensity scintillation index of the spherical wave has similar variation characteristics to that of the plane wave. The parameter change has a greater influence on the intensity scintillation index of the spherical wave. When the transmission distance is 420 m and 1320 m respectively, the peak intensity scintillation index of the spherical wave is slightly higher than that of the plane wave. This is because the spherical wave is affected by the wavefront curvature and turbulence in the moderate-turbulence region around the peak, which enhances the intensity fluctuation. When the transmission distance is 10020 m, the intensity scintillation index of the two inner scales is higher, and it decreases when α is larger. This is because the influence of spherical wave on the change of α increases in long-distance transmission.

(3) Analysis of the variation characteristics of light



(a) Plane wave (b) Spherical wave

Figure 8. Optical intensity scintillation index versus propagation distance under the generalized von Kármán spectrum.



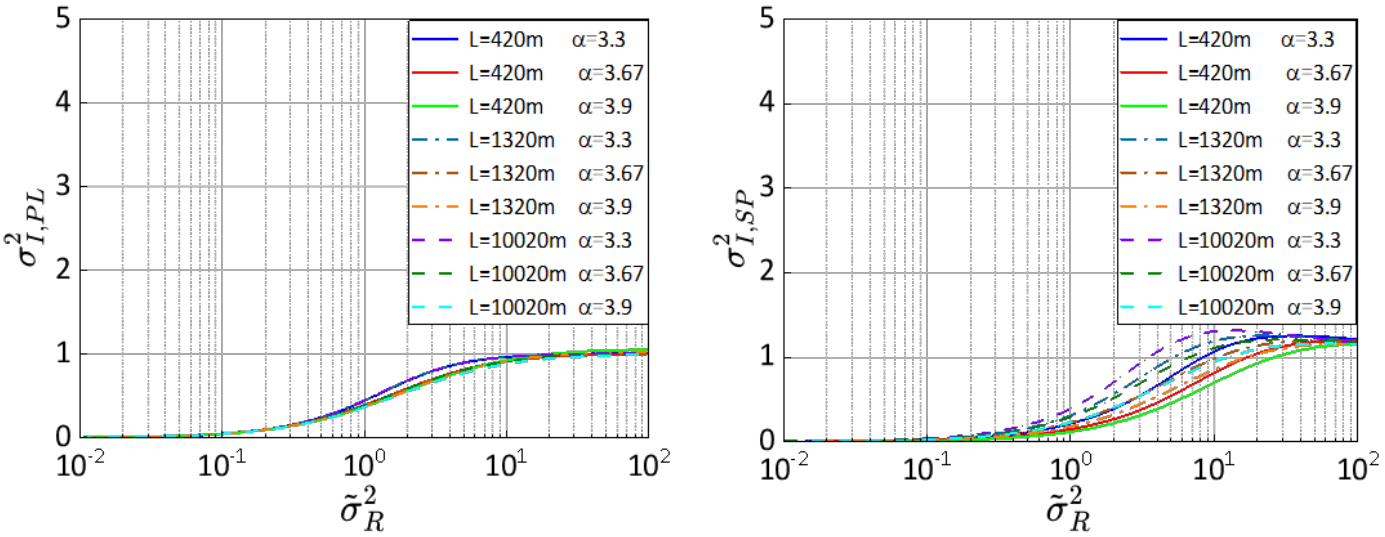
(a) Plane wave (b) Spherical wave

Figure 9. Optical intensity scintillation index versus α under the generalized von Kármán spectrum.

intensity scintillation index with generalized Rytov variance $\tilde{\sigma}_R^2$

According to the expression (91) of the intensity scintillation index of the plane wave with arbitrary turbulence intensity under the generalized von Kármán spectrum, the wavelength $\lambda = 525$ nm, $\tilde{C}_n^2 = 10^{-14} m^{3-\alpha}$,$3 < \alpha < 4$ are selected, the inner scale is l_0 = 1 mm and 10 mm, and the outer scale is $L_0 = 1$ m. The curve of the intensity scintillation index of the plane wave with the generalized Rytov variance is obtained, as shown in Figure 10 (a). According to the expression (138) of the intensity scintillation index of spherical waves with arbitrary turbulence intensity under the generalized von Kármán spectrum, the curve of the intensity scintillation index of spherical waves with the generalized Rytov variance $\tilde{\sigma}_R^2$ is obtained, as shown in Figure 10 (b). The solid lines represent the results for $L = 420$ m, the dash-dotted lines those for $L = 1320$ m, and the dashed lines those for $L = 10020$ m.

According to Figure 10 (a), under the condition of generalized von Kármán spectrum, the intensity scintillation index of plane wave increases monotonically with $\tilde{\sigma}_R^2$ and gradually saturates. Different propagation distances and spectral indices slightly shift the transition region. According to Figure 10 (b), the intensity scintillation index of the spherical wave increases monotonically with $\tilde{\sigma}_R^2$ and tends to be saturated. The intermediate



(a) Plane wave (b) Spherical wave

Figure 10. Optical intensity scintillation index versus $\tilde{\sigma}_R^2$ under the generalized von Kármán spectrum.

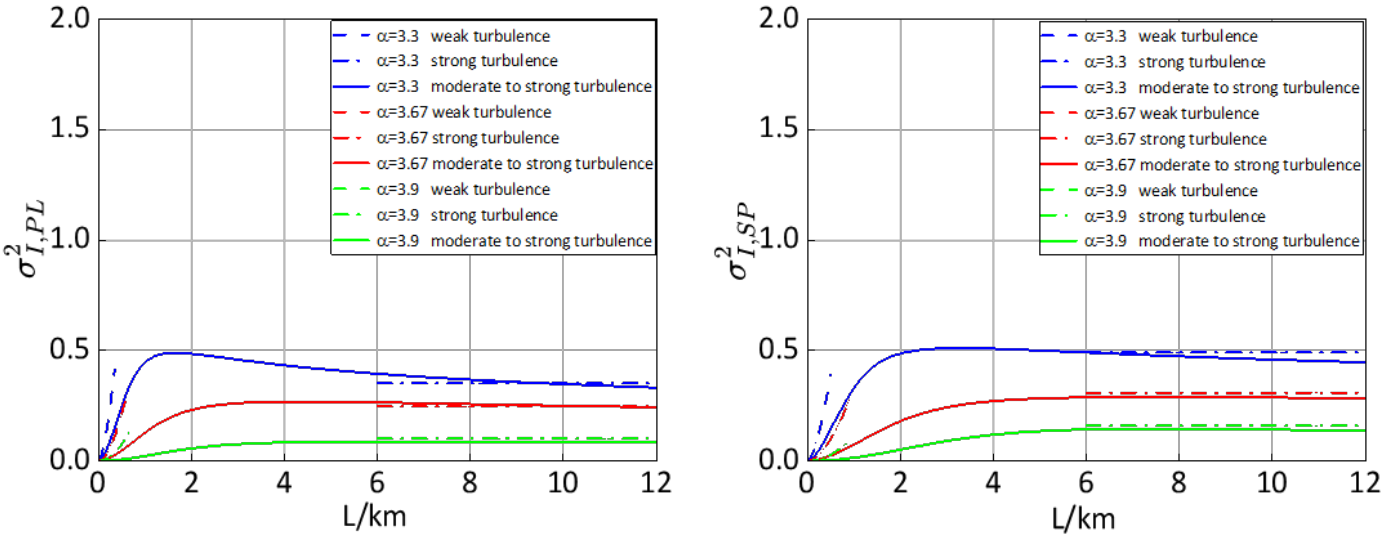
transition process is more obvious than the plane wave. The intensity scintillation index curve has a more prominent bulge in the middle turbulent region, and the peak value is slightly higher than that of the plane wave. The distribution of the intensity scintillation index curve at different transmission distances is more discrete. This is because the point source divergence characteristics of the spherical wave are more susceptible to the filtering effect of the spatial frequency. By comparing Figure 10 (a) and (b), it can be seen that the light intensity scintillation index curve of the plane wave is more concentrated and the change is gentler, and the light intensity scintillation index curve of the spherical wave is more dispersed and the peak characteristics are more prominent. With the increase of $\tilde{\sigma}_R^2$, the intensity scintillation index of plane wave and spherical wave tends to be saturated, because the propagation mode of light wave mainly affects the change process of intensity scintillation and the strength of peak value.

3.4.3 Analysis of the variation characteristics of the intensity scintillation index of the plane wave and spherical wave of the generalized modified atmospheric spectrum

(1) Analysis of the variation characteristics of light intensity scintillation index with transmission distance

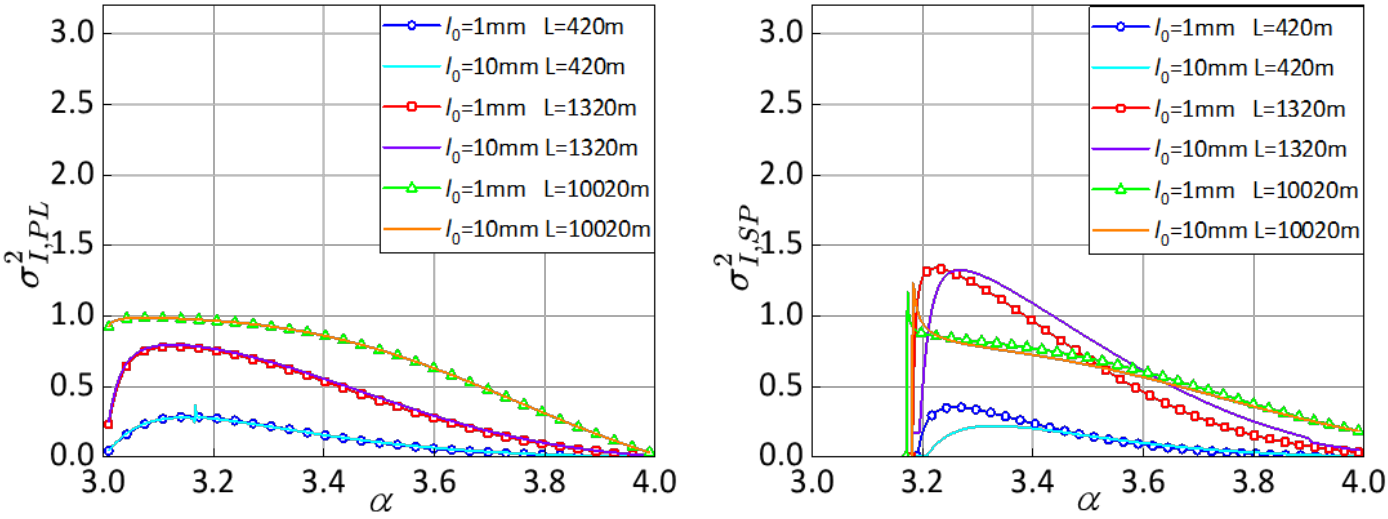
According to the generalized modified atmospheric spectrum under the condition of arbitrary turbulence intensity plane wave intensity scintillation index expression (93), weak turbulence plane wave intensity scintillation index expression (44) and saturated strong turbulence plane wave intensity scintillation index expression (59), $\lambda = 525$ nm, non-Kolmogorov refractive index structure constant $\tilde{C}_n^2 = 10^{-14} m^{3-\alpha}$, selecting $\alpha = 3.3,\ 3.67,\ 3.9$, transmission distance $L \sim$ 0-12 km, inner scale $l_0 = 1$ mm, spectrum correction parameters $a_1 = 1.802$, $b_1 = 0.254$ and $\beta = 7/6$, receiving aperture diameter D = 105 mm. The curve of the plane wave intensity scintillation index with the transmission distance is obtained, as shown in Figure 11 (a). According to the generalized modified atmospheric spectrum under arbitrary turbulence intensity spherical wave intensity scintillation index expression (140), weak turbulence spherical wave intensity scintillation index expression (101) and saturated strong turbulence spherical wave intensity scintillation index expression (108), the curve of spherical wave intensity scintillation index with transmission distance is obtained, as shown in Figure 11 (b). The solid line represents the intensity scintillation index of any turbulence intensity, the dashed line represents the intensity scintillation index of weak turbulence, and the dash-dotted line represents the intensity scintillation index of strong turbulence.

According to Figure 11 (a), under the condition of generalized modified atmospheric spectrum, the intensity scintillation index of plane wave first increases to the peak value and then slowly decreases and saturates with the increase of transmission distance, indicating that the atmospheric turbulence effect accumulates rapidly in the early stage of transmission, and the growth of the intensity scintillation index is gradually suppressed at long transmission distances. The expression of the



(a) Plane wave (b) Spherical wave

Figure 11. Optical intensity scintillation index versus propagation distance under the generalized modified atmospheric spectrum.



(a) Plane wave (b) Spherical wave

Figure 12. Optical intensity scintillation index versus α under the generalized modified atmospheric spectrum.

scintillation index of weak and strong turbulence is similar to the expression of the scintillation index of any turbulence intensity in short and long distances. According to Figure 11 (b), it is shown that the variation of the scintillation index of the spherical wave is similar to that of the plane wave, but the peak value is slightly higher than that of the plane wave, and the peak position moves slightly backward. This is due to the combined effect of the wavefront curvature and turbulence of the spherical wave, which enhances the intensity fluctuation. As the transmission distance increases, the intensity scintillation index gradually becomes saturated. By comparing Figure 11 (a) and (b), it can be seen that the intensity scintillation index of plane wave and spherical wave is relatively close. Both of them satisfy that the smaller α is, the stronger the intensity scintillation is, indicating that the refractive index fluctuation of higher spatial frequency under small α has a greater influence on the intensity fluctuation. The intensity scintillation index of the plane wave drops more obviously after reaching the peak, because the light wave propagation mode affects the peak and transition process of the intensity scintillation index. Under the same parameters, the wavefront curvature and geometric expansion effect of spherical wave alleviate the accumulation of light intensity fluctuation, making the intensity scintillation index of spherical wave more stable and

saturated than that of plane wave. This is because the propagation mode of light wave adjusts the intensity scintillation index in different atmospheric turbulence intensity intervals by changing the spatial filtering characteristics.

(2) Analysis of the variation characteristics of light intensity scintillation index with α

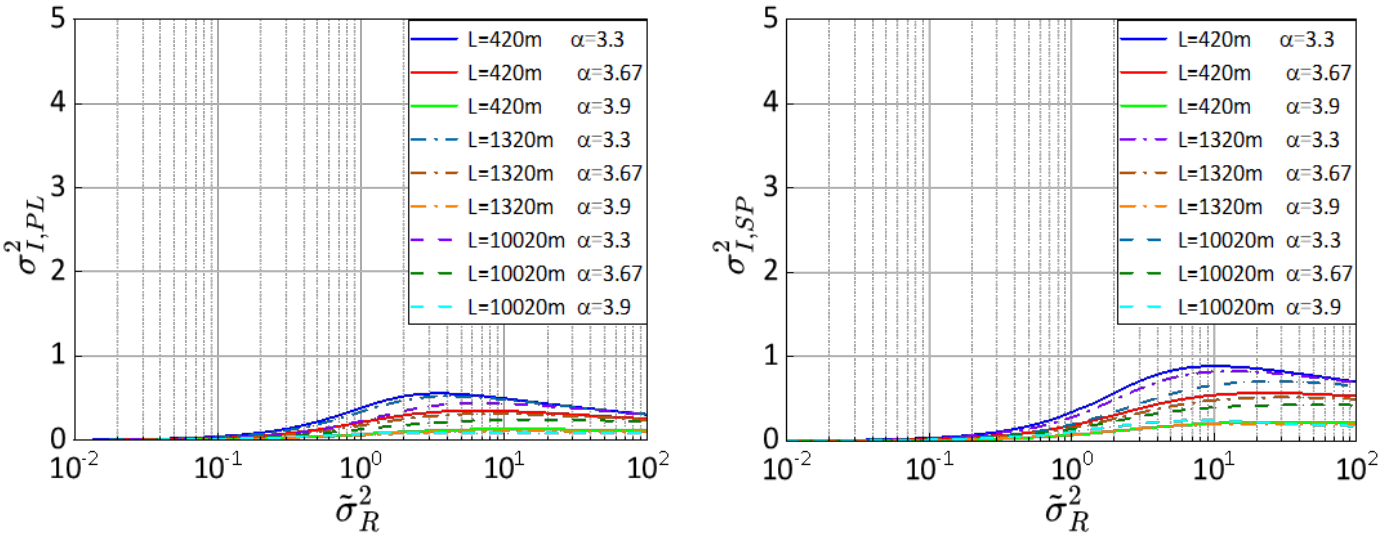
According to the expression (93) of the plane wave intensity scintillation index of arbitrary turbulence intensity under the generalized modified atmospheric spectrum condition, λ = 525 nm, the non-Kolmogorov refractive index structure constant $\tilde{C}_n^2 = 10^{-14}m^{3-\alpha}$, selecting $3 < \alpha < 4$, the transmission distance is L = 420 m, 1320 m and 10020 m, the inner scale is $l_0 = 1$ mm and 10 mm, the spectral correction parameters are $a_1 = 1.802$, $b_1 = 0.254$ and $\beta = 7/6$, and the receiving aperture diameter D = 105 mm. The curve of the plane wave intensity scintillation index with α is obtained, as shown in Figure 12 (a). According to the expression (140) of the intensity scintillation index of the spherical wave with arbitrary turbulence intensity of the generalized modified atmospheric spectrum, the curve of the intensity scintillation index of the spherical wave with α is obtained, as shown in Figure 12 (b). The results for l_0 = 1 mm are represented by the solid lines with markers, and those for l_0 = 10 mm by the solid lines without markers.

According to Figure 12 (a), under the generalized modified atmospheric spectrum condition, the variation of the intensity scintillation index of the plane wave shows non-monotonicity. The increase of the inner scale suppresses the atmospheric turbulence effect and reduces the intensity fluctuation. When the transmission distance is 420 m and 1320 m, the peak value of the intensity scintillation index of the plane wave appears at $\alpha \approx 3.1$, and decreases to the minimum when $\alpha \approx 4$. This is because the small α enhances the refractive index fluctuation of the higher spatial frequency and increases the intensity scintillation index. When the transmission distance is 10020 m, the intensity scintillation index of the two groups maintains a high value and decreases with the increase of α, which is due to the cumulative effect of atmospheric turbulence under long-distance transmission. According to Figure 12 (b), the spherical wave exhibits a stronger intensity scintillation response in a specific α range, and its peak gradient with α is steeper. This is because the spherical wave is not only affected by α, but also by wavefront curvature, geometric diffusion and power spectrum parameter coupling. By comparing Figure 12 (a) and (b), it can be seen that the two wave fronts tend to be saturated in the long-distance strong turbulence region, but the spherical wave is more affected by the change of the inner scale and α, and the intensity scintillation index curve of the spherical wave has obvious abrupt variation. This is because the spherical wave is affected by stronger phase disturbance and intensity fluctuation in the generalized modified atmospheric spectral model.

(3) Analysis of the variation characteristics of light intensity scintillation index with generalized Rytov variance $\tilde{\sigma}_R^2$

According to the expression (93) of the plane wave intensity scintillation index of arbitrary turbulence intensity under the generalized modified atmospheric spectrum, λ = 525 nm, the non-Kolmogorov refractive index structure constant $\tilde{C}_n^2 = 10^{-14}m^{3-\alpha}$, selecting $3 < \alpha < 4$, the transmission distances are L = 420 m, 1320 m and 10020 m, the inner scales are $l_0 = 1$ mm and 10 mm, the spectral correction parameters are $a_1 = 1.802$, $b_1 = 0.254$ and $\beta = 7/6$, and the receiving aperture diameter D = 105 mm. The curve of the plane wave intensity scintillation index with $\tilde{\sigma}_R^2$ is obtained, as shown in Figure 13 (a). According to the expression (140) of the intensity scintillation index of spherical wave with arbitrary turbulence intensity under the condition of generalized modified atmospheric spectrum, the curve of the intensity scintillation index of spherical wave with $\tilde{\sigma}_R^2$ is obtained, as shown in Figure 13 (b). The solid lines represent the results for L = 420 m, the dash-dotted lines those for L = 1320 m, and the dashed lines those for L = 10020 m.

According to Figure 13 (a), under the condition of generalized modified atmospheric spectrum, the intensity scintillation index of plane wave increases first and then tends to saturation with the increase of $\tilde{\sigma}_R^2$. Different propagation distances and different α will change the peak height and position. The intensity scintillation index curve of smaller α is higher as a whole. This is because under the condition of small α, the refractive index fluctuation of higher spatial frequency enhances the intensity scintillation, and long-distance transmission accumulates this effect. According to Figure 13 (b), the intensity scintillation index of spherical wave shows a similar change rule, the peak value is larger, and the overall intensity scintillation index curve is higher, which is more affected by the transmission distance and α. This is



(a) Plane wave (b) Spherical wave

Figure 13. Optical intensity scintillation index versus $\tilde{\sigma}_R^2$ under the generalized modified atmospheric spectrum.

because the wavefront curvature of spherical wave and atmospheric turbulence enhance the intensity fluctuation during transmission. By comparing Figure 13 (a) and (b), it can be seen that the intensity scintillation index of the plane wave changes more smoothly and the peak value is lower. The intensity scintillation index peak of the spherical wave is slightly higher and tends to be saturated at a larger $\tilde{\sigma}_R^2$. This is because the propagation mode of the light wave mainly affects the enhancement process and peak characteristics of the intensity scintillation.

Overall, the plane- and spherical-wave results differ mainly because of wavefront geometry and the way turbulence accumulates along the path. Plane waves have approximately parallel wavefronts, whereas spherical waves exhibit diverging wavefronts, resulting in different weighting of refractive-index fluctuations at various positions along the propagation path and across different spatial scales. As the propagation distance increases, turbulence-induced phase perturbations are progressively converted into intensity fluctuations, leading to an increase in the intensity scintillation index in the weak-turbulence regime. With further increases in turbulence strength, multiscale scattering and wave interference effects limit the growth of intensity fluctuations, potentially causing the intensity scintillation index to reach a peak and enter the saturation regime. Under strong-turbulence conditions, enhanced multiple scattering and statistical averaging effects cause the intensity scintillation index to approach a relatively stable level. As a result, the two wave types show different scintillation levels, peak positions and saturation behavior in Figures 5– 13.

4 The variation characteristics of phase structure function of different atmospheric turbulence power spectrum models

In the study of atmospheric turbulence, the phase fluctuation reflects the degree of distortion of the wavefront after passing through the medium with random refractive index fluctuation. In wireless optical communication systems, phase fluctuations lead to a decrease in beam coherence. Wavefront phase structure function $D_\phi(\rho)$ [10, 31], also known as phase structure function, can reflect the degradation law of beam spatial coherence. The phase structure function reflects the spatial correlation and distortion degree of the wavefront phase under the action of turbulence by characterizing the phase difference between different spatial positions. The change under the smaller spatial interval can reflect the local high spatial frequency phase fluctuation. By studying the phase structure function under different generalized atmospheric turbulence power spectra, a beam coherence degradation model from inner-scale turbulent motion to outer-scale energy injection can be established, which provides a theoretical basis for studying the evolution boundary of beam spatial coherence in complex atmospheric environment.

The phase structure functions below are derived under the following approximations. In the derivation of the phase structure function, the geometrical optics approximation is used to describe phase perturbations caused by refractive-index fluctuations,

while the Markov approximation is adopted where applicable to simplify the longitudinal correlation of refractive-index fluctuations. For certain analytical expressions, the turbulence inner scale is assumed to approach zero to simplify the integration of the power spectrum, whereas the corresponding scale parameters are retained in models that account for finite inner and outer scales.

4.1 Phase structure function of plane wave

For the plane wave transmitted from the light source point to the receiving point, the expression of phase fluctuation [32] is

$$\phi(\mathbf{r}) = k \int_0^L n_1(\mathbf{r}, z)\, dz \tag{145}$$

The phase structure function describes the mean square error of the phase between two points in space. The expression of phase structure function of plane wave [10, 33] is

$$D_\phi(\rho) = \langle [\phi(\mathbf{r}+\rho) - \phi(\mathbf{r})]^2 \rangle = 2[B_\phi(0) - B_\phi(\rho)] \tag{146}$$

where ρ is the distance between two points in space. $B_\phi(\rho) = \langle \phi(\mathbf{r})\phi(\mathbf{r}+\rho) \rangle$ is a phase correlation function, which describes the spatial correlation of phase fluctuation.

Substituting Eq. (145) into the phase correlation function, the expression [32] is

$$B_\phi(\rho) = k^2 \int_0^L \int_0^L \langle n_1(\mathbf{r}, z_1) n_1(\mathbf{r}+\rho, z_2) \rangle\, dz_1 dz_2 \tag{147}$$

Under the Markov approximation, $\langle n_1(z_1) n_1(z_2) \rangle = \delta(z_1 - z_2) B_n(\rho, z)$, and the double integral is simplified as

$$B_\phi(\rho) = k^2 \int_0^L B_n(\rho, z)\, dz \tag{148}$$

The relationship between the refractive-index correlation function B_n and the power spectrum Φ_n of the refractive index in the transverse plane [4] is

$$B_n(\rho, z) = 2\pi \int d^2\kappa\, \Phi_n(\kappa, z) e^{i\kappa\cdot\rho} \tag{149}$$

Substituting into the expansion of the phase structure function, the phase structure function of the plane wave is obtained as

$$D_\phi(\rho) = 4\pi k^2 \int_0^L dz \int d^2\kappa\, \Phi_n(\kappa, z) \left[1 - e^{i\kappa\cdot\rho}\right] \tag{150}$$

If the refractive index is isotropic in the cross section, the three-dimensional power spectrum depends only on the magnitude κ of the wavenumber. The three-dimensional power spectrum is expressed as

$$\Phi_n(\boldsymbol{\kappa}, z) = \Phi_n(\kappa, z) \tag{151}$$

where $\kappa = \sqrt{\kappa_x^2 + \kappa_y^2}$.

By using the polar coordinate transformation $d^2\kappa = \kappa\ d\kappa\ d\theta$ and the Bessel function $J_0(\kappa\rho) = \frac{1}{2\pi}\int_0^{2\pi} e^{i\kappa\rho\cos\theta}\ d\theta$, the phase structure function of plane wave at any turbulence intensity is expressed as

$$D_\phi(\rho) = 8\pi^2 k^2 \int_0^L dz \int_0^\infty \kappa \Phi_n(\kappa, z)[1 - J_0(\kappa\rho)] d\kappa \tag{152}$$

For the two-dimensional isotropic spectrum, the polar coordinate transformation $\int d^2\kappa = 2\pi \int_0^\infty \kappa\ d\kappa$ is used. Since the generalized power spectral function is position independent, the path integral $\int_0^L dz$ is directly reduced to the distance L, and the expression is simplified to

$$D_\phi(\rho) = 8\pi^2 k^2 L \int_0^\infty \kappa \Phi_n(\kappa)[1 - J_0(\kappa\rho)]\, d\kappa \tag{153}$$

where k is the wavenumber, L is the transmission distance, J_0 is the first kind of 0-order Bessel function, and $D_\phi(\rho)$ is a dimensionless physical quantity.

4.1.1 *Plane-wave phase structure function for non-Kolmogorov spectra*

Non-Kolmogorov spectrum is the basis for studying the evolution of atmospheric turbulence. The phase structure function under this spectrum is derived, which can quantify the power-law degradation caused by the atmospheric turbulence energy cascade process on the coherence of the beam. By studying the phase structure function of the non-Kolmogorov spectrum, the characteristics of the beam from fully coherent

to partially coherent with the spatial distance ρ are described.

(1) Inertial range ($l_0 \ll \rho \ll L_0$)

Substitute (6) into (153), the expression of phase structure function, which reduces to the classical power-law result for $\alpha = 11/3$ [34], is

$$D_\phi(\rho) = 8\pi^2 k^2 L A(\alpha) \tilde{C}_n^2 \int_0^\infty \kappa^{1-\alpha}[1 - J_0(\kappa\rho)]d\kappa \tag{154}$$

Let $u = \kappa\rho$, then $\kappa = u/\rho$, $d\kappa = du/\rho$, the integral expression in (154) is

$$\int_0^\infty \kappa^{1-\alpha}[1 - J_0(\kappa\rho)]d\kappa = \rho^{\alpha-2} \int_0^\infty u^{1-\alpha}[1 - J_0(u)]du \tag{155}$$

According to the properties of Mellin transform and the integral table of Bessel function ($3 < \alpha < 4$ interval), the definite integral in (155) is

$$Q(\alpha) = \int_0^\infty u^{1-\alpha}[1 - J_0(u)]du = \frac{\Gamma(2 - \frac{\alpha}{2})}{2^{\alpha-2}(\alpha - 2)\Gamma(\frac{\alpha}{2})} \tag{156}$$

Substituting Eq. (156) into Eq. (154) and combining the constant factor $8\pi^2 \cdot 2^{2-\alpha} = 2^{5-\alpha}\pi^2$, the expression of the phase structure function is

$$D_\phi(\rho) = \left[\frac{2^{5-\alpha}\pi^2 A(\alpha)\Gamma(2 - \frac{\alpha}{2})}{(\alpha - 2)\Gamma(\frac{\alpha}{2})}\right] k^2 L \tilde{C}_n^2 \rho^{\alpha-2} \tag{157}$$

In the inertial range, the phase structure function increases with $\rho^{\alpha-2}$ power law, which reflects the statistical variation of wavefront phase difference with spatial scale under turbulence. As the spatial distance increases, the randomness of the wavefront accumulates rapidly, and the spatial coherence of the beam attenuates in a power-law manner.

(2) Dissipation range ($\rho \ll l_0$)

In the dissipative region, the non-Kolmogorov spectrum without inner scale cannot be used directly, because the spectrum will lead to the inconsistency of the integral with physical reality when $\kappa \to \infty$. The non-Kolmogorov spectral expression is modified by introducing an inner scale cutoff factor.

$$\Phi_n(\kappa, \alpha) = A(\alpha)\tilde{C}_n^2 \kappa^{-\alpha} \exp\left(-\frac{\kappa^2}{\kappa_m^2}\right) \tag{158}$$

where $\kappa_m = c(\alpha)/l_0$ is the cutoff wavenumber associated with the inner scale.

Substituting Eq. (158) into Eq. (153), the phase structure function can be expressed as

$$D_S(\rho) = 8\pi^2 k^2 L A(\alpha)\tilde{C}_n^2 \int_0^\infty \kappa^{1-\alpha} \exp\left(-\frac{\kappa^2}{\kappa_m^2}\right)[1 - J_0(\kappa\rho)]d\kappa \tag{159}$$

When the space distance ρ is very small, the integral is limited by $\exp(-\kappa^2/\kappa_m^2)$, mainly in the vicinity of $\kappa \approx \kappa_m \approx 1/l_0$, satisfying the condition $\kappa\rho \ll 1$. The series expansion of the first kind of 0-order Bessel function $J_0(\kappa\rho)$ is $J_0(\kappa\rho) \approx 1 - (\kappa\rho)^2/4$, then $1 - J_0(\kappa\rho) \approx \kappa^2\rho^2/4$, and the approximation term is substituted into the integral formula

$$D_S(\rho) \approx 8\pi^2 k^2 L A(\alpha)\tilde{C}_n^2 \int_0^\infty \kappa^{1-\alpha} \exp\left(-\frac{\kappa^2}{\kappa_m^2}\right)\left(\frac{\kappa^2\rho^2}{4}\right)d\kappa \tag{160}$$

The term independent of the integral variable κ is extracted, and the phase structure function is obtained as

$$D_S(\rho) \approx 2\pi^2 k^2 L A(\alpha)\tilde{C}_n^2\rho^2 \int_0^\infty \kappa^{3-\alpha} \exp\left(-\frac{\kappa^2}{\kappa_m^2}\right)d\kappa \tag{161}$$

Substituted into the gamma function integral formula $\int_0^\infty t^n e^{-t}dt = \Gamma(n+1)$, the integral term expression in Eq. (161) is

$$\int_0^\infty \kappa^{3-\alpha} \exp\left(-\frac{\kappa^2}{\kappa_m^2}\right)d\kappa = \frac{1}{2}\kappa_m^{4-\alpha}\Gamma\left(\frac{4-\alpha}{2}\right) \tag{162}$$

Substituting Eq. (162) into Eq. (161), the expression of the phase structure function under the smaller spatial interval in the dissipative region is obtained as follows

$$D_S(\rho) \approx \left[\pi^2 A(\alpha)\Gamma\left(\frac{4-\alpha}{2}\right)\kappa_m^{4-\alpha}\right] k^2 L \tilde{C}_n^2 \rho^2 \tag{163}$$

When the transverse spatial interval is less than the inner scale l_0 and enters the dissipation region, the

refractive index fluctuation of high spatial frequency is significantly attenuated by viscous dissipation, which makes the refractive index field have strong correlation and smoothness in the local spatial range. Therefore, the phase difference between adjacent positions is mainly determined by the local phase gradient, and the phase structure function increases approximately quadratically with the spatial interval, indicating that the wavefront is dominated by smooth local phase changes in a small spatial range.

4.1.2 *The phase structure function of plane waves in the generalized von Kármán spectrum*

Non-Kolmogorov has the problem of energy divergence in the low frequency region. The phase structure function under the generalized von Kármán spectrum is derived, and the physical limitation of the outer scale L_0 is introduced. The coherence degradation of the beam is not endless. It is shown that when the spatial distance is close to or exceeds the outer scale, the phase correlation tends to be saturated, which reflects the physical upper limit of atmospheric turbulence on phase interference. The phase structure function under the generalized von Kármán spectrum defines the maximum range of coherence damage caused by atmospheric turbulence, which provides a theoretical basis for the design of large-aperture wireless optical communication systems. When dealing with the generalized von Kármán spectrum including the inner scale l_0 and the outer scale L_0, the analytical form of the phase structure function $D_\phi(\rho)$ becomes very complicated due to the non-power-law characteristics of the power spectrum in the high-frequency dissipation region and the low-frequency energy input region. To keep the physical meaning clear, the expression is written in terms of the cutoff wavenumbers κ_0 and κ_m defined above.

Substituting the above generalized von Kármán spectrum (7) into Eq. (153), the expression of the phase structure function of the plane wave is obtained as

$$D_\phi(\rho) = 8\pi^2 k^2 L A(\alpha) \tilde{C}_n^2 \int_0^\infty \frac{\kappa \exp(-\kappa^2/\kappa_m^2)}{(\kappa^2+\kappa_0^2)^{\alpha/2}} [1 - J_0(\kappa\rho)] d\kappa \tag{164}$$

The integral term in Eq. (164) can be divided into a constant term without Bessel function and a term with Bessel function. The integral term becomes

$$\begin{aligned} &\int_0^\infty \frac{\kappa \exp(-\kappa^2/\kappa_m^2)}{(\kappa^2+\kappa_0^2)^{\alpha/2}} [1 - J_0(\kappa\rho)] \, d\kappa \\ &= \int_0^\infty \frac{\kappa e^{-\kappa^2/\kappa_m^2}}{(\kappa^2+\kappa_0^2)^{\alpha/2}} d\kappa - \int_0^\infty \frac{\kappa e^{-\kappa^2/\kappa_m^2}}{(\kappa^2+\kappa_0^2)^{\alpha/2}} J_0(\kappa\rho) \, d\kappa \end{aligned} \tag{165}$$

The integral term (165) involves the product of exponential function, power function and Bessel function. Using the integral identity of the second kind of confluent hypergeometric function $U(a, b, \kappa)$, its expression is

$$\begin{aligned} &\int_0^\infty \frac{\kappa \exp(-\beta_6\kappa^2)}{(\kappa^2+\gamma^2)^{\mu+1}} d\kappa = \frac{1}{2}\gamma^{-2\mu} U(1, 1-\mu, \beta_6\gamma^2) \\ &\int_0^\infty \frac{\kappa \exp(-\beta_6\kappa^2)}{(\kappa^2+\gamma^2)^{\mu+1}} J_0(\rho\kappa) \, d\kappa = \frac{\gamma^{-2\mu}}{2} \sum_{n=0}^\infty \frac{(-1)^n}{n!} \left(\frac{\gamma\rho}{2}\right)^{2n} \\ &\qquad \times U(n+1, n+1-\mu, \beta_6\gamma^2) \end{aligned} \tag{166}$$

where β_6 corresponds to the inner scale-dependent $1/\kappa_m^2$. γ corresponds to the outer scale dependent cutoff frequency κ_0. $\mu + 1$ corresponds to $\alpha/2$.

Substituting Eq. (166) into Eq. (164), the expression of the plane wave phase structure function with inner and outer scales is

$$\begin{aligned} D_\phi(\rho) = \frac{4\pi^2 A(\alpha) k^2 L \tilde{C}_n^2}{\kappa_0^{\alpha-2}} \Bigg[&\left(\frac{\kappa_0^2}{\kappa_m^2}\right)^{\frac{\alpha}{2}-1} \exp\left(\frac{\kappa_0^2}{\kappa_m^2}\right) \Gamma\left(1-\frac{\alpha}{2}, \frac{\kappa_0^2}{\kappa_m^2}\right) \\ &- \mathcal{H}(\rho, \kappa_0, \kappa_m) \Bigg] \end{aligned} \tag{167}$$

where $\Gamma(a, x)$ is the upper incomplete Gamma function. The spatial correlation term $\mathcal{H}(\rho, \kappa_0, \kappa_m)$ describes the phase correlation varying with the observation distance ρ, and its series expansion form is

$$\mathcal{H}(\rho, \kappa_0, \kappa_m) = \sum_{n=0}^\infty \frac{(-1)^n}{n!} \left(\frac{\kappa_0\rho}{2}\right)^{2n} U\left(n+1, n+2-\frac{\alpha}{2}, \frac{\kappa_0^2}{\kappa_m^2}\right) \tag{168}$$

where $U(a, b, x)$ is a confluent hypergeometric function.

Under the generalized von Kármán spectrum, the phase structure function of plane wave shows different characteristics in three regions. In the dissipative region $\rho < l_0$, the phase structure function is mainly affected by the $n = 1$ term in the $\mathcal{H}$ term, which is proportional to ρ^2, and the function shows a square law growth. In the inertial region $l_0 \ll \rho \ll L_0$, the series terms and the correction factors combine so that the phase structure function approaches the power-law form. In the energy input region $\rho \to \infty$, due to $\mathcal{H} \to 0$, the phase structure function tends to the

finite saturation value determined by the outer scale L_0, which solves the problem of infinite divergence of non-Kolmogorov theory in the low frequency band.

4.1.3 *The phase structure function of plane wave for generalized correction of atmospheric spectrum*

In the real atmospheric environment, the atmospheric turbulence spectrum not only exhibits non-Kolmogorov power-law characteristics, but also has protrusions at the edge of the dissipation zone and is physically limited by the inner scale l_0 and the outer scale L_0. The phase structure function under the generalized modified atmospheric spectrum is derived on the basis of the bump spectral model [35], which can reflect the influence of the high spatial frequency energy change represented by the Hill protrusion near the dissipative region on the local phase fluctuation, and reflect the variation characteristics of the spatial coherence of the light field during the transition from the inertial region to the dissipative region. The phase structure function under the generalized modified atmospheric spectrum reveals that in some specific application scenarios, ignoring the inner scale effect will lead to the deviation of the system coherence, and the actual communication performance in the complex atmospheric environment cannot be accurately evaluated. In order to maintain the consistency of the description of physical quantities, the phase structure function under the generalized modified atmospheric spectrum is derived.

The generalized modified atmospheric power spectrum model is proposed. The power spectrum is expressed by the expressions including the Hill protrusion correction term f_{bump}, the inner scale index truncation and the outer scale truncation.

$$\Phi_n(\kappa) = A(\alpha)\tilde{C}_n^2\kappa^{-\alpha}\underbrace{\left[1 + a_1\left(\frac{\kappa}{\kappa_l}\right) - b_1\left(\frac{\kappa}{\kappa_l}\right)^{\beta}\right]}_{f_{bump}\ \text{(Hill bump correction)}} \times \exp\left(-\frac{\kappa^2}{\kappa_l^2}\right)\left[1 - \exp\left(-\frac{\kappa^2}{\kappa_0^2}\right)\right] \tag{169}$$

Substituting Eq.(169) into Eq. (153), the expression of the phase structure function of the plane wave is

$$D_\phi(\rho) = 8\pi^2k^2LA(\alpha)\tilde{C}_n^2\sum_{n=1}^{\infty}\frac{(-1)^{n+1}}{(n!)^2}\left(\frac{\rho}{2}\right)^{2n} \times \left[I_0 + \frac{a_1}{\kappa_l}I_1 - \frac{b_1}{\kappa_l^{\beta}}I_\beta\right] \tag{170}$$

Each component I_i is the spectral integral defined in Eqs. (193)–(194), with the corresponding power correction $\delta_i \in \{0, 1, \beta\}$. I_0 represents the background energy of non-Kolmogorov turbulence, I_1 represents the high-frequency fluctuation caused by the linear term of the Hill bump, and I_β represents the slope correction caused by the power term of the Hill bump. a_1, b_1, β are the Hill bump correction coefficients. κ_0 and κ_l are the spatial cutoff frequencies related to the outer scale and the inner scale, respectively.

Under the generalized modified atmospheric spectrum, the Hill protrusion increases the refractive index fluctuation energy in a specific spatial frequency range near the dissipative region, and changes the phase fluctuation of the corresponding spatial scale, so that the phase structure function can describe the phase statistical characteristics of the transition from the inertial region to the dissipative region near the inner scale in more detail. In the dissipative region $\rho < l_0$, the phase structure function is mainly affected by the $n = 1$ series term, and the function shows a smooth growth of ρ^2. In the inertial region $l_0 \ll \rho \ll L_0$, the phase structure function degenerates into a power-law form. In the energy input region $\rho \to \infty$, the correlation term in the phase structure function tends to zero, eliminating the defect of infinite divergence of the ideal power-law spectrum. When $a_1 = b_1 = 0$, the phase structure function of the generalized modified atmospheric spectrum automatically reduces to the phase structure function of the generalized von Kármán spectrum. When $L_0 \to \infty, l_0 \to 0$, the phase structure function of the generalized modified atmospheric spectrum reduces to the phase structure function of the non-Kolmogorov spectrum.

4.2 Phase structure function of spherical wave

In practical engineering applications, light waves are mostly transmitted in the form of spherical waves. The purpose of deducing the phase structure function of spherical wave can reveal the decoupling law between the geometric shape of light wave transmission and the inhomogeneity of atmospheric turbulence. The spherical wave diverges with the transmission distance,

and the wavefront cross section expands continuously. Compared with the phase structure function of plane wave, the phase structure function of spherical wave can quantify the effect of geometric divergence on alleviating coherence degradation, which provides a physical basis for optimizing the layout of wireless optical communication. For the spherical wave propagating from the light source point (z=0) to the receiving point ($z = L$), the phase fluctuation expression [34] is

$$\phi(\mathbf{r}) = k\int_0^L n_1\left(\frac{z}{L}\mathbf{r}, z\right)dz \tag{171}$$

The coordinate term $\frac{z}{L}\mathbf{r}$ reflects the characteristic that the wave surface diverges linearly with the propagation distance z.

The structure function expression of the phase of the spherical wave [34] is

$$D_\phi(\rho) = \langle[\phi(\mathbf{r}+\rho) - \phi(\mathbf{r})]^2\rangle = 2[B_\phi(0) - B_\phi(\rho)] \tag{172}$$

Substituting Eq. (171) into the phase correlation function $B_\phi(\rho)$, the expression is

$$B_\phi(\rho) = k^2\int_0^L\int_0^L \left\langle n_1\left(\frac{z_1}{L}\mathbf{r}, z_1\right) n_1\left(\frac{z_2}{L}(\mathbf{r}+\rho), z_2\right)\right\rangle dz_1 dz_2 \tag{173}$$

By using Markov approximation, $\langle n_1(z_1)n_1(z_2)\rangle = \delta(z_1 - z_2)B_n(\Delta\mathbf{r}, z)$ is obtained. By using δ function, the double integral is simplified to single integral. The transverse coordinate difference is $\frac{z}{L}\rho$, and the (173) formula becomes

$$B_\phi(\rho) = k^2\int_0^L B_n\left(\frac{z}{L}\rho, z\right)dz \tag{174}$$

Substituting Eq. (174) into Eq. (172), the phase structure function of spherical wave is expressed as

$$D_\phi(\rho) = 4\pi k^2\int_0^L dz\int d^2\kappa\Phi_n(\kappa, z)\left[1 - e^{i\kappa\cdot(\frac{z}{L}\rho)}\right] \tag{175}$$

Since $\int_0^{2\pi} 1d\theta = 2\pi$, and according to the definition of Bessel function $\int_0^{2\pi} e^{i\frac{z}{L}\kappa\rho\cos\theta}d\theta = 2\pi J_0\left(\frac{z}{L}\kappa\rho\right)$, the integral term in Eq. (175) is

$$\int_0^{2\pi}(1 - e^{i\frac{z}{L}\kappa\rho\cos\theta})d\theta = 2\pi\left[1 - J_0\left(\frac{z}{L}\kappa\rho\right)\right] \tag{176}$$

The two-dimensional integral is transformed into one-dimensional integral $\int d^2\kappa = 2\pi\int_0^\infty \kappa d\kappa$, and the expressions of (151) and (176) are substituted into (175). The phase structure function of spherical wave under arbitrary turbulence intensity is expressed as

$$D_\phi(\rho) = 8\pi^2k^2\int_0^L dz\int_0^\infty \kappa\Phi_n(\kappa, z)\left[1 - J_0\left(\frac{z}{L}\kappa\rho\right)\right]d\kappa \tag{177}$$

Suppose that the refractive index fluctuation along the propagation direction is statistically uniform $\Phi_n(\kappa, z) \approx \Phi_n(\kappa)$, and the dimensionless variable $\xi = z/L$ ($dz = Ld\xi$), the expression is simplified as

$$D_\phi(\rho) = 8\pi^2k^2L\int_0^1 d\xi\int_0^\infty \kappa\Phi_n(\kappa)\left[1 - J_0(\xi\kappa\rho)\right]d\kappa \tag{178}$$

Through Eq.(178), it can be seen that the phase structure function of the spherical wave has a path weighting factor $\xi = z/L$ more than the phase structure function of the plane wave, resulting in that the atmospheric turbulence near the wave source has little effect on the phase fluctuation.

4.2.1 *Phase structure function of spherical wave of non-Kolmogorov spectrum*

Compared with the plane wave phase structure function, the main difference of the spherical wave phase structure function is that the independent variable of the Bessel function changes from $\kappa\rho$ to $\kappa\rho\xi$ which reflects the divergence characteristics of the spherical wave front.

(1) Inertial range ($l_0 \ll \rho \ll L_0$)

Substituting the non-Kolmogorov spectrum Eq. (6) into Eq. (178), the expression of the spherical wave phase structure function is obtained as follows:

$$D_\phi(\rho) = 8\pi^2k^2LA(\alpha)\tilde{C}_n^2\int_0^1\int_0^\infty \kappa^{1-\alpha}[1 - J_0(\kappa\rho\xi)]d\kappa d\xi \tag{179}$$

Let $u = \kappa\rho\xi$, then $\kappa = u/(\rho\xi)$, the integral term in (179) is

$$\int_0^\infty \kappa^{1-\alpha}[1-J_0(\kappa\rho\xi)]d\kappa = (\rho\xi)^{\alpha-2}Q(\alpha) \tag{180}$$

where $Q(\alpha)$ is the same integral constant as in Eq. (156), i.e.,

$$Q(\alpha) = \frac{\Gamma(2-\frac{\alpha}{2})}{2^{\alpha-2}(\alpha-2)\Gamma(\frac{\alpha}{2})} \tag{181}$$

Substituting Eq. (180) into Eq. (179), the expression of the phase structure function of the spherical wave is

$$D_\phi(\rho) = \left[\frac{1}{\alpha-1}\cdot\frac{2^{5-\alpha}\pi^2 A(\alpha)\Gamma(2-\frac{\alpha}{2})}{(\alpha-2)\Gamma(\frac{\alpha}{2})}\right]k^2 L\tilde{C}_n^2\rho^{\alpha-2} \tag{182}$$

Under the non-Kolmogorov spectrum, the phase structure function of the spherical wave degenerates to $1/(\alpha-1)$ times that of the plane wave under the same atmospheric turbulence intensity and path. When $\alpha = 11/3$, the phase structure function of spherical wave is about 3 / 8 of that of plane wave. The spherical wave does not change the power-law growth characteristics of the phase structure function with distance $\rho^{\alpha-2}$.

(2) Dissipation range ($\rho \ll l_0$)

Substituting the spectral formula (158) with the inner-scale cutoff into formula (178), the phase structure function of the spherical wave is expressed as

$$D_\phi(\rho) = 8\pi^2 k^2 L A(\alpha)\tilde{C}_n^2 \int_0^1 d\xi \times \int_0^\infty \kappa^{1-\alpha}\exp\left(-\frac{\kappa^2}{\kappa_m^2}\right)[1-J_0(\kappa\rho\xi)]\,d\kappa \tag{183}$$

When the space distance ρ is very small, because κ is limited by κ_m ($\kappa \approx 1/l_0$) in the integral, the condition $\kappa\rho\xi \ll 1$ is satisfied. The second-order Taylor expansion of 0-order Bessel function $J_0(\kappa\rho\xi)$ is carried out, and $1-J_0(\kappa\rho\xi) \approx (\kappa\rho\xi)^2/4$ is obtained. The approximate term is substituted into the integral formula, and the phase structure function expression of spherical wave is obtained.

$$D_\phi(\rho) \approx 8\pi^2 k^2 L A(\alpha)\tilde{C}_n^2 \int_0^1 d\xi \times \int_0^\infty \kappa^{1-\alpha}\exp\left(-\frac{\kappa^2}{\kappa_m^2}\right)\left(\frac{\kappa^2\rho^2\xi^2}{4}\right)d\kappa \tag{184}$$

For the ξ integral $\int_0^1 \xi^2 d\xi = 1/3$, this is the path weighting factor introduced by the propagation geometry during the propagation of spherical waves. For the κ integral, after extracting the constant term, the integral term in Eq. (184) is

$$\int_0^\infty \kappa^{3-\alpha}\exp\left(-\frac{\kappa^2}{\kappa_m^2}\right)d\kappa = \frac{1}{2}\kappa_m^{4-\alpha}\Gamma\left(\frac{4-\alpha}{2}\right) \tag{185}$$

Substituting Eq. (185) into Eq. (184), the expression of the phase structure function of the spherical wave is

$$D_\phi(\rho) \approx \left[\frac{1}{3}\cdot\pi^2 A(\alpha)\Gamma\left(\frac{4-\alpha}{2}\right)\kappa_m^{4-\alpha}\right]k^2 L\tilde{C}_n^2\rho^2 \tag{186}$$

Under the non-Kolmogorov spectrum, the spherical wave phase structure function no longer obeys the $\rho^{\alpha-2}$ power law in the small spatial interval range of the dissipative region, but is proportional to ρ^2, reflecting that the contribution of atmospheric turbulence near the light source ($\xi \to 0$) to the phase fluctuation at a small spatial interval can be almost ignored, which reflects the smoothing characteristics of the point source divergence wavefront. In the inertial region, the phase structure function of the spherical wave is $1/(\alpha-1)$ times that of the plane wave.

4.2.2 *Phase structure function of spherical wave of generalized von Kármán spectrum*

The generalized von Kármán spectrum (7) is substituted into Eq. (178), and $[1-J_0(\kappa\rho\xi)]$ is expanded as a series. The integral form of the phase structure function $D_\phi(\rho)$ is

$$D_\phi(\rho) = 8\pi^2 k^2 L A(\alpha)\tilde{C}_n^2 \int_0^1\int_0^\infty \frac{\kappa\exp(-\kappa^2/\kappa_m^2)}{(\kappa^2+\kappa_0^2)^{\alpha/2}} \times \sum_{n=1}^{\infty}\frac{(-1)^{n+1}}{(n!)^2}\left(\frac{\kappa\rho\xi}{2}\right)^{2n} d\kappa\,d\xi \tag{187}$$

Using the confluent hypergeometric function, after integrating κ, the semi-analytical expression of the path factor ξ is obtained as

$$\int_0^\infty \frac{\kappa^{2n+1}\exp(-\kappa^2/\kappa_m^2)}{(\kappa^2+\kappa_0^2)^{\alpha/2}}d\kappa = \frac{n!}{2\kappa_0^{\alpha-2n-2}}U\left(n+1, n+2-\frac{\alpha}{2}, \frac{\kappa_0^2}{\kappa_m^2}\right) \tag{188}$$

Substituting Eq. (188) into Eq. (187) and eliminating the κ integral term, the series form of the distribution with path ξ is obtained as follows:

$$D_\phi(\rho) = 4\pi^2 k^2 L A(\alpha) \tilde{C}_n^2 \kappa_0^{2-\alpha} \int_0^1 \sum_{n=1}^{\infty} \frac{(-1)^{n+1}}{n!} \left(\frac{\rho\xi\kappa_0}{2}\right)^{2n} \times U\left(n+1, n+2-\frac{\alpha}{2}, \frac{\kappa_0^2}{\kappa_m^2}\right) d\xi \tag{189}$$

After performing the path integral $\int_0^1 \xi^{2n} d\xi = \frac{1}{2n+1}$, the expression of the spherical wave phase structure function including the inner and outer scale correction is obtained as follows:

$$D_\phi(\rho) = 4\pi^2 k^2 L A(\alpha) \tilde{C}_n^2 \kappa_0^{2-\alpha} \sum_{n=1}^{\infty} \frac{(-1)^{n+1}}{n!(2n+1)} \left(\frac{\kappa_0\rho}{2}\right)^{2n} \times U\left(n+1, n+2-\frac{\alpha}{2}, \frac{\kappa_0^2}{\kappa_m^2}\right) \tag{190}$$

Under the generalized von Kármán spectrum, the key term that distinguishes the phase structure function of spherical wave from that of plane wave is the factor $(2n+1)$, which reduces the weight of the corresponding series term and reflects the weakening effect of path weighting on the cumulative contribution of phase fluctuation during the divergent propagation of spherical wave. In the inertial region, the series in the spherical wave phase structure function is affected by the low-order term, which reflects the limitation of the inner and outer scales of atmospheric turbulence, and shows the power law of the spherical wave phase structure function close to $\rho^{\alpha-2}$.

4.2.3 *Phase structure function of spherical wave for generalized correction of atmospheric power spectrum*

Substituting Eq. (169) into Eq. (178), the phase structure function of spherical wave is expressed as

$$D_\phi(\rho) = 8\pi^2 k^2 L A(\alpha) \tilde{C}_n^2 \int_0^1 \int_0^\infty \kappa^{1-\alpha} \left[1 + a_1 \frac{\kappa}{\kappa_l} - b_1 \left(\frac{\kappa}{\kappa_l}\right)^\beta\right] e^{-\frac{\kappa^2}{\kappa_l^2}} \times \left(1 - e^{-\frac{\kappa^2}{\kappa_0^2}}\right) [1 - J_0(\kappa\rho\xi)]\, d\kappa\, d\xi \tag{191}$$

Using the series expansion of J_0, the $[1 - J_0(\kappa\rho\xi)]$ in Eq. (191) is expanded as

$$1 - J_0(\kappa\rho\xi) = \sum_{n=1}^{\infty} \frac{(-1)^{n+1}}{(n!)^2} \left(\frac{\kappa\rho\xi}{2}\right)^{2n} \tag{192}$$

Since the integral operator $\int_0^1 \ldots d\xi$ and the spatial frequency κ are independent of each other, the path factor ξ is first integrated, $\int_0^1 \xi^{2n} d\xi = 1/(2n+1)$, which makes the spatial frequency term of the spherical wave have the unique denominator correction factor (2n+1) of the spherical wave.

The correction term in the generalized correction atmospheric power spectral function is expanded, and three corrections corresponding to Hill protrusions are defined for $\delta_i \in \{0, 1, \beta\}$. The integral form of each term conforms to Eq.(193), and its expression is

$$I_i = \int_0^\infty \kappa^{2n+1-\alpha+\delta_i} \left[e^{-\frac{\kappa^2}{\kappa_l^2}} - e^{-\kappa^2\left(\frac{1}{\kappa_l^2}+\frac{1}{\kappa_0^2}\right)}\right] d\kappa \tag{193}$$

By using the Gamma-function integral $\int_0^\infty t^{s-1} e^{-pt} dt = \Gamma(s) p^{-s}$, Eq.(193) is analytically reduced to

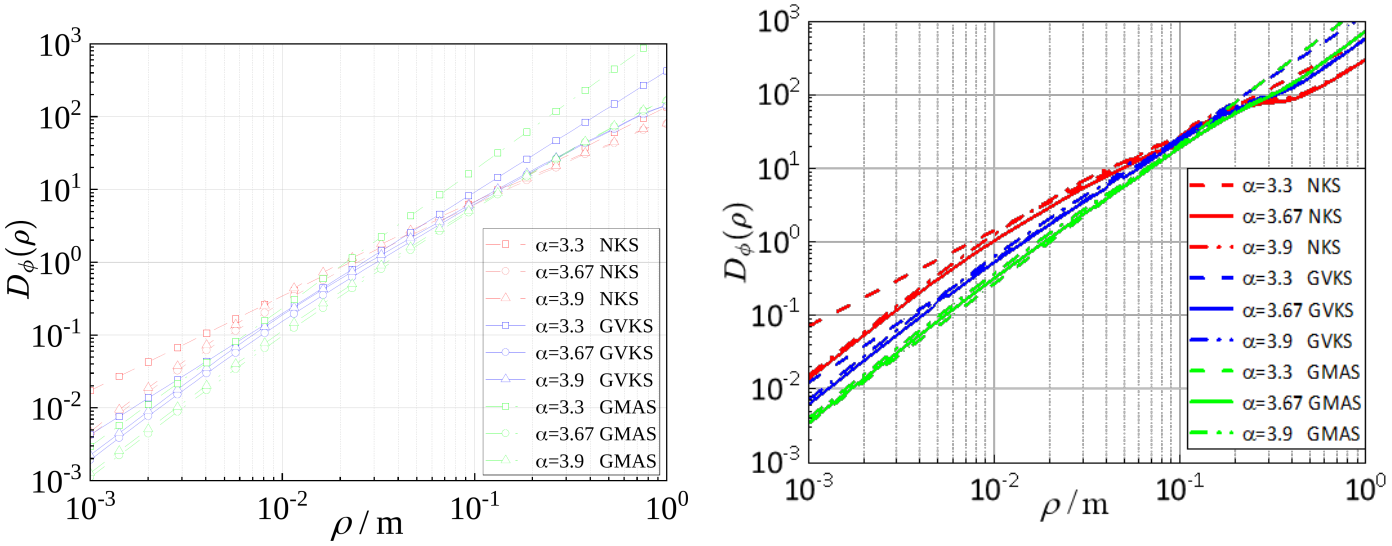
$$I_i = \frac{1}{2}\Gamma(s_i) \left[\kappa_l^{2s_i} - \left(\frac{1}{\kappa_l^2} + \frac{1}{\kappa_0^2}\right)^{-s_i}\right], \quad s_i = n + 1 - \frac{\alpha - \delta_i}{2} \tag{194}$$

Substituting Eq. (192) and Eq. (194) into Eq. (191), the expression of the spherical wave phase structure function is obtained as follows:

$$D_\phi(\rho) = 8\pi^2 k^2 L A(\alpha) \tilde{C}_n^2 \sum_{n=1}^{\infty} \frac{(-1)^{n+1}}{(n!)^2(2n+1)} \left(\frac{\rho}{2}\right)^{2n} \times \left[I_0 + \frac{a_1}{\kappa_l} I_1 - \frac{b_1}{\kappa_l^\beta} I_\beta\right] \tag{195}$$

where I_0 is the basis term, I_1 the linear term, and I_β the power term.

Under the generalized modified atmospheric spectrum, the spherical wave phase structure function is less sensitive to the high-frequency fluctuation caused by the Hill protrusion than the plane wave due to the (2n + 1) weight. In the dissipation region $\rho < l_0$, the phase structure function of the spherical wave follows the ρ^2 law, but its growth slope is lower than that of the plane wave. In the inertial range with $a_1 = b_1 = 0$, $l_0 \to 0$, $L_0 \to \infty$ and $\alpha = 11/3$, the expression degenerates to the classical spherical wave structure function $D_\phi(\rho) = 3/8 \times 6.88(\rho/r_0)^{5/3}$.



(a) Phase structure function of a plane wave

(b) Phase structure function of a spherical wave

Figure 14. Phase structure functions of plane and spherical waves under the three spectral models.

4.3 Analysis of the variation characteristics of the phase structure function of different wavefronts

By studying the phase structure function of plane wave and spherical wave under different power spectrum, it can be seen that under the same turbulence conditions, the $D_\phi(\rho)$ of plane wave is greater than that of spherical wave. The wave front of the plane wave remains parallel during transmission, and the disturbance is accumulated along the path. Due to the divergence characteristics of the wave front, the spherical wave is affected by turbulence, which is reflected in the statistical weight attenuation. Using formula (157), formula (167), formula (170), formula (182), formula (190) and formula (195), the variation curves of phase structure function $D_\phi(\rho)$ of plane wave and spherical wave with the separation distance ρ under three spectral conditions are obtained respectively, as shown in Figure 14. The wavelength is $\lambda = 0.525$ μm, transmission distance L = 10020 m, refractive index structure constant $\tilde{C}_n^2 = 10^{-16} m^{3-\alpha}$, outer scale L_0=10 m, inner scale l_0=10 mm. α is 3.3, 3.67 and 3.9, respectively. The generalized modified atmospheric spectral constants are a_1=1.802, b_1=0.254 and β=7/6. The distribution characteristics of the phase structure function for separation distances in the range of 10^{-3} to 1 m are described by the double logarithmic coordinates. In Figure 14, the value of the spectral index is distinguished by different symbols. The dashed lines represent the phase structure function under the non-Kolmogorov spectrum condition, the solid lines represent the phase structure function under the generalized von Kármán spectrum condition, and the dotted lines represent the phase structure function under the generalized modified atmospheric spectrum condition.

Figure 14 (a) and (b) show the variation of phase structure function $D_\phi(\rho)$ of plane wave and spherical wave with separation distance ρ, respectively, showing the dependence of phase structure function on power spectrum model and power law characteristics. The non-Kolmogorov spectral phase structure function without considering the inner and outer scales strictly follows the power-law growth $\propto \rho^{\alpha-2}$, which appears as a straight line in the double logarithmic coordinates. The generalized von Kármán spectral phase structure function increases linearly in the small-scale region, and is limited by the outer scale L_0 in the large-scale region, which reduces the slope and tends to saturation. The generalized modified atmospheric spectral phase structure function reflects the high-frequency convex characteristics of refractive index fluctuations due to the compensation term in the range close to the inner scale l_0. With the increase of power-law spectral index, the slope of each curve increases obviously, and the curves with different α values intersect near $\rho \approx 0.1$m, which reflects the redistribution characteristics of turbulent energy distribution with the change of power-law spectral index. Figure 14 shows that under the same physical parameters, the numerical difference between the phase structure function of spherical wave and plane wave is mainly due to the path weighting effect caused by the wavefront geometry. The plane wave is equally weighted by the influence of turbulence on the transmission path. The spherical wave front diverges with distance, and the turbulence near the light source has less influence. The path weighting

factor $\xi^{\alpha-2}$ leads to the overall weakening of the phase fluctuation, so that the value of the spherical wave is lower than that of the plane wave. The growth slopes of both are dominated by $\alpha - 2$ power law in the double logarithmic coordinates, and the spherical wave shows higher spatial correlation at the same separation distance ρ due to the lower intercept. The response of the spherical wave to the high-frequency bulge caused by the inner scale is smoother, and the process of saturation due to the limitation of the outer scale is more delayed than that of the plane wave, which reflects the unique weighting mechanism of the point source divergence characteristics to the turbulent spatial sampling efficiency.

Through the comparative analysis of Figure 14, the phase structure function reflects the multi-scale effect of atmospheric turbulence on beam modulation. In the dissipative region, the influence of the inner-scale l_0 in the atmospheric turbulence on the beam is characterized by a smooth wavefront tilt, and the spatial coherence degradation of the beam is slow. In the inertial region, due to the influence of α, the energy distribution of atmospheric turbulence redistributes with the change of spatial distance, and the spatial coherence of the beam degrades rapidly. In the energy input region, the influence of the atmospheric turbulence outer-scale L_0 on the beam, the phase fluctuation reaches saturation, and the spatial coherence of the beam degenerates to the limit.

5 Conclusion

This paper compares three non-Kolmogorov turbulence spectra and their effects on optical wave statistics. The spectral characteristics of the non-Kolmogorov spectrum, generalized von Kármán spectrum, and generalized modified atmospheric turbulence spectrum are analyzed, highlighting their differences in describing turbulent energy distributions across different spatial frequencies. The effects of propagation distance, power-law spectral index, and inner scale on the intensity scintillation index of plane and spherical waves are investigated numerically, the outer-scale effect is incorporated through the spectral models and spatial filtering functions, and the corresponding analytical expressions for the phase structure function are derived. The results indicate that different power spectrum models exhibit distinct predictions of intensity scintillation and phase fluctuations. The inner and outer scales primarily affect high- and low-spatial-frequency turbulence components, respectively, thereby influencing the intensity scintillation index and phase structure function. Furthermore, differences in wavefront geometry lead to different responses of plane and spherical waves to atmospheric turbulence, resulting in variations in scintillation magnitude and its evolution with propagation distance. These results link the spectral parameters to the intensity and phase statistics and can be used as a reference for turbulence-mitigation studies. It should be noted that the present study is primarily based on selected atmospheric turbulence power spectrum models and their associated theoretical assumptions, with analytical derivations and parametric comparisons of the intensity scintillation index and phase structure function. The reported trends are constrained by the forms of the spectral models, the selected parameter values—including the power-law exponent and inner and outer scales, with the outer scale fixed in the numerical examples—and the propagation conditions. Their applicability to realistic, inhomogeneous, anisotropic, and time-varying atmospheric environments remains to be further assessed. Moreover, the present study mainly presents theoretical and numerical parametric analyses and does not yet include systematic validation of model prediction accuracy using independent outdoor measurement data. Therefore, the conclusions should be interpreted within the scope of the adopted models and parameter ranges.

Future work will combine numerical wave-optics simulations with observations of optical propagation through the actual atmosphere to cross-validate the intensity scintillation indices and phase structure functions of plane and spherical waves predicted by the three power spectrum models and to quantify differences between model predictions and measurements. Building on these results, more complex turbulence conditions, including inhomogeneous, anisotropic, and time-varying environments, will be considered to extend the applicability of the models. We will also explore the use of the resulting statistical relationships in free-space optical communication link performance evaluation and in optimizing adaptive-optics wavefront compensation parameters.

Data Availability Statement

Data will be made available on request.

Funding

This work was supported without any funding.

Conflicts of Interest

Xizheng Ke served as an Editor-in-Chief of the *Optical Wireless Communication* at the time of manuscript submission. To ensure the integrity of the peer-review process, Xizheng Ke was not involved in the editorial handling, peer review, or decision-making process for this manuscript, which was handled independently by another editor. The remaining authors declare no conflicts of interest.

AI Use Statement

The authors declare that no generative AI was used in the preparation of this manuscript.

Ethical Approval and Consent to Participate

Not applicable.

References

[1] Kolmogorov, A. N. (1991). The local structure of turbulence in incompressible viscous fluid for very large Reynolds numbers. *Proceedings: Mathematical and Physical Sciences, 434*(1890), 9-13. https://www.jstor.org/stable/51980

[2] Pope, S. B. (2000). Turbulent Flows. Cambridge: Cambridge University Press. https://www.cambridge.org/is/universitypress/subjects/physics/nonlinear-science-and-fluid-dynamics/turbulent-flows

[3] Fante, R. L. (1980). Electromagnetic beam propagation in turbulent media: an update. *Proceedings of the IEEE, 68*(11), 1424-1443. [CrossRef]

[4] Andrews, L. C., & Phillips, R. L. (2005). *Laser Beam Propagation through Random Media* (2nd ed.). Bellingham: SPIE Press. https://spie.org/samples/PM354.pdf

[5] Tatarskii, V. I., & Zavorotnyi, V. U. (1985). Wave propagation in random media with fluctuating turbulent parameters. *Journal of the Optical Society of America A, 2*(12), 2069-2076. [CrossRef]

[6] Yura, H. T. (1974). Physical model for strong optical-amplitude fluctuations in a turbulent medium. *Journal of the Optical Society of America, 64*(1), 59-67. [CrossRef]

[7] Clifford, S. F., Ochs, G. R., & Lawrence, R. S. (1974). Saturation of optical scintillation by strong turbulence. *Journal of the Optical Society of America, 64*(2), 148-154. [CrossRef]

[8] Hill, R. J., & Clifford, S. F. (1981). Theory of saturation of optical scintillation by strong turbulence for arbitrary refractive-index spectra. *Journal of the Optical Society of America, 71*(6), 675-686. [CrossRef]

[9] Andrews, L. C., Phillips, R. L., Hopen, C. Y., & Al-Habash, M. A. (1999). Theory of optical scintillation. *Journal of the Optical Society of America A, 16*(6), 1417-1429. [CrossRef]

[10] Fried, D. L. (1965). Statistics of a geometric representation of wavefront distortion. *Journal of the optical society of America, 55*(11), 1427-1435. [CrossRef]

[11] Reynolds, O. (1895). On the dynamical theory of incompressible viscous fluids and the determination of the criterion. *Philosophical Transactions of the Royal Society of London. A, 186*, 123-164. [CrossRef]

[12] Toselli, I., Andrews, L. C., Phillips, R. L., & Ferrero, V. (2008). Free-space optical system performance for laser beam propagation through non-Kolmogorov turbulence. *Optical Engineering, 47*(2), 026003-026003. [CrossRef]

[13] Ata, Y., Baykal, Y., & Gökçe, M. C. (2022). Performance of a free-space optical communication system employing receive diversity techniques in anisotropic atmospheric non-Kolmogorov turbulence. *Journal of the Optical Society of America B, 39*(8), 2100-2108. [CrossRef]

[14] Toselli, I., Agrawal, B., & Restaino, S. (2011). Light propagation through anisotropic turbulence. *Journal of the Optical Society of America A, 28*(3), 483-488. [CrossRef]

[15] Andrews, L. C., Phillips, R. L., & Hopen, C. Y. (2001). Laser Beam Scintillation with Applications. Bellingham: SPIE Press. [CrossRef]

[16] Toselli, I., Andrews, L. C., Phillips, R. L., & Ferrero, V. (2009). Free space optical system performance for a Gaussian beam propagating through non-Kolmogorov weak turbulence. *IEEE Transactions on Antennas and Propagation, 57*(6), 1783-1788. [CrossRef]

[17] Stribling, B. E., Welsh, B. M., & Roggemann, M. C. (1995, June). Optical propagation in non-Kolmogorov atmospheric turbulence. In *Atmospheric propagation and remote sensing IV* (Vol. 2471, pp. 181-196). SPIE. [CrossRef]

[18] Beland, R. R. (1995, April). Some aspects of propagation through weak isotropic nonkolmogorov turbulence. In *Beam Control, Diagnostics, Standards, and Propagation* (Vol. 2375, pp. 6-16). SPIE. [CrossRef]

[19] Toselli, I., Andrews, L. C., Phillips, R. L., & Ferrero, V. (2007, May). Angle of arrival fluctuations for free space laser beam propagation through non Kolmogorov turbulence. In *Atmospheric Propagation IV* (Vol. 6551, pp. 149-160). SPIE. [CrossRef]

[20] Cui, L., Xue, B., Zheng, S., Xue, W., Bai, X., Cao, X., & Zhou, F. (2012). Atmospheric spectral

model and theoretical expressions of irradiance scintillation index for optical wave propagating through moderate-to-strong non-Kolmogorov turbulence. *Journal of the Optical Society of America A, 29*(6), 1091-1098. [CrossRef]

[21] Hill, R. J., & Clifford, S. F. (1978). Modified spectrum of atmospheric temperature fluctuations and its application to optical propagation. *Journal of the Optical Society of America, 68*(7), 892-899. [CrossRef]

[22] Xue, B., Cui, L., Xue, W., Bai, X., & Zhou, F. (2011). Generalized modified atmospheric spectral model for optical wave propagating through non-Kolmogorov turbulence. *Journal of the Optical Society of America A, 28*(5), 912-916. [CrossRef]

[23] Andrews, L. C. (1992). An analytical model for the refractive index power spectrum and its application to optical scintillations in the atmosphere. *Journal of modern optics, 39*(9), 1849-1853. [CrossRef]

[24] Yi, X., Liu, Z., & Yue, P. (2012). Inner-and outer-scale effects on the scintillation index of an optical wave propagating through moderate-to-strong non-Kolmogorov turbulence. *Optics Express, 20*(4), 4232-4247. [CrossRef]

[25] Ma, J., Fu, Y. L., Yu, S. Y., Xie, X. L., & Tan, L. Y. (2018). Further analysis of scintillation index for a laser beam propagating through moderate-to-strong non-Kolmogorov turbulence based on generalized effective atmospheric spectral model. *Chinese Physics B, 27*(3), 034201. [CrossRef]

[26] Toselli, I., Andrews, L. C., Phillips, R. L., & Ferrero, V. (2007). Scintillation index of optical plane wave propagating through non Kolmogorov moderate-strong turbulence. *Proceedings of SPIE, 6747*, 67470B. [CrossRef]

[27] Yi, X., Liu, Z., & Yue, P. (2013). Optical scintillations and fade statistics for FSO communications through moderate-to-strong non-Kolmogorov turbulence. *Optics & Laser Technology, 47*, 199-207. [CrossRef]

[28] Deng, P., Yuan, X. H., & Huang, D. (2012). Scintillation of a laser beam propagation through non-Kolmogorov strong turbulence. *Optics Communications, 285*(6), 880-887. [CrossRef]

[29] Cui, L., Xue, B., Xue, W., Bai, X., Cao, X., & Zhou, F. (2012). Expressions of the scintillation index for optical waves propagating through weak non-Kolmogorov turbulence based on the generalized atmospheric spectral model. *Optics & Laser Technology, 44*(8), 2453-2458. [CrossRef]

[30] Andrews, L. C., Al-Habash, M. A., Hopen, C. Y., & Phillips, R. L. (2001). Theory of optical scintillation: Gaussian-beam wave model. *Waves in Random Media, 11*(3), 271-291. [CrossRef]

[31] Lawrence, R. S., & Strohbehn, J. W. (1970). A survey of clear-air propagation effects relevant to optical communications. *Proceedings of the IEEE, 58*(10), 1523-1545. [CrossRef]

[32] Lutomirski, R. F., & Yura, H. T. (1971). Wave structure function and mutual coherence function of an optical wave in a turbulent atmosphere. *Journal of the Optical Society of America, 61*(4), 482-487. [CrossRef]

[33] Sasiela, R. J., & Shelton, J. D. (1993). Transverse spectral filtering and Mellin transform techniques applied to the effect of outer scale on tilt and tilt anisoplanatism. *Journal of the Optical Society of America A, 10*(4), 646-660. [CrossRef]

[34] Chesnokov, S. S., & Skipetrov, S. E. (1997). Optical resolution through atmospheric turbulence with finite outer scale. *Optics Communications, 141*(3-4), 113-117. [CrossRef]

[35] Andrews, L. C., Vester, S., & Richardson, C. E. (1993). Analytic expressions for the wave structure function based on a bump spectral model for refractive index fluctuations. *Journal of Modern Optics, 40*(5), 931-938. [CrossRef]



Rui Wang received the Ph.D. degree from Xi'an University of Technology, Xi'an, China, and is currently a faculty member at Xi'an University of Finance and Economics, Xi'an, China. Research interest: optical wireless communication. (Email: 2005010006@xaufe.edu.cn)



Xizheng Ke received the Ph.D. degree in science and is currently a Professor at Xi'an University of Technology, Xi'an, China. He is a Fellow of the Chinese Institute of Electronics and a Foreign Academician of the Russian Academy of Natural Sciences. Research interest: optical wireless communication. (Email: xzke@263.net)